Republic of Iraq
Ministry of Higher Education and Scientific Research
University of Kerbala-College of Science
Chemistry Department

Preparation and Study of MoO₃/TiO₂ Nano-composite and Application in Decolorization

A Thesis

Submitted to the Council of the College of Science/ University of Kerbala in a Partial Fulfillment of the Requirements for the Degree of Master of Science in Chemistry

By

Amani Jabbar Obaid

B.Sc. Chemistry (2016) /University of Kerbala

Supervisor

Prof. Dr. Luma Majeed Ahmed

2021 AD   **1442 AH**

بسم الله الرحمن الرحيم

﴿ اللّهُ لاَ إِلَـهَ إِلاَّ هُوَ الْحَيُّ الْقَيُّومُ لاَ تَأْخُذُهُ سِنَةٌ وَلاَ نَوْمٌ لَّهُ مَا فِي السَّمَاوَاتِ وَمَا فِي الأَرْضِ مَن ذَا الَّذِي يَشْفَعُ عِنْدَهُ إِلاَّ بِإِذْنِهِ يَعْلَمُ مَا بَيْنَ أَيْدِيهِمْ وَمَا خَلْفَهُمْ وَلاَ يُحِيطُونَ بِشَيْءٍ مِّنْ عِلْمِهِ إِلاَّ بِمَا شَاء وَسِعَ كُرْسِيُّهُ السَّمَاوَاتِ وَالأَرْضَ وَلاَ يَؤُودُهُ حِفْظُهُمَا وَهُوَ الْعَلِيُّ الْعَظِيمُ ﴾

صدق الله العلي العظيم

سورة البقرة (٢٥٥)

Supervisor Certification

I certify that this thesis **" Preparation and Study of MoO$_3$/TiO$_2$ Nano-composite and Application in Decolorization** " was conducted under my supervision at the department of chemistry, College of science, University of Kerbala, as a partial fulfillment of the requirements for the degree of Master of Science in Chemistry.

Signature:

Name: **Dr. Luma Majeed Ahmed**

Title: Professor
Address: University of Kerbala, College of Science, Department of Chemistry.
Date: /   / 2021

Report of the Head of Chemistry Department

According to the recommendation presented by the Chairman of the Postgraduate Studies Committee, I forward this thesis**" Preparation and Study of MoO₃/TiO₂ Nano-composite and Application in Decolorization** " for examination.

Signature:
Asst. Prof. Dr. Adnan Ibrahim Mohammed

Head of Chemistry Department
Address: University of Kerbala, College of Science, Department of Chemistry.
Date: /   / 2021

Report of Linguistic Evaluator

"I certify that the linguistic evaluation of this thesis " **Preparation and Study of MoO₃/TiO₂ Nano-composite and Application in Decolorization** " was assessed by myself and it is linguistically accepted.

Signature:
Name**: Dhiya Khaleel Nile**
Title: Instructor
Address: University of Kerbala, College of Education for the Humanities, Department of English
Date: /   / 2021

Report of Scientific Evaluator

I certify that the scientific evaluation of this thesis " **Preparation and Study of MoO$_3$/TiO$_2$ Nano-composite and Application in Decolorization** " was assessed by myself and it is scientifically accepted.

Signature:

Name: **Dr. Lekaa Hussain Khdaim**
Title: Assistant Professor
Address: University of Kufa, College of Education for Girls, Department of Chemistry

Date: /   / 2021

Signature:

Name: **Amjed Mirza Oda**
Title: Assistant Professor
Address: University of Babylon, College of Basic Education, Science Department

Date: /   / 2021

Dedication

To Imam Mahdi (calf God reappearance)

To my great mother, for her support, assistance, and kindness, all thanks and appreciation to you.

To my father

To my supervisor

To my dear friend (Saja, Thaqeef)

Who helped me all the time

Amani

2021

Acknowledgments

Initially, I want to thank the almighty Allah for giving me the strength and guidance throughout my entire life and during this work in particular.

I would like to deliver my deepest gratitude to my supervisor, **Prof. Dr. Luma Majeed Ahmed**, for her dedication, encouragement, and outstanding scientific support during the whole work.

Also, I want to thank all faculty members of the Department of Chemistry in College of Science in University of Kerbala, for their worthless support of the work.

Finally, thanks to my family, friends, and co-workers for helping hands, comradeship, and a nice atmosphere.

Amani

ABSTRACT

This project consists of three main parts:

Part one includes the preparation of molybdenum trioxide as α-MoO_3 nanobelts using a hydrothermal method. In this way, the dimensions of the prepared material were controlled by the reaction between sodium molybdate dihydrate as a precursor and dilution HCl. The α-MoO_3/TiO_2 nanocomposite was prepared in a w/w ratio of 0.25 (α-MoO_3): 9.75 (TiO_2) using the ultrasonic waves technique, which is fast, simple, and regarded as a friendly environment method.

Part two deals with the characterization of prepared α-MoO_3, α-MoO_3/TiO_2 nanocomposite, and commercial TiO_2. The XRD analysis conformed that the α-MoO_3 and its nanocomposite with TiO_2 are successfully prepared based on appeared the strong intensity peaks at miller indices (020), (040), and (060). SEM analysis indicated the shape of prepared α-MoO_3 and found to be nanobelts, while the shapes of TiO_2 and α-MoO_3/TiO_2 nanocomposite are semi-spherical and semi-spherical agglomerate respectively . The FT-IR spectra were confirmed to synthesis the α-MoO_3 and α-MoO_3/TiO_2 nanocomposite with appeared the peaks of metal-oxygen bonds at 675 cm^{-1} for Ti-O and at 559 cm^{-1} for Mo-O. The calculated band gaps (Bg) by the Tauc equation detected that all the catalysts are a photocatalyst, and demonstrate the commercial TiO_2 and the nanocomposite are having an indirect band gap, but the α-MoO_3 is having a direct band gap with 3 e V, 2.95 e V, and 2.8 eV respectively.

Part three focuses on the ability and tests their efficiency of the α-MoO_3, TiO_2, and its nanocomposite α-MoO_3/TiO_2 on the decolorization of chlorazol black BH dye as a studied model. The influence of different parameters on photo-decolorization of chlorazol black BH dye by using

the commercial TiO_2, prepared α-MoO_3/TiO_2 nanocomposite was illustrated. The parameters include the dose of photocatalysts, temperature, and initial pH of the solution. The thermodynamic parameters were calculated using the Arrhenius equation, the Eyring-Polanyi equation, and the Gibbs equation proved this photoreaction is an exothermic, less random, and nonspontaneous reaction using TiO_2, while with using α-MoO_3/TiO_2 nanocomposite is endothermic, less random, and nonspontaneous reaction.

The activity of photodecolorization for chlorazol black BH dye obtained to be maximum with the using the prepared α-MoO_3/TiO_2 nanocomposite that leads to increase the acidity of α-MoO_3 after incorporated the α-MoO_3 in the crystal lattice of TiO_2. This photoreaction follows the pseudo-first-order kinetics dependent on chlorazol black BH dye.

Contents Table

List of Tables

List of Figures

List of Abbreviations and Symbols

List of Abbreviations and Symbols	
Abbreviations and Symbols	**The Meaning**
AOPs	Advanced Oxidation Processes
BET	surface area analysis
$\mathbf{B_g}$	Band Gap
$\mathbf{C_o}$	Initial concentration
$\mathbf{C_B}$	Conduction Band
$\mathbf{C_t}$	Concentration of Substrate at Time T of Irradiation
$\mathbf{e^-}$	Negative electron
$\mathbf{E_a}$	Activation Energy
$\mathbf{E_g}$	Energy Gap
FTIR	Fourier Transformation Infrared
FWHM	Full width half – maximum
$\mathbf{h^+}$	Positive Hole
HOMO	Highest Occupied Molecular Orbital
$\mathbf{I_o}$	Light Intensity
k	The Scherrer's constant
$\mathbf{k_{app.}}$	Apparent Rate constant
L	Crystallite Size, Mean Crystallite Size
LUMO	Lowest Occupied Molecular Orbital
PDE	Photo decolourization Efficiency
SEM	Scanning Electron Microscopy
SEM-EDX	Energy Dispersive X-Ray Spectroscopy
T	Temperature
UV-Vis	Ultra Violet light in the range from 315 to 380 nm
$\mathbf{V_B}$	Valance Band
XPS	X-ray photoelectron spectroscopy
XRD	X-Ray Diffraction
α	Absorbance coefficient
β	Full Half-Maximum Intensity Width in Degrees
θ	Bragg Angle
λ	Wavelength

Chapter One
Introduction

1.1 General Introduction

Throughout the last few decades, the wastewater amount in world has increase due to the rise in human activities in some industries such as textile, cosmetics, industries that contain the residual dyes , and other usages [1-3]. This caused interest in seeking a safer way to treat recalcitrant organic contaminants through used an advanced oxidation process (AOPs) [4]. The AOPs are one of the emerging technologies that can turn organic contaminants into harmless products such as carbon dioxide (CO_2), water (H_2O), and mineral salts. So this process is beneficial since no require further separation of the by-product in an aqueous solution [5, 6]. In the other words, AOPs are a set of techniques that usually utilize the strong oxidizing species such as hydroxyl radicals ($^.OH$) that have a high in situ generated oxidation potential ($E^o = 2.8$ V), which then activates a series of reactions that break down a macromolecule into smaller and less dangerous components, the AOP approach uses a variety of techniques to generate hydroxyl radicles ($^.OH$) as shown in Figure (1-1), [7-11].
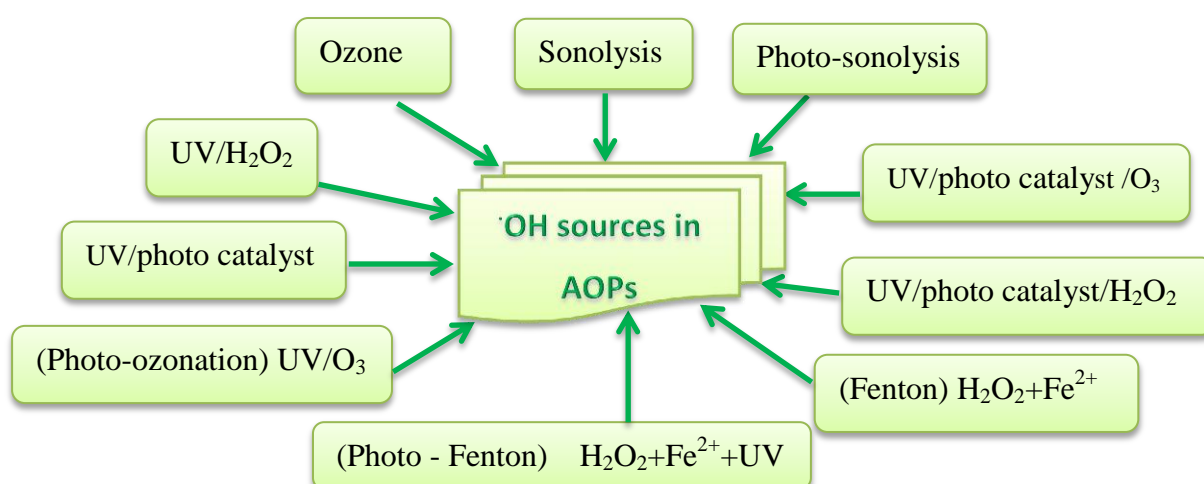
Figure (1-1). The schematic diagram for most Advanced Oxidation Processes applications as sources of $^.OH$ in photo or dark reaction [7].

Consequently, a more promising (AOPs) technology has been extensively studied in which a wide range of organic dyes can be rapidly and non-selectively oxidized. The (AOPs) have the benefit of being completely environmentally friendly over both chemical and biological processes [12-15], cost-effective, generated large amounts of hydroxyl radicals, minimized the time of photo or dark reaction, and reduced the dangerous organic contaminations[16,17].On the other side, the drawbacks of AOPs are inhibiting the rate of reaction by growing the scavenger's material, and it is possible to manufacture undesirable hazardous products that have prevented the completion of the mineralization process, may use further cost steps or adjust the pH leading to problems effectively [7,18].

1.2 Semiconductors

Semiconductors are described as solid materials that are crystalline or amorphous, and are regarded as an intermediate state between a metal and an insulator [19]. In general, the classification of solid materials based on the band gap (Bg) [energy gap (Eg)] values can be indicated in the table (1-1) [7, 20].

Table (1-1). Classification of solid materials according to energy gap magnitudes at room temperature.

Type of solid	Metal	Semimetal	Semiconductor	Insulator
Eg values (eV)	No Eg	$Eg \approx 0$	$0 < Eg < 4$ or 5	$Eg \geq 4$ or 5

Each solid material can be characterized by two energetic bands according to the band theory: a valence band (VB) called the high molecular orbital occupied (HOMO) has lower energy, filled with electrons , and a conductivity band (CB) called the lower unoccupied
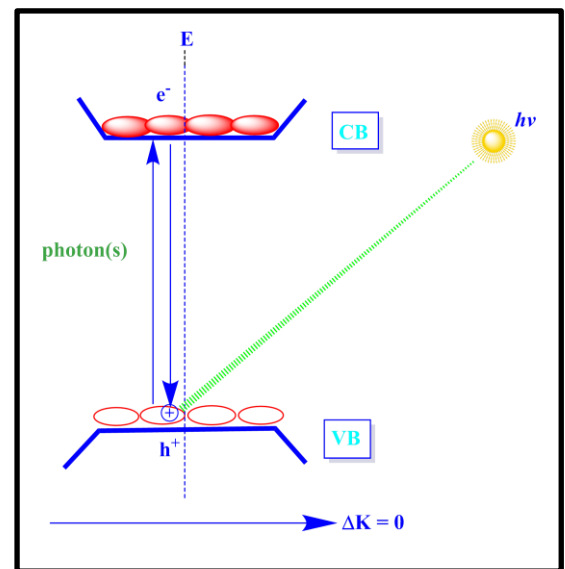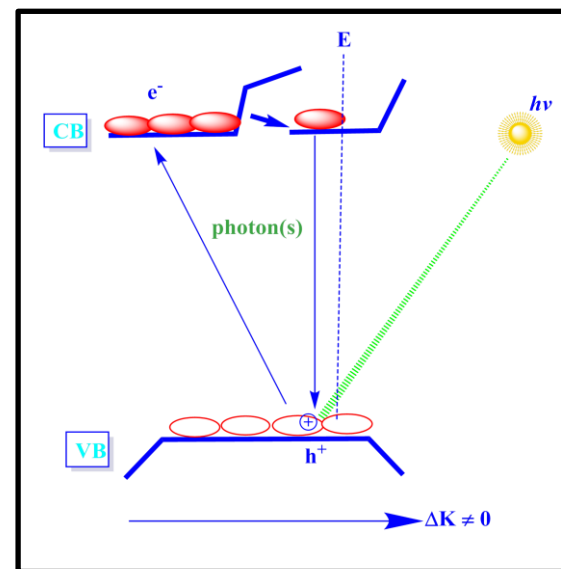
molecular orbital (LUMO), has higher energy.   Based on the solid material types, the energetic distance between VB and CB alters, and can be 0.7-5 eV for semiconductors, 6-7 eV for isolators, but the distance between them in metals overlaps [7, 21]. Some impurities or defects in the semiconductor crystal lattice lead to response to additional electronic levels (donor or acceptor ones) placed inside the forbidden semiconductor gap and produced p-type and n-type of semiconductor, the generated requirements are listed in table (1-2) [22].

Table (1-2).The generated requirements of p-type and n-type of semiconductor.

p-type	*n-type*
The empty acceptor level is placed near to the valence band and can be withdrawn the valence band electrons, leaving behind an electronic hole, this case called an electron-defect one.	The donor level is placed close to the conductivity band and called as an electron-excess semiconductor one.
When Fermi level lies close to VB can be produced p-type semiconductor	When Fermi level lies close to CB that will give n-type semiconductor
Such as NiO.	Such as TiO_2.

In fact, the Fermi level is a key factor that has detected this type of semiconductor, meaning the chemical potential of electrons in a semiconductor, which depends on the presence of the majority charge carriers in the semiconductor [23-28]. Several metal oxides such as (TiO_2, ZrO_2,   ZnO, MoO_3, and WO_3) and metal chalcogenides such as (CdS, CdSe, and ZnS) can be used as photocatalysts with direct or indirect bandgap [21, 29, 30]. The types of band gaps are depending on the symmetry of the crystal lattice band structure as shown in table (1-3) [31-35].

Table (1-3). The comparison between the direct and indirect band gaps.

Direct band gap	*Indirect band gap*
The transitions of the electrons are allowed, so the energy and electrons momentum must be conserved.	The transitions of the electrons are forbidden therefore the momentums cannot be conserved.
The transition of the electron carrying out directly via photon (is a type of elementary particle, quantum light and all other forms of electromagnetic radiation).	The transition of the electron carrying out indirectly via phonon (is the quanta of crystal lattice vibration energy) .
The change in the wave factor is equal to zero, ($\Delta k = 0$).	The change in the wave factor is not equal to zero, ($\Delta k \neq 0$).
The transition electron from the valence band to the conductance band is excited perpendicularly.	The transition electron from the valence band to the conductance band is no perpendicularly transition of the electron.
Such as ZnO (3.2-3.4 eV), CdS (2.4 eV) and ZnS (3.6 eV).	Such as TiO_2 (3.0-3.2 eV), spinel Mn_3O_4 (2.1 eV).

1.3 Photocatalysis

It is a process that enhances the rate of chemical reactions in a catalytic system by light. The photocatalytic system has two types homogeneous and heterogeneous photocatalysis [35, 36]. In the first type, both the photocatalyst and chemical reactants are in the same phases, but the last type is achieved with various phases [36]. Heterogeneous photocatalytic systems are the most widely applied during the

4

photocatalytic processes, because of photocatalysts such as metal oxide are typically used as activators with an appropriate wavelength and easily produce radical chain reactions. Photocatalysts are the most preferred in photocatalytic oxidation of dye waste-water because they are inexpensive, have low to no toxicity, have tunable properties that can be adjusted such as size reduction, doping, or sensitizers, have multi-electron transfer facilities, and can be used for longer periods without losing photocatalytic activity [37-39].

The catalytic material is known as photocatalyst when it absorbs UV or visible or solar light with energy greater than or equal to its bandgap ($hv \geq E_{Bg}$) and enhances the chemical transformation rate of the reactants [25, 40]. This behavior leads to generate holes (h^+_{VB}) on the valence band and electrons (e^-_{CB}) on the conduction band, which migrate to the photocatalyst surface and react with other species in series of redox reactions. The holes (h^+_{VB}) can be reacted with hydroxyl ion in an aqueous solution and produced hydroxyl radicals. Moreover, electrons (e^-_{CB}) can be reacted with environment oxygen and at last formed a double amount of hydroxyl radical, which regards as a powerful force for photoreaction. As shown in figure (1-2) [7, 38, 41].
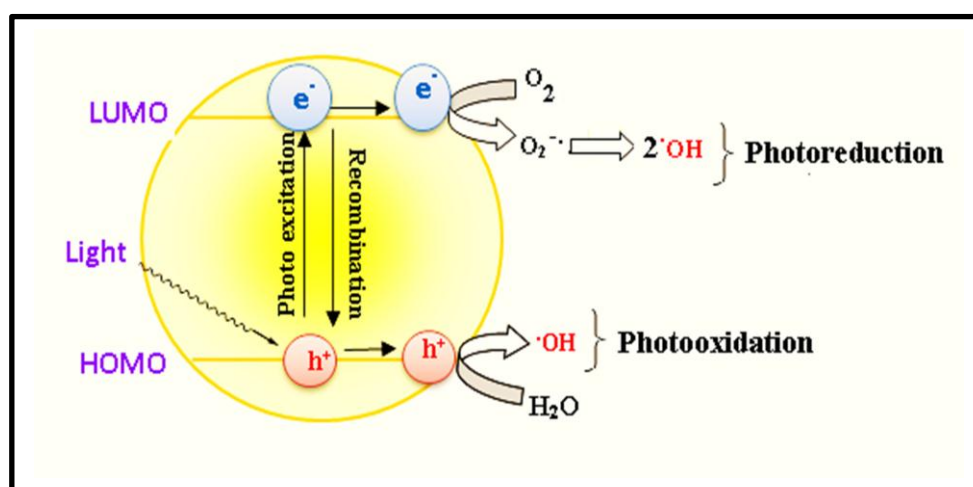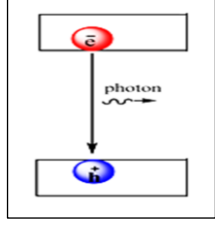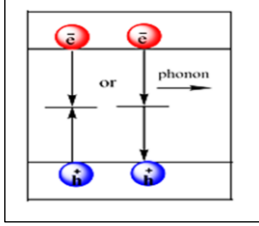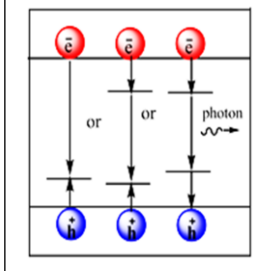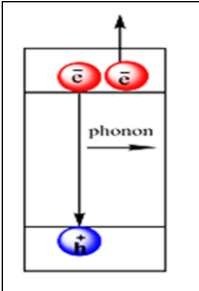
Figure (1-2). Essential process in (photocatalyst/ light/ aqueous solution) system.

However, the advantages of absorbs light photon in photoreaction lead to a high quantum yield, high conversion efficiency, high activity, and high stability. On the contrary, the efficiency of the photocatalyst can be decreased by the recombination process, that occur when the electrons return to the valence band from the conductive band and lose energy as heat [37, 38]. There are four common types of recombination shown in Table (1-4) [7, 42-44].

Table (1-4). The Common Types of Recombination in Semiconductor Photocatalyst.

Types	info	Schematic diagram
Direct recombination (band-to-band recombination)	The transition happens in the direct band gap semiconductor as a radiative transition. It is produced from drops of the Free photo electron in CB directly into the free photo hole in the VB and associated together. Ex. ZnO and WO$_3$ have a direct band gap	
Volume recombination (centers recombination or Trap-assisted recombination)	This kind arises when semiconductor defects are caused by impurities that provide new levels (as traps of photoelectron and photohole). It contributes to the release of heat as a phonon in the semiconductor indirect band gap. Ex. Pure TiO2 and metal defect of TiO2, which created an indirect band gap.	
Surface recombination (recombination of an exciton)	If the traps capture the photo electron-hole as exciton at or near the semiconductor surface or semiconductor interface, this occurs at low temperature. That attitude to dangling bonds induced by the sudden discontinuation of the semi-conductor crystal with energy just below the band gap value. Ex. In solar cells and light-emitting diode (LED) with shallow levels, this happed.	
Auger recombination	Three carriers are involved in this recombination: Free photo electron, free photo whole recombine, and the energy emitting as heat or as a photon (non-radiative process). The energy transition deals with intra-band transitions, resulting when either electron rises at higher levels of conduction band or hole deeper push into the valence band. Ex. This case can be obtained with a short lifetime when heavy doping defects (like Ag) in direct-gap semiconductors under present sunlight	

In order to reduce the recombination process must increase the separation of the charge on the photocatalyst surface, and increase the lifetime of the photo hole.

Three common methods are used to divide these modification methods: i) Surface Sensitization ii) Composite Semiconductor and iii) Modification by loaded Metal on Semiconductor [7]. As seen in figure (1-3)
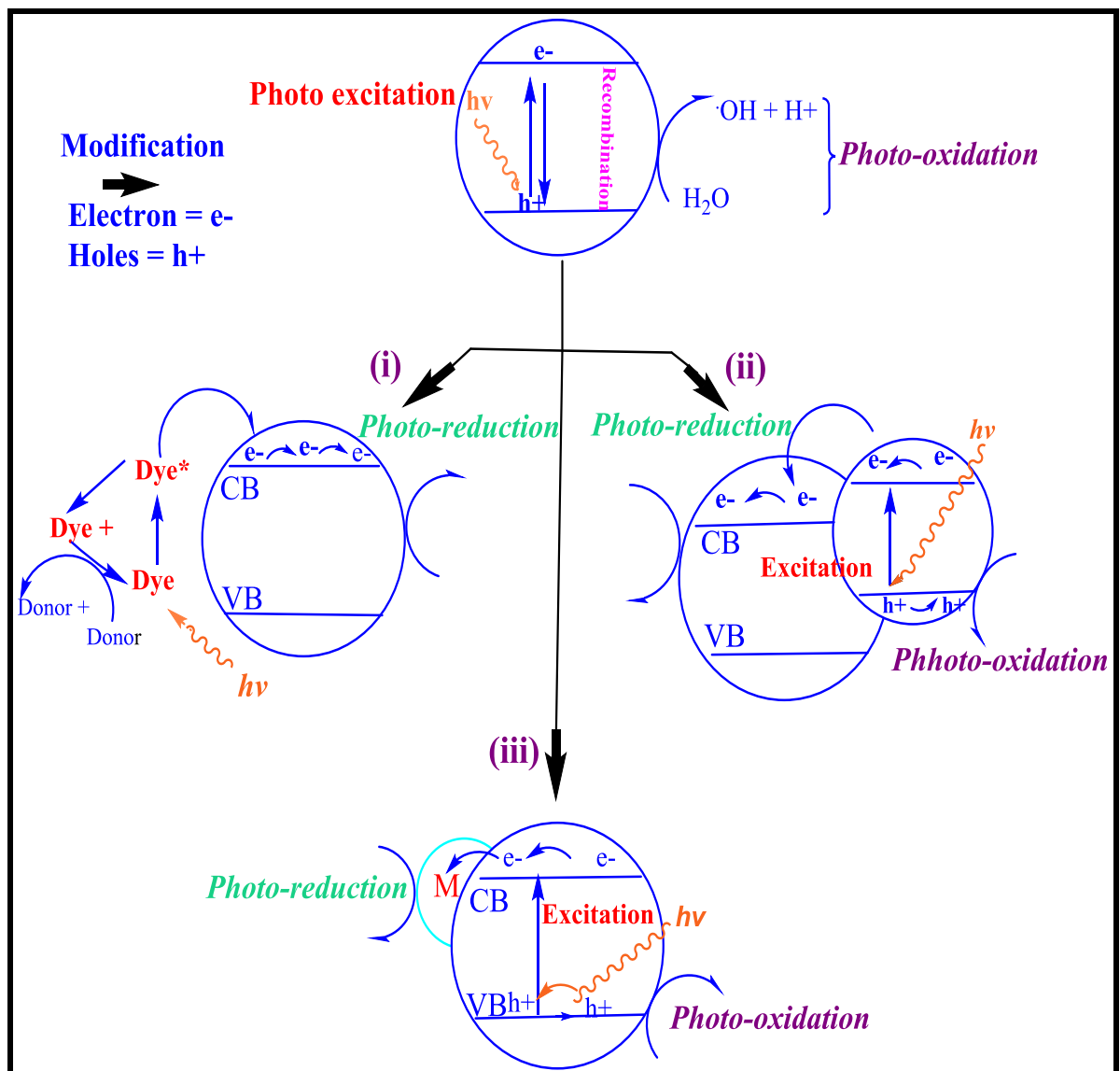
Figure (1-3). The common modification methods of photocatalyst surface [45].

1.4 Bulk and Nanoparticles Metal Oxide Properties

The metal oxide is known to be bulk or nanoparticle's most significant photocatalysts. The bulk metal oxide has dimensions greater than 100 nm, but there must be a nano-structure containing one or more external dimensions between 1 and 100 nm. The nanoparticle has special physical activity such as light absorption of specific wavelengths and catalytic activity. Hence, that leads to uptakes the interest in having unique features such as electrical, dielectric, optical, magnetic [46]. These characteristics of nanoparticles are industrially significant. Metal oxide nanoparticle is one of the major industrial materials and is manufactured in large quantities industrially and is the most frequently used. They are also used in products familiar to ordinary consumers such as fuel additives, sunscreens, pharmaceutical products, and cosmetics, in addition to industrial applications as transition metal oxide catalysts such ZnO, TiO_2, MoO_3, etc. [47].
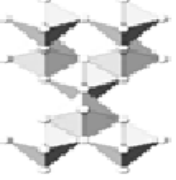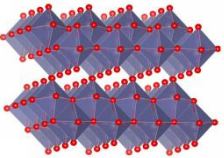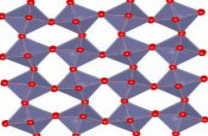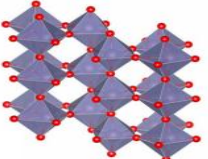
1.5 TiO_2 and MoO_3 as a Catalysts

Titanium dioxide (TiO_2) also known as titanium oxide or titanium (IV) oxide or titania, is a semiconductor the preferred catalyst for the photocatalytic treatment of dye wastewater due to its have a high capacity to generate a high oxidizing electron-hole pair, its strong chemical stability, non-toxicity and long term photostability [48,49]. TiO_2 naturally occurs in three common crystalline polymorphs, anatase, rutile, and brookite as explained in table (1-5).   Anatase and rutile crystal phases having the band gap of 3.2 eV and 3.0 eV for anatase and rutile respectively [35, 50]. It is also a versatile transition metal oxide and a useful material in a variety of present and future applications such as

catalysis, electronics, photonics, sensing, medicine, and controlled drug release [12, 49, 51, 52].

Molybdenum trioxide (MoO_3) is one of the most intriguing transition metal oxides due to its distinct layered structure and electrochemical properties. MoO_3 has intriguing structural, chemical, electrical, and optical properties. It is an n-type wide band gap (2.39-2.90 eV) semiconductor that can be used for a variety of technological applications such as photochromic materials. As shown in the table (1-5), there are three basic MoO_3 polytypic available, thermodynamically stable orthorhombic MoO_3 (α-type), metastable monoclinic MoO_3 (β-type), and hexagonal MoO_3 (h-type). Because the α-MoO_3 has band gap energy of about 3.0 eV, it can be used for photocatalytic applications in the solar spectrum's blue region. Molybdenum oxides are versatile oxide compounds that have well-known applications in electronics, catalysis, energy-storage units, sensors, field emission devices, lubricants, superconductors, bio systems, thermal materials [53, 54, 55]. Some main properties of TiO_2 and MoO_3 crystals are displaying in the table (1-5).

Table (1-5). Some main properties of TiO₂ and MoO₃ Crystals [51,52,55-59].

Type		Crystalline Structure type	Crystal structures	Color	Lattice Constant (Å)	Stability	Density (g cm⁻³)	Band gab type
TiO2	**Rutile**	Tetragonal		White	a= 4.5936 c= 2.9587	Stable	4.13	Indirect
	Anatase	Tetragonal		White	a= 3.784 c= 9.515	Metastable	3.79	
	Brookite	Orthorhombic		White	a= 9.184 b= 5.447 c= 5.154	Metastable	3.99	
MoO3	**α-MoO₃**	Orthorhombic		Deep grey	a= 3.962 b= 13.85 c= 3.697	Stable	-	Direct
	β-MoO₃	Monoclinic		Yellow-green	a= 7.4245 b= 7.4783 c= 7.6897	Metastable	4.70	
	h-MoO₃	hexagonal		Sandy	a= 10.53 b= 10.53 c= 3.730	Metastable	-	

1.6 Methods of Preparation and Modification of Nano-materials

The various techniques that are used to prepare the nanoparticles (NP's) are classified into two approaches [60, 61]:

1. (Bottom –up approach) such as Sol-Gel, Green synthesis, Co-precipitation method, hydrothermal method, and Solvothermal method.

2. (Top- down approach) such as Chemical vapor Deposition, ultrasonic method, Leaser ablation, and mechanical milling.

1.6.1 Hydrothermal Method for the Preparation of Nanomaterials

This method choses to prepare MoO_3, hence, must describe it here. The term "hydrothermal/solvothermal process" is characterized as the performance of chemical reactions in solvents contained in sealed vessels in which the temperature of solvents can be heated concurrently with autogenously pressures to their critical points. When water is used as the solvent, the term "hydrothermal" is used, but, when organics are used as solvents, the process is referred to as solvothermal process [60-63].

Hydrothermal synthesis is one of the most widely used methods for nanomaterials preparation. It is essentially a reaction-based approach to the solution. The formation of nanomaterials can happen in hydrothermal synthesis in a large temperature range from room temperature to very high temperatures [64]. Depending on the vapor pressure of the main composition in the reaction, either low pressure or high-pressure conditions may be used to control the morphology of the materials to be

prepared and several factors are influencing this method, such as precursors, additives, and reaction time [65]. Many kinds of nanomaterials have been successfully synthesized by the utilization of this method. Additionally, the prepared nanomaterials can be produced by the hydrothermal method with high vapor pressures and minimum loss of materials [66]. To synthesize the nanomaterials compositions must be well controlled in hydrothermal synthesis through a liquid phase or multiphase chemical reactions [67]. The hydrothermal synthesis method is regarded as one of the most promising methods for preparing nanomaterials. This method also has major advantages, it can produce highly crystalline and pure nanoparticles with well-controlled dimensions [68, 69]. On the other hand, the disadvantages of hydrothermal synthesis are as follows [70, 71]:

    i.   It needs expensive autoclaves.

    ii. The safety issues during the reaction process.

    iii. Impossibility of observing the reaction process (close system).

1.6.2   Ultrasonic Method for the Preparation of Nanomaterials

Sonochemistry is the study of chemical reactions using high-frequency ultrasound in the range of 20 kHz to 10 MHz. Ultrasonic waves are used in a liquid suspension by either immersing an ultrasound probe directly in the suspension, which is known as direct sonication or by immersing an ultrasound probe indirectly in the suspension, which is known as indirect sonication, or by immersing the container of the sample in an ultrasonic bath containing a liquid such as D.W and is called an indirect sonication. The physical mechanism responsible for the

sonochemical process is acoustic cavitation, which includes the forming, growth, and collapse of bubbles within a liquid. These bubbles behave as individual micro-reactors, releasing vast quantities of energy in the form of pressure (1000 bar) and temperature (5000 K) as they collapse frequently [72]. Based on the hot spot mechanism, since this bubble collapses, the chemical bonds are broken; because this collapse happened in less nanosecond, with very high cooling rates, preventing the products from organizing and crystallizing, and resulting in amorphous nanomaterials [73]. Many factors influence the rate of a sonochemical reaction, including the volatile nature of the precursors, solvents with low vapor pressure, and a low sonication temperature for the preparation of nanoparticles. The benefit of this approach over other methods of nanoparticle synthesis is that it can generate a wide range of nanophase materials by simply changing the reaction medium and it is also environmentally friendly [74].

1.7 Literature Review for Prepared MoO_3/TiO_2 Composite

To enhance the dye adsorption on photocatalyst surfaces and to achieve effective decolorization or degradation, the composites were created to develop the photocatalytic materials with high adsorption, reduce efficient electron-hole recombination, catalyst separation ease, and dye degradation effectiveness [75]. The MoO_3 semiconductor was incorporated with TiO_2 (an n-type semiconductor with a band gap of 3.0-3.2 eV) to prevent the electron-hole pair recombination and extend the range of useful excitation light toward the visible spectra. The MoO_3, an n-type semiconductor, is considered to form a composite with TiO_2 because it has a suitable band gap of about 2.85 eV for visible light absorption and a high oxidation power of photogenerated holes in the

valence band, which can easily convert absorbed water or hydroxide ions into $^{\cdot}OH$ radical. The improvement of photocatalytic activity can be attributed to the reduction of the electron-hole recombination rate during using of MoO_3/TiO_2 as a composite heterostructure [76, 77]. In this manner, there are some researchers interested in the combination of MoO_3 with TiO_2 in various procedures.

In 2012, Lande and co-workers [78], the MoO_3-TiO_2 nanocrystalline composite material was created using the sol-gel method. The synthesized material has been characterized using X-ray diffraction, scanning electron microscopy with electron dispersion spectroscopy, transmission electron microscopy, and (FTIR) spectroscopy. Melanoidin is a dark brown pigment found in the wastewater of the sugar industry. Under UV-visible radiation, the synthesized MoO_3-TiO_2 nanomaterial was found to be effective in degrading molasses.

In 2015, Luo and co-workers [76], the MoO_3/TiO_2 composite was generated using a simple sol-gel method. The (XRD), BET surface area analysis, (EDS), (XPS), and photoluminescence (PL) emission spectrum were used to characterize the composite. The results of the study show that BET-specific composite surface areas are significantly enhanced, and the composite has higher photocatalytic activity than pure TiO_2 for the degradation of Rhodamine B (RhB) under visible light irradiation.

In 2016, Liu and co-workers [79] prepared MoO_3/TiO_2 composite nanorods films. This composite has been successfully the novel prepared through the combination of hydrothermal and electrodeposition methods. The improved electrochromic properties are primarily attributed to the porous space inside the collection of the nanorods, which promotes the

ion diffusion becomes easier, and it also gives greater surface area for charge-transfer reactions.

In 2017, Kumar and co-workers [80], MoO_3/TiO_2 composite nanopowders were synthesized using a mechanochemical synthesis technique and characterized using PXRD, SEM with EDS, FT-IR, Raman, and TGA/DTA. The TGA/DTA analysis revealed that with a negligible weight loss, the nanopowders are stable up to 7800 ^{o}C. The synthesized oxide nanocomposite can therefore be used at elevated temperatures as a solid lubricant.

In 2018, Su and co-workers [81], used $(NH_4)_6Mo_7O_{24}.4H_2O$ and $TiCl_4$ to hydrothermally produced TiO_2-MoO_3 nanocomposite at 180 ◦C as the source of Mo and Ti, respectively. It is possible to confirm the TiO_2 and MoO_3 nanocrystalline in the products by using the (XRD). (TEM) has demonstrated that with the rise in the amount of Ti-doping, the size of MoO_3 becomes smaller. The TiO_2-MoO_3 nanocomposites displayed strong adsorption activity is approximately 290 mg g^{-1} for Rhodamine B (RhB), 180 mg g^{-1} for Methylene blue (MB), and 59 mg g^{-1} for the Cr (VI) of the heavy metal ion.

In 2020, Jesionowski and co-workers [82], synthesized the TiO_2-MoO_3 composite, they were successfully using a template-assisted microwave method at molar ratios TiO_2:MoO_3, 8:2, 5:5, and 2:8. The XRD and Raman spectroscopy, SEM, TEM, and HRTEM analysis have described the synthesized material systems comprehensively. The proposed template-assisted microwave synthesis allowed TiO_2 particles to be incorporated with the surface of hexagonal particles of MoO_3, resulted in a stable junction between TiO_2 and molybdenum trioxide. At the molar ratio 5:5 from TiO_2:MoO_3 composite, the best system was

obtained. The successful intercalation of lithium ions into the TiO_2-MoO_3 composite material has been confirmed by X-ray photoelectron spectroscopy (XPS).

1.8 Adsorption

Adsorption is a surface phenomenon in which the molecules or ions in the liquid or gas phase (adsorbate) are concentrated on the solid (adsorbent) surface [83, 84]. It can be categorized into chemisorption (based on covalent bonding) and physisorption (based on van der Waals forces) [85, 86]. In the heterogeneous photocatalytic mechanism, adsorption is an essential feature, which corresponds to the principle of Langmuir. Ultimately, the surface adsorption is influenced by ionic strength and pH value [87]. Adsorption has some important benefits and drawbacks, as any other process. The benefits may summarize as:

i. High ability and speed in removing pollutants from wastewater by converting to H_2O and CO_2.
ii. Finding various types of the catalyst.

While the drawbacks are summarized as: [88, 89]

i. The catalyst loses step-by-step actionable.
ii. Some types of the catalyst are high cost.
iii. Surfaces of active sites of the catalyst are mostly blocked with the present high amount of the macromolecular compounds like "dyes" in solution, this known poisoning.

1.8.1 Adsorption on the Semiconductor Surface

An adsorption process at the active catalyst site is used to treat pollutants in common wastewater [86]. The second most essential aspect

of a photocatalytic process is the extent of active surface area. The larger the available active surface area, the more reactants on the surface can be adsorbed. Consequently, photocatalytic degradation efficiency can be improved. The most convenient way to elevate the surface area is being by nano-structuring. As a result of the nanostructure, the surface area to volume ratio increases [90]. In fact, the adsorption process is based on a sequence of numerous steps. The first step is adsorption, which is performed by diffusion of the reactant molecule via fluid liquid or gas onto the semiconductor (photocatalyst) surface. The second step takes place if the active site has adsorbed the reactant molecule in the photocatalystis [91]. The photocatalysis produces charge carriers (e-/h$^+$) that are formed not only through the active sites of the photocatalyst activity used, but also through the use of semiconductor at any portion that is effectively absorbed in the presence of light for the reactant. In the third step, an activated complex is formed for bond formation and bond dissociation, which requires less activation energy than the activated complex of the uncatalyzed path. The rate of adsorption is affected by the particle size of the photocatalyst as well as the concentration of reactants and products. The adsorption process on the photocatalyst surface is considered the most important step in photocatalysis for reducing recombination [92, 93].

1.8.2 Adsorption of Oxygen and Water

The reactive species in the n-type semiconductor is the photo hole that is produced with the photoelectron; when a photon is absorbed by photocatalyst, the carries are formed with high light quantum energy, and then the accumulation of the electrons on the particles should be avoided, as it can lead to an increase in the rate of the hole- electron recombination

rate and lower the quantum yield. Therefore, the efficiency of the photocatalytic degradation process with the presence of an electron acceptor in the solution is essentially the typical proposed mechanism and steps are explained in figure (1-4) for the adsorption of dissolved oxygen and water hydroxyl ion [94].
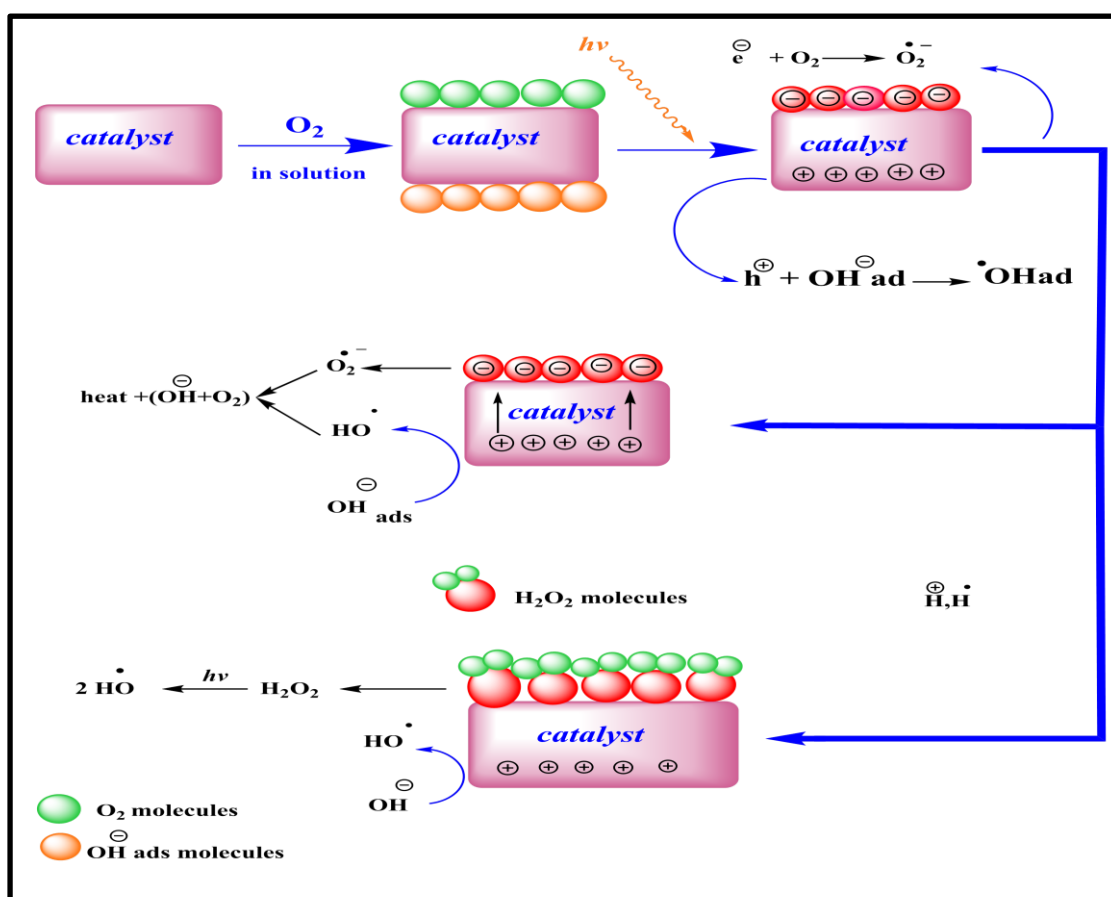
Figure (1-4). Schematic description of adsorption of the oxygen and water on the surface of a catalyst via using a photocatalyst under illumination.

1.8.3 Adsorption Dyes

Dye contamination, due to its toxicity and even carcinogenicity, has posed a serious threat to the aqueous environment and human health in recent years [95-97]. Dyes, on the other hand, are indispensable in everyday life and are inextricably linked to the textile, cosmetics, printing, and pharmaceutical industries [98, 99]. Therefore, several

resources have been devoted to the search for the successful removal of dyes from the aqueous solution. Adsorption is a simple, economical, and effective method for dye removal, compared to other techniques, such as ion exchange and membrane filtration [100, 101].   But another new problem is the set of adsorbents after adsorption. Therefore, high-efficiency adsorbents, fast regeneration, and low cost to the removal of dyes from wastewater are urgently desired. Several materials, such as zeolite, active carbon, alumina, polymer, etc [102, 103], have been identified as adsorbents to remove the organic dye contaminants from the wastewater, the process of dye adsorption has been explained in Figure (1-5).
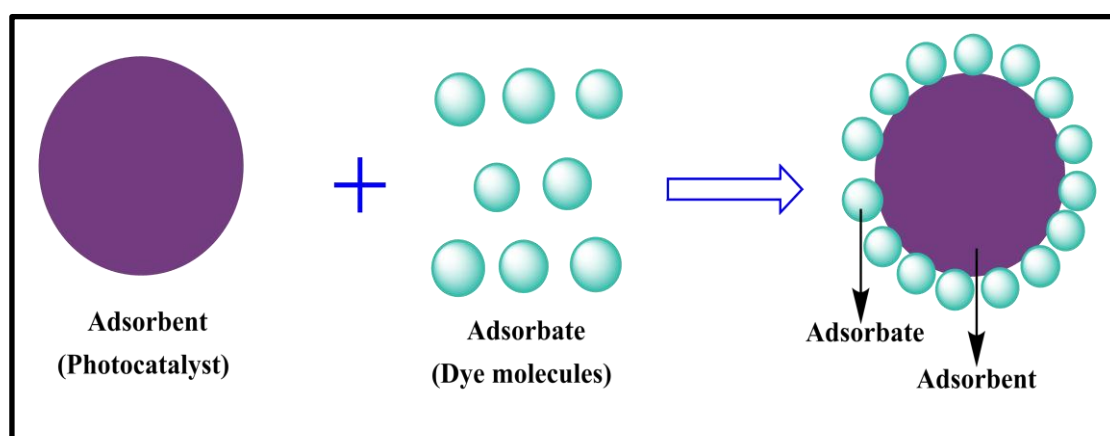
Figure (1-5). The dye adsorption process using adsorbent modification from [104].

1.9 Dyes

Dyes are a colored substance that binds to the substrate to which it is applied. It is colored because it absorbs light in the visible spectrum at a specific wavelength [104-106]. Dyes are primary ionizing and aromatic compounds with the various chromophore molecules that are responsible for their color, where, the color of dyes is due to the chromogene-chromophore structure (acceptor of electrons), while, the dyeing ability is

due to the presence of auxochrome groups (donor of electrons). Dyes are categorized as natural or synthetic based on their raw ingredients. Natural textile dyes are mainly obtained from plant and animal sources, while synthetic dyes are typically aromatic compounds generated via the chemical synthesis process. Furthermore, synthetic dyes are presently the most favorable due to their availability, superior coloring, and low cost [107, 108]. Dyes are also categorized based on their constituents, applications, colors, and chemical structure such as azo dyes, nitro dyes, nitroso dyes, triarylmethane dyes, and anthraquinone dyes these types are based on their chemical composition [109, 110]. Dyes are employed in the manufacturing of textile, cosmetics, pigment, leather tanning, and a variety of other industries use them to color their products. These factories' effluents cause potential hazards to the environment and human health. As a result, dye removal from wastewater has gotten a lot of attention in recent years. So far, chemical, physical, and biological approaches have all been employed, with adsorption proving to be the most successful method for removing dyes. [111,112].

1.9.1 Azo Dyes

The majority of synthetic azo aromatic dye (as monoazo or diazo or triazo or polyazo) consist of one, two, three, or more (N = N) groups and are related to benzene and naphthalene rings, which are often substituted by some functional groups, such as (methyl, nitro, triazine amine, chloro, hydroxyl, and sulphonate) [113,114]. Azo dyes are widely employed in the pharmaceutical, food, dyeing textile, cosmetics, and paper printing industries. Approximately 80% of azo dyes are closely used in the textile industry due to their high stability, low cost, and color variety [115]. Chlorazol black BH is a diazo dye, the chemical

structure of this dye is illustrated in figure (1-6). Some properties of Chlorazol black BH dye are explained in the table (1-6) [116,117].
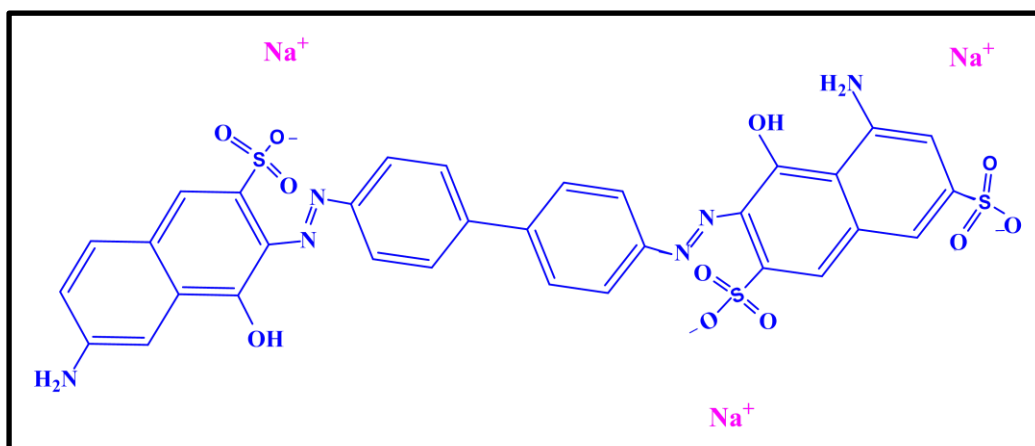
Figure (1-6). The structural formula of Chlorazol black BH dye.

Table (1-6). Some properties of chlorazol black BH dye.

Properties	
IUPAC name	Trisodium,5-amino-3-[[4-[4-[(7-amino-1-hydroxy-3-sulfonatonaphthalen-2-yl)diazenyl]phenyl]phenyl]diazenyl]-4-hydroxynaphthalene-2,7-disulfonate.
Synonym	Direct Blue 2
Molecular formula	$C_{32}H_{21}N_6Na_3O_{11}S_3$
Family sub. (class)	Azo dyes
Molecular weight	830.71 g mol^{-1}
λ$_{max}$	500-550 nm

1.9.2 Photocatalytic Degradation of Chlorazol Black BH Dye

The decolorization or degradation of any dye was simple in heterogeneous photocatalysts, but it was dependent on the quality and nature of the photocatalyst used in these processes, with the photo semiconductors having a strong positive charge on their particle for dye adsorption. The following equations (1-1) to (1-9) and figure (1-7) were used to carry out the dye adsorption steps under illumination [77].

21

Catalyst + BH Dye $\longrightarrow$ BH Dye- Catalyst   (1-1)

BH Dye- Catalyst + hv $\longrightarrow$ BH Dye- Catalyst* (e⁻, h⁺)   (1-2)

BH Dye- Catalyst (h⁺) + H_2O $\longrightarrow$ Catalyst - (BH Dye, HO•) + H⁺   (1-3)

BH Dye- Catalyst (h⁺) + OH⁻ $\longrightarrow$ (BH Dye, HO•)- Catalyst   (1-4)

BH Dye- Catalyst (e−) + O_2 $\longrightarrow$ (BH Dye, O_2)-Catalyst   (1-5)

(BH Dye, O2)-Catalyst + H⁺ $\longrightarrow$ (BH Dye, HOO•)-Catalyst   (1-6)

(BH Dye, HOO•) - Catalyst + H˙ $\longrightarrow$ BH Dye- Catalyst + H_2O_2 (1-7)

BH Dye- Catalyst + H_2O_2+ hv $\longrightarrow$ BH Dye- Catalyst +2 HO•   (1-8)

Or

BH Dye- Catalyst + H_2O_2+ e− $\longrightarrow$ BH Dye- Catalyst + HO• + OH⁻   (1-9)

Figure (1-7). Schematic the description of adsorption of dye on the surface of the catalyst, modification from the references [77,118].

1.10 The Aims of the Study

The aims of this project are to:

1- Prepare MoO_3 by hydrothermal method.

2- Prepare (MoO_3/TiO_2) composite.

3- Study the properties of prepared MoO_3, commercial TiO_2, and the prepared (MoO_3/TiO_2) composite by X-ray diffraction (XRD), scan electronic Microscope (SEM), Fourier-transform infrared spectroscopy (FTIR), and Band gap (Bg).

4- Investigate the photocatalytic activity for the prepared MoO_3, commercial TiO_2, and (MoO_3/TiO_2) composite by studying the effect of the following parameters on a decolorized colored solution:

    a) Weight of catalyst.

    b) Temperature.

    c) Initial pH of the solution.

Chapter Two
Experimental

2.1 Chemicals

All of the chemicals used in this project were utilized without being purified in any way as shown in tables (2-1) A and B.

Table (2-1) A. Used liquid chemicals.

No.	Chemicals	Company Supplied	Percentage
1.	Absolute ethanol (C_2H_5OH)	Chem.lab, Belgium.	(100) %
2.	Hydrochloric acid (HCl)	J.K. Baker, Netherlands.	(36.5,38.0) %
3.	Sulphuric acid (H_2SO_4)	CDH, India	(97.98) %

Table (2-1) B. Used solid chemicals

No.	Chemicals	Company Supplied	Purity
1.	1,10- Phenanthroline ($C_{12}H_8N_2$)	Ridel-De-Haen AG, Seelze, Hannover, Germany.	(99.98) %
2.	Chlorazol black BH dye ($C_{32}H_{21}N_6Na_3O_{11}S_3$)	Merck, Germany	(99.98) %
3.	Iron (III)sulfate hydrate ($Fe_2(SO_4)_3.H_2O$)	Evans, Mf-Dica, England	(99.98) %
4.	Potassium oxalate ($K_2C_2O_4.H_2O$)	Riedel-De-Haen AG, Seelze, Hannover, Germany.	(99.98) %
5.	Sodium hydroxide (NaOH)	Sigma Chemical Company, USA	(99.98) %
6.	Sodium molybdate ($Na_2MoO_4.2H_2O$)	Merck, Germany	(99.98) %
7.	Titanium dioxide (TiO_2)	Riedel-De-Haen AG, Seelze, Hannover, Germany	(99.98) %

2.2 Instruments

Table (2-2) shows the instruments used in this study as well as the companies and places.

Table (2-2): Employed Instruments.

No.	Instrument	Company	Place
1.	Centrifuge	Hettich- Universal II-Germany	University of Kerbala, Science college
2.	Digital pH meter	OAICTON-2100, Singapore	University of Kerbala, Science college
3.	Double -beam-UV-Visible spectrophotometer	AA-1800, Shimadzu, Japan.	University of Kerbala, Science college
4.	Fourier-transform infrared spectroscopy (FTIR)	FT-IR-8400S, Shimadzu, Japan	University of Kerbala, Science college
5.	High-Pressure Mercury Lamp -UV (A) (400W)	Rudium, China.	University of Kerbala, Science college
6.	Hotplate Magnetic Stirrer	Heido-MrHei-Standard, Germany	University of Kerbala, Science college
7.	Oven	Memmert, Germany	University of Kerbala, Science college
8.	Scan Electron Microscopy (SEM)	FESEM FEI Nova Nano SEM 450 device	University of Tehran
9.	Sensitive balance	BL 210 S, Sartorius-Germany	University of Kerbala, Science college.
10.	Spectrophotometer	Spectro SC, LaboMed, Inc	University of Kerbala, Science college
11.	Steeliness steel Teflon tube autoclave	TOPT-HP100 TOPTION UK	University of Kerbala, Science college
12.	Ultrasonic	DAIHAN Scientific, Korea.	University of Kerbala, Science college.
13.	X-Ray Diffraction	Rigaku Ultima IV	University of Tehran.

2.3 Photocatalytic Reactor Set

Figure (2-1) depicts the photocatalytic reactor unit that was used to conduct all photo experiments.
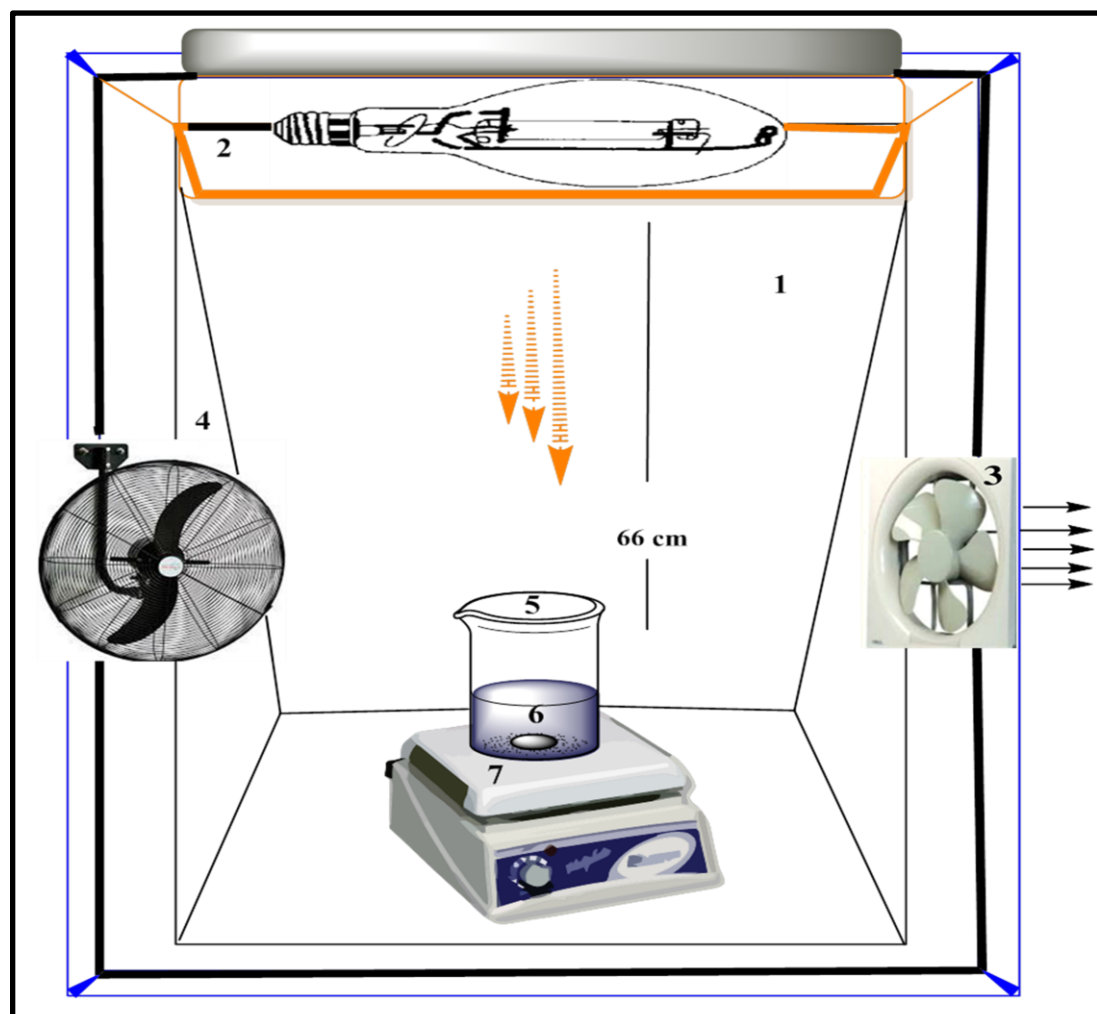
Figure (2-1). Homemade photoreactor. Where: wooden box (1), High-pressure mercury lamp (400 W) (2), Vacuum fan (3), Fan (4), Pyrex glass beaker 400 cm^3 (5), Teflon bar (6), Magnetic stirrer (7).

2.4 Preparation of MoO$_3$ Nanoparticles

MoO$_3$ nanoparticles had been prepared via the modified hydrothermal method in references [54,119], which is briefly explained as follows:

The (0.28 g) of sodium molybdate (Na$_2$MoO$_4$.2H$_2$O) was dissolved in 68 mL of distilled water, and then 7 mL of 2M of hydrochloric acid (HCl) was dropped by drop added to the solution with continuous stirring for 15 minutes. The faint yellow solution was transferred to a Teflon-lined stainless autoclave (100 mL capacity) as shown in figure (2-2 a).

Hydrothermal reactions were performed at 180 ℃ for 5 h, and then it was cooled at room temperature. The solid product was filtered and washed with distilled water and ethanol to remove impurities and non-reactive materials. The bluish-gray product was allowed to dry in an oven at 80℃ for 1 h and then dried overnight in a desiccator. Figure (2-2 b) illustrates the bluish-gray product. The chemical equations of MoO$_3$ preparation were followed below.

$$Na_2MoO_4.2H_2O + 2HCl \rightarrow H_2MoO_4 + 2NaCl + 2H_2O \qquad (1)$$

$$H_2MoO_4 \rightarrow MoO_3 + 2H_2O \qquad (2)$$

(a)　　　　　　　　　　　　　　　　　(b)
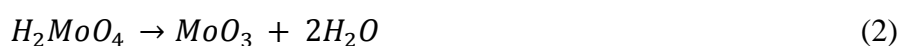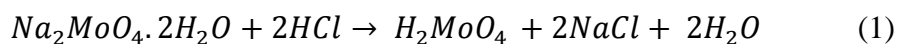
Figure (2-2).　The real image for used steeliness steel Teflon tube autoclave (a), the real image for produced bluish-gray MoO$_3$ (b).

2.5　Ultrasonic Synthesis of MoO$_3$/TiO$_2$ Nanocomposite

Ultrasonic is recognized as one of the most environmentally and friendly technology in the field of green chemistry.

The ratio 0.025% of (MoO$_3$/TiO$_2$) nanocomposite was synthesized using ultrasonic waves to give a suitable energy to bind both metal oxides. Figure (2-3) illustrates the steps for the synthesis of (MoO$_3$/TiO$_2$) nanocomposite.
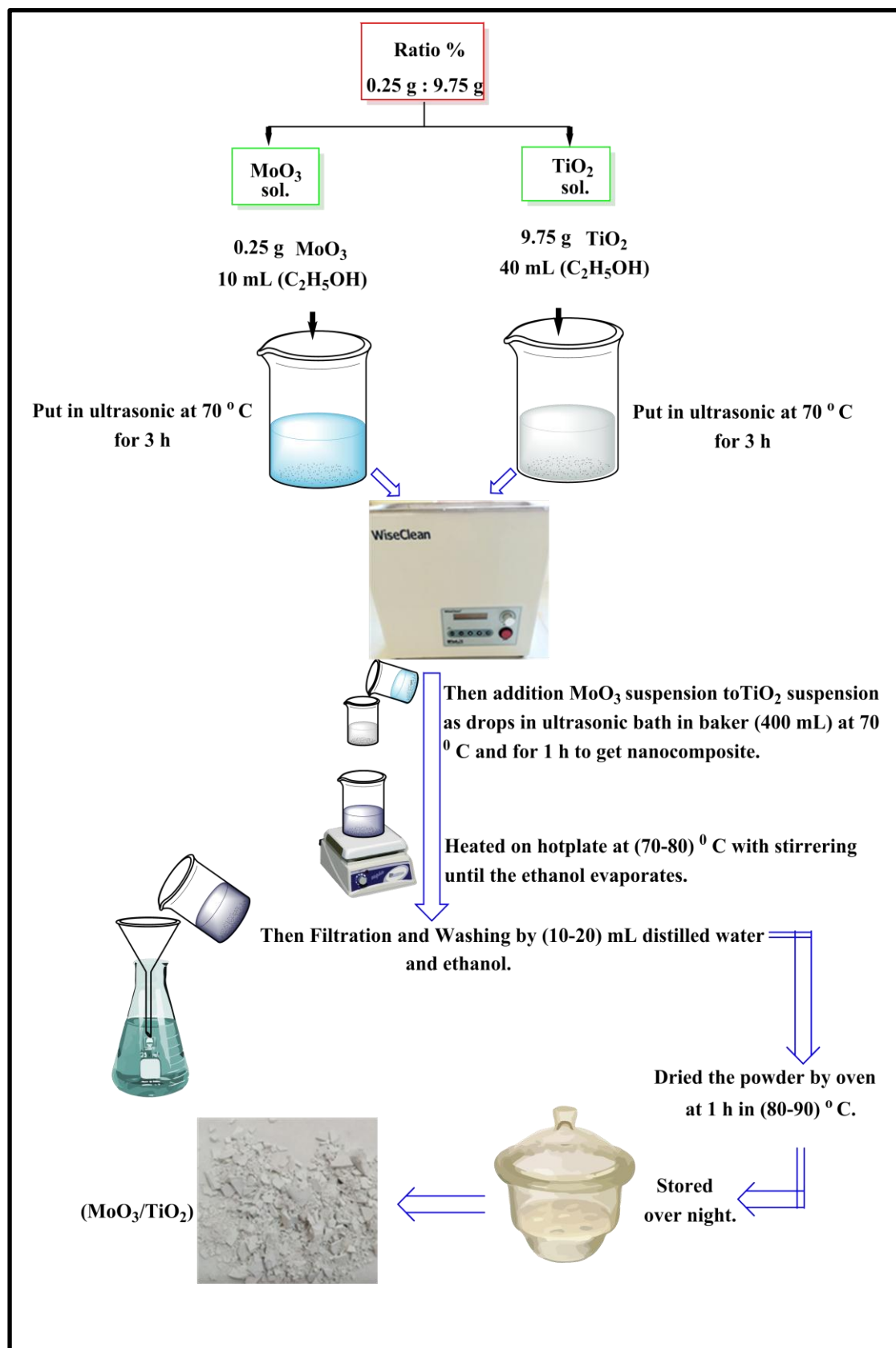
Figure (2-3).The schematic diagram for steps of prepared (MoO₃/TiO₂) nanocomposite.

2.6 Characterization

2.6.1 X-Ray Diffraction Patterns (XRD)

Photocatalysts are mostly inorganic solid materials that are typically crystals and the crystalline form is often determined by an X-ray diffraction (XRD) pattern [120]. XRD is considered a good tool to determine the essence of the crystalline and components of crystal substances as a thin layer of crystal or as powder form. Since, based on the quantity of the respective crystalline substance, the power of a diffracted beam contributes to the ability to use the XRD data to calculate the mean crystallite size (L) employing Scherrer's equation [121].

$$L = \frac{k\,\lambda}{\beta\cos\theta} \qquad\qquad\qquad\qquad (2.1)$$

Here: k is the Scherrer's dimensionless shape constant (used 0.89 for nanobelts shape, and 0.94 for spherical shape), λ is the wavelength of Cu kα (used 0.15406 nm), 2θ a Bragg diffraction angle and β is (FWHM) the full width of half-maximum intensity in degrees, which must convert to radians by multiplying it by (π/180).

2.6.2 Scanning Electron Microscopy (SEM)

The shape and surface characteristics of the nanostructures for the photocatalysts were analyzed using scanning electron microscopy. Measurements were made using the FESEM FEI Nova Nano SEM 450 device at the University of Tehran/Islamic Republic of Iran.

2.6.3 FT-IR Spectra

The infrared spectrum was measured at wavelengths ranging from 400 to 4000 cm^{-1} for all samples (TiO_2, MoO_3, and MoO_3/TiO_2). Potassium bromide (KBr) was used to make a tablet of both of these compounds after it was grinding it well.

2.6.4 Band Gap Energy Measurements

Using from UV- Visible spectrophotometer, direct and indirect band gap energy was calculated in (eV) to determine the absorbance coefficient (α) from absorbance (A) and thickness (t) for all samples based on the equation (2.2). And by using the Tauc equation (2.3) [122,123].

$$\alpha = 2.3026 \; x \; \frac{A}{t} \tag{2.2}$$

$$\alpha h v = A(h v - E_g)^{\frac{1}{m}} \tag{2.3}$$

Here: h is Plank's constant that equal (6.63 x 10^{-34} joule sec), v is the frequency of the light is equal to (C/ λ), here, C is a light speed that equal to 2.998 x 10^8 ms^{-1}, *A* is optical constant, m is constantly equal to ½ for direct transition or 2 for indirect transition.

2.7 Light Intensity Measurements

Employing a chemical actinometric method [124], the intensity of the light (I_o) for the UV-A light source was done. This method was carried out by employing 100 mL of actinometric solution, which contained from (40 mL of 0.15 M), of $Fe_2(SO_4)_3.H_2O$ mixed with (50mL of 0.45M) of $K_2C_2O_4.H_2O$ and (10 mL of 0.05M) of H_2SO_4 in photocatalytic reactor then irradiation under presence atmospheric

oxygen. The yellowish-green solution was produced as $K_3[Fe(C_2O_4)_3].H_2O$ complex under irradiation.

In order to find the light intensity, over must analyze this actinometric complex by taken about 3 mL of irradiated solution with regular periods at (5, 10, and 15) min and centrifuged (4000 rpm, in 10 min). Exact 2.5 mL of filtered solutions were added to 0.5 mL of (1%) from 1, 10- phenanthroline. The reddish-orange complex was obtained immediately, the absorption of this colored solution was recorded at 510 nm.

The following equations below explain a summary of the processes and reactions that happened [125].

$$[Fe^{3+}[(C_2O_4)_3]^{3-} + h\nu \longrightarrow [Fe^{2+}(C_2O_4)_2]^{2-} + C_2O_4^{\cdot-} \tag{2.4}$$

$$[Fe^{3+}[(C_2O_4)_3]^{3-} + h\nu \longrightarrow Fe^{2+} + 2(C_2O_4)^{2-} + C_2O_4^{\cdot-} \tag{2.5}$$

$$[Fe^{3+}(C_2O_4)_3]^{3-} + C_2O_4^{\cdot-} \longrightarrow [Fe^{2+}(C_2O_4)_2]^{2-} + C_2O_4^{\cdot-} + 2CO_2 \tag{2.6}$$

$$2[Fe^{3+}(C_2O_4)_3]^{3-} \longrightarrow 2[Fe^{2+}(C_2O_4)_2]^{2-} + C_2O_4^{2-} + 2CO_2 \tag{2.7}$$
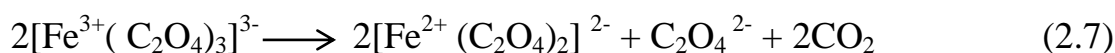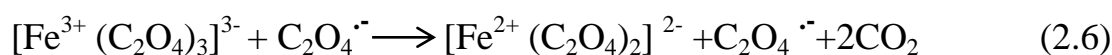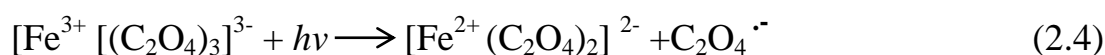
And the following equations were calculated the light intensity (I_o) [126]:

$$\text{Moles of } Fe^{2+} = \frac{V_1 \times V_3 \times A_{(510nm)}}{V_2 \times l \times \varepsilon_{(510nm)} \times 10^3} \tag{2.8}$$

$$I_o = \frac{\text{moles of } Fe^{+2}}{\Phi_\lambda \times t} \tag{2.9}$$

$I_o = 2.95 \times 10^{-7}$ Enstine s^{-1}

Here: $V_1 = 100$ cm^3 is the total of irradiation volume, $V_3 = 3$ cm^3 is summation of the irradiation solution volume (2.5 mL) that added to (0.5 mL) from 1, 10-phenonethroline solution, $V_2 = 2.5$ cm^3 is volume of irradiation solution, l is the optical path length (1 cm), A_{510} is the average absorbance of ferrioxalate solution after different internals irradiation

time, that mixed with 1,10-phenonethroline, (molar absorptivity $\varepsilon = 1.045$ x 10^4 L mol^{-1} cm^{-1}) , $(\Phi\lambda = 1.2)$ is the quantum yield and (t) is the average of irradiation time (10 min).

2.8 Calibration Curve of Chlorazol Black BH Dye

Calibration Curve for Chlorazol black BH dyes was performed by preparing series standard concentrations within the range (1-50) ppm of the chlorazol black BH dye solution. The absorbance for these concentrations was recorded at the wavelength (501 nm) that found after scan the dye solution from range 200-800 nm, according to figure (2-4). The results of table (2-3) were drawn between absorption and concentration as explained in figure (2-5)
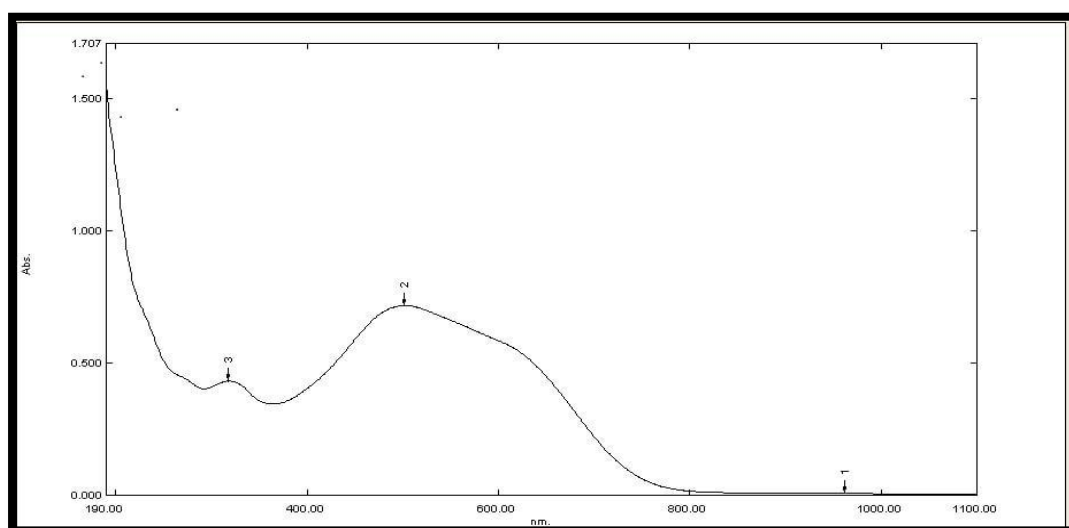
Figure (2-4). The Scan of Chlorazol black BH dye solution.

Table (2-3). Calibration Curve Data of Chlorazol black BH dye.

C/ppm	Abs.
1	0.018
5	0.075
10	0.165
15	0.231
20	0.269
25	0.362
30	0.424
40	0.644
50	0.790
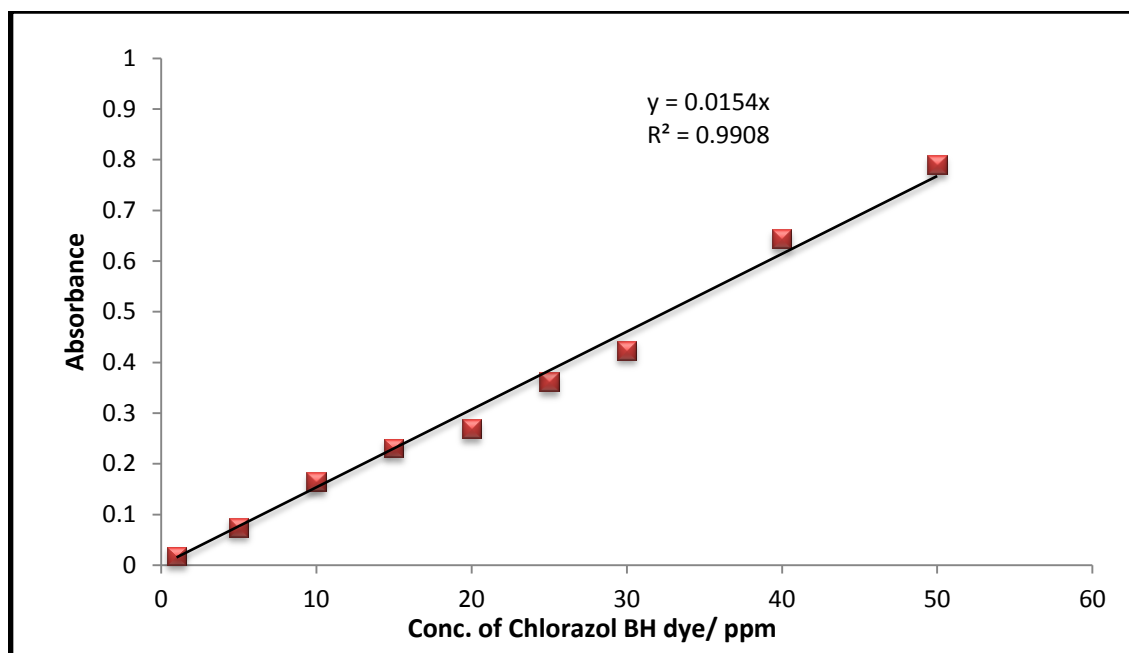
Figure (2-5). Calibration curve at different concentrations of Chlorazol BH black dye.

2.9 Photocatalytic Decolorization Reaction of Chlorazol Black BH Dye

The photocatalysts that were prepared (MoO_3, MoO_3/TiO_2) and commercial (TiO_2) were applied experimentally. These experiments were conducted using a high-pressure mercury lamp (400 Watt, λ=365 nm) as a source of UV-A radiation in the photo-reactor unit. The suspension solutions were prepared by adding 50 ppm of 100 mL Chlorazol BH dye solution to the quantity of photocatalysts. Suspensions were stirred in darkness for 30 min before irradiation using a magnetic stirrer to maintain adsorption equilibrium. The formed suspension was periodically irradiated with light intensity (2.95×10^{-7} enstine s^{-1}) by UV-A light. Using a syringe approximately 4 mL was removed and then doubled separately with a centrifuge for 15 min at 5000 rpm to ensure the removal of all fine parts of the photocatalyst.

The absorption of producing filter was read at 500 nm. Depending on the dye calibration curve in figure (2.5), the dye concentrations before irradiation (C_o) and after irradiation (C_t) were identified. The Langmuir-Hinshelwood model is a good express which utilized to determine the apparent reaction rate constant ($k_{app.}$) at low concentration of dye with intervals time (t) as shown in equation (2.10) [127]. A plot of $\ln(C_o/C_t)$ versus (t) will yield a slope as a value of k_{app}.

$$\ln\left(\frac{C_o}{C_t}\right) = k_{app}t \tag{2.10}$$

The (PDE %) is the efficiency of the photocatalytic decolorization percentage was calculated from equation (2.11) [128].

$$PDE \% = \frac{(C_o - C_t)}{C_o} \times 100 \tag{2.11}$$

2.10 Activation Energy

The apparent activation energy (Ea) of decolorization for chlorazol black BH dye was detected in the temperature range (283.15- 298.15) K and based on the plotted Arrhenius equitation (2.12) [129].

$$\ln k_{app} = \frac{-E_a}{RT} + \ln A \tag{2.12}$$

Here: k_{app} is an apparent constant rate, T is the reaction temperature, R is a constant gas equal (8.314 J mol^{-1} K^{-1}) and A is a frequency constant.

2.11 Thermodynamic Parameters

Thermodynamic parameters have played a significant role in determining the direction of the reaction. From the Eyring equation (2.13) can be calculated the enthalpy change ($\Delta H^{\#}$) and entropy change ($\Delta S^{\#}$) values [130].

$$\ln\left(\frac{K_{app}}{T}\right) = \frac{-\Delta H^{\#}}{RT} + \left(\ln\left(\frac{K_B}{h}\right) + \frac{\Delta S^{\#}}{R}\right) \tag{2.13}$$

Here: k_{app} is an apparent rate constant, T is the temperature of the reaction, k_B is Boltzmann's constant equal (1.381×10^{-23} J K^{-1}), R is gas constant equal (8.314 J mol^{-1} K^{-1}) and h is Plank's constant equal (6.63×10^{-34} J s).

Using the Gibbs equation (2.14) the free energy ($\Delta G^{\#}$) was calculated [131].

$$\Delta G^{\#} = \Delta H^{\#} - T\Delta S^{\#} \tag{2.14}$$

Chapter Three
Results and Discussion

3.1 Characterization of photocatalysts

In this project, the characterizations of studied samples were measured using XRD, SEM, FTIR technique, and Bandgap (Bg) measurements.

3.1.1 X-ray Diffraction patterns (XRD)

The proper crystal structure is very important for the photocatalyst, and XRD is one of the most effective techniques for determining the molecular structure of a crystal. All the prepared and commercial samples of MoO_3, MoO_3-TiO_2, and TiO_2 were analyzed by XRD as shown in figure (3-1). Based on the results of the XRD, the synthesized MoO_3 was found to be an orthorhombic (α-MoO_3) and complies with the standard diffraction data of α-MoO_3 (JCPDS Card No. 005-0508) [132]. The essential diffraction peaks of orthorhombic α-MoO_3 demonstrated at (2θ) 12.80◦, 25.76◦, 27.35◦, 39.059◦, 58.906◦, and 67.630◦ with miller indicates (0 2 0), (0 4 0), (021), (0 6 0), (0 8 1) and (0 10 0) planes respectively [137, 138]. Indeed, the stronger intensities at 2θ for 12.8^o, $25.7^{o,}$ and 39.0^o with reflection peaks (0 k 0), where k is 2, 4, 6, are confirmed that the synthesis α-MoO_3 is being as nanobelts [133].

Furthermore, the rutile-TiO_2 peaks appeared at diffractions (110), (101), (111), (211), (220) and (301) at 2θ positions are 27.46°, 36.10°, 41.26°, 54.34°, 56.32°, and 69.02° respectively, and these magnitudes are in agreement with the standard diffraction data (JCDS card No.00-021-1276) [134,135].

The main peaks are shifted to the high 2θ from 27.358º (α-MoO_3) and 27.475º (TiO_2) to 27.480º, from 36.118º (TiO_2) to 36.122º, from 39.059º (α-MoO_3) to 39.230º, 41.279º (TiO_2) to 41.287º, during the incorporation between α-MoO_3 and rutile-TiO_2 as nanocomposite.
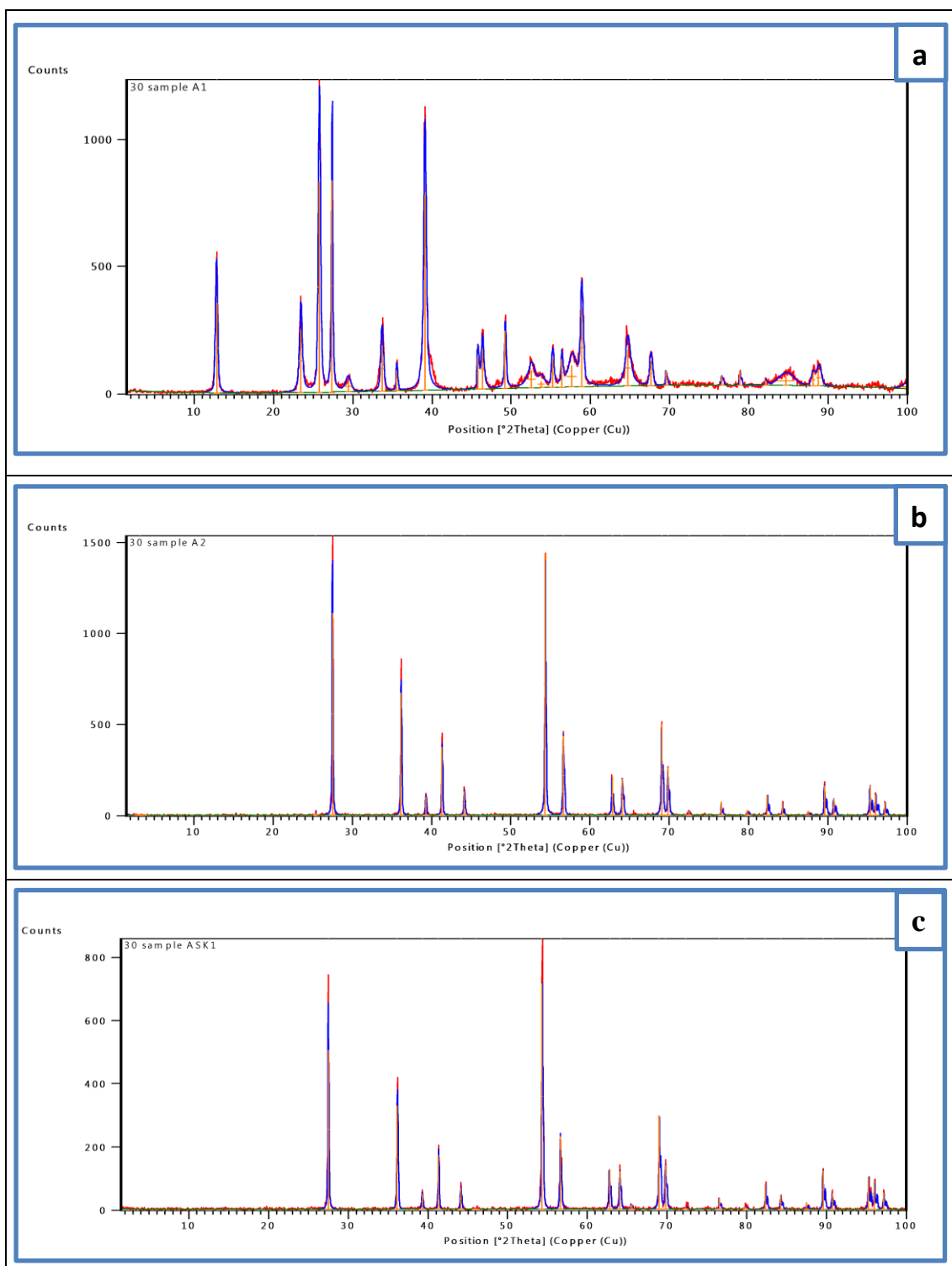
Figure (3-1). The XRD patterns of samples α-MoO$_3$ (a), TiO$_2$ (b), and α-MoO$_3$/TiO$_2$ nanocomposite (c).

That attitude generates a metallic bond between two metals Mo and Ti [136-138]. Since both Mo and Ti have a coordination number equal to 6 [139], and the Mo ion is smaller than Ti, with an ionic radius 0.59 Å and 0.67 Å, respectively [140,141], hence, the Mo^{6+} is appropriate to incorporate with Ti^{4+} in crystal. Depending on the XRD data, the mean crystallite sizes (L) in nm were calculated using Scherrer's equation (2-1), and the results are shown in table (3-1).

The mean crystal size of α-MoO_3 elevates with incorporation with rutile- TiO_2 from 30. 5511 nm to 57.6063 nm, that due to the mean crystal size of rutile- TiO_2 is large than the mean crystal size value of α-MoO_3.

Table (3-1). The values of mean crystal sizes (L) for the samples synthesis α-MoO_3, α-MoO_3/TiO_2 nanocomposite, and commercial TiO_2.

Samples	α-MoO_3	TiO_2	α-MoO_3/TiO_2
Mean Crystal sizes (from XRD data) / nm	**30.5511**	**72.3799**	**57.6063**

3.1.2 Scan Electron Microscopy (SEM)

Scan electron microscopy (SEM) is intended to characterize physically apparent properties such as morphology of size and shape for macromaterials and nanomaterials. SEM images for α-MoO$_3$, TiO$_2$, and α-MoO$_3$/TiO$_2$ nanocomposite, were obtained from the micro and nanoscale levels and shown in Figures from (3.2) to figure (3-4).
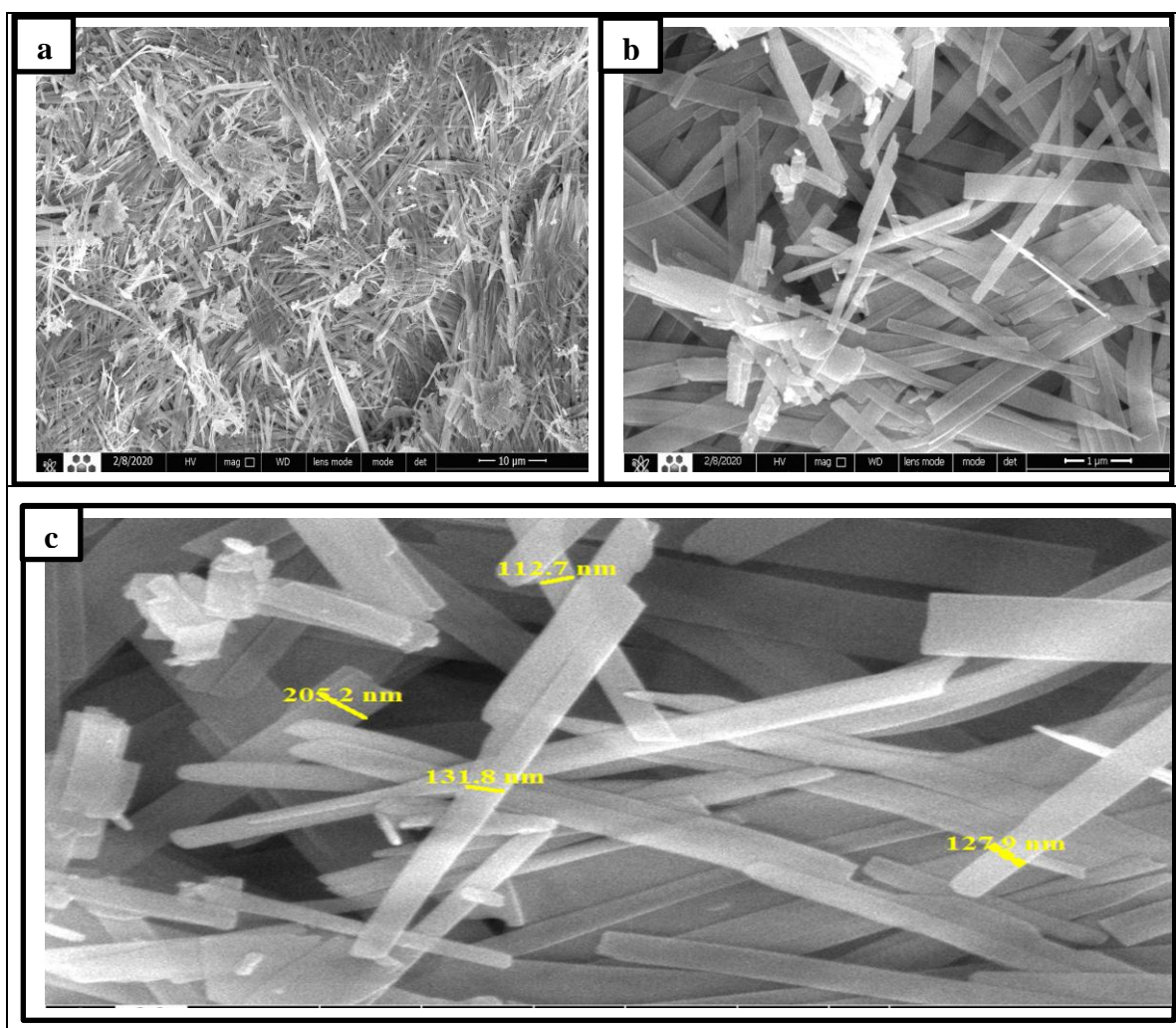
Figure (3-2). SEM images of synthesis α-MoO$_3$, a) the overall product, b) a magnified region of the surface structure, c) more magnified to appear nanobelts shape.

Figure (3-2) is displaying the synthesis of regular α-MoO$_3$, and the shape found to be nanobelts at various magnifications, this result is in agreement with the result in XRD analysis and literature works [132,133,142]. Figure (3-2) a, depicts nanobelts with widths ranging from (112.7, 127.9, 131.8, to 205.2) nm and length of the range (1-10) μm. The

39

produced nanobelts are rectangular flat tips, smooth surfaces distribute densely and uniformly with four sharp corners on the upper ends and are straight, the nanobelts surfaces, as well as the sharp edges, are encased in smooth facets [143,144].
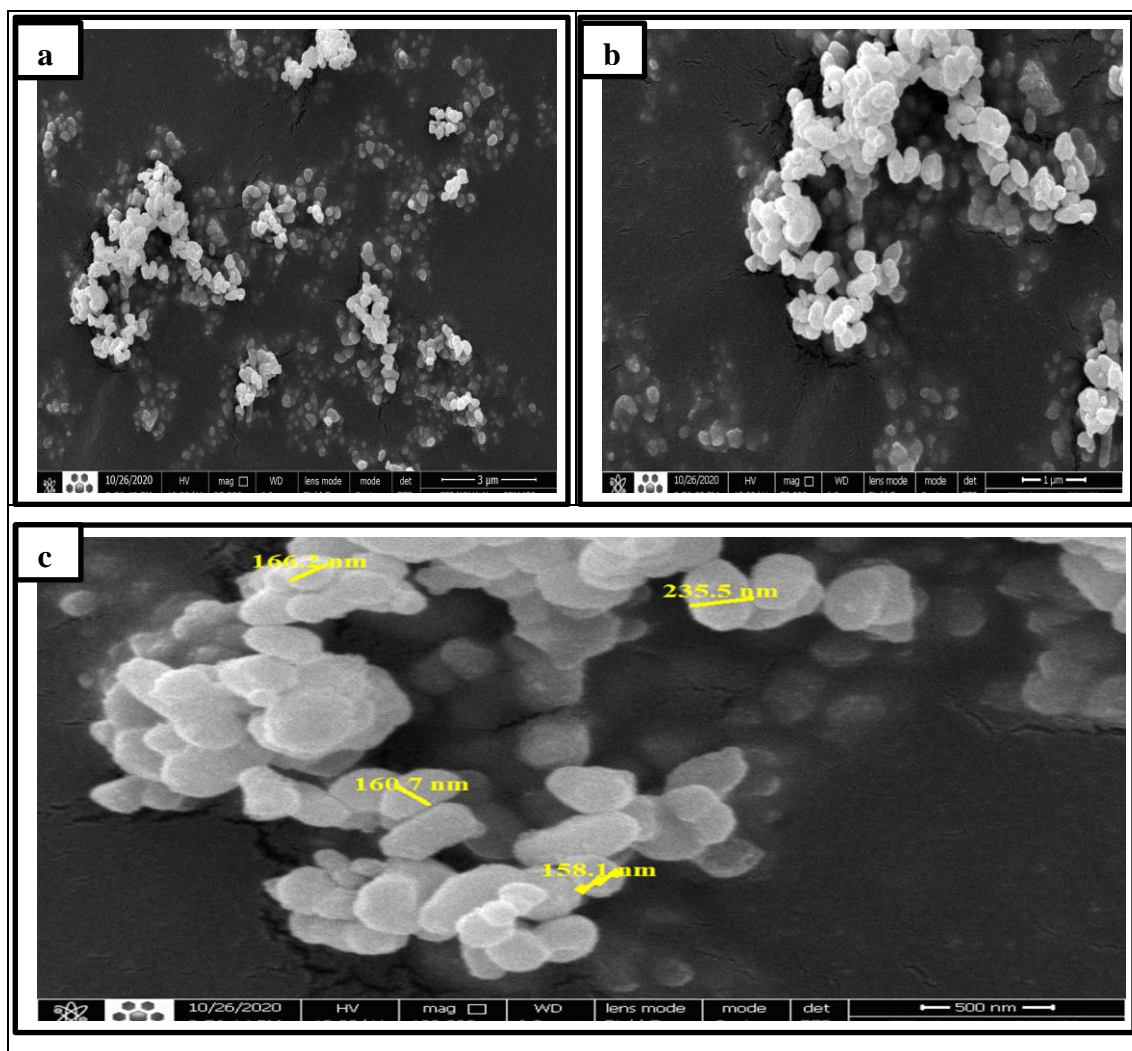
Figure (3-3). SEM images of commercial TiO$_2$, a) the overall product, b) a magnified region of the surface structure, c) more magnified to appear spherical shape.

Rutile-TiO$_2$ and synthesized α-MoO$_3$/TiO$_2$ nanocomposite have a semi-spherical and semi-spherical agglomerate shape respectively; because the amount of TiO$_2$ is very high compared to the amount of α-MoO$_3$ that leads to increase the lightness of α-MoO$_3$ [145]. Figures (3-3) and (3-4) indicate that the spheres exhibit a wide range of widths, ranging from 150 to 250 nm, and the length ranging from 1-5 μm for TiO$_2$ (micro-sized) and its nanocomposite. The surface of TiO$_2$ and α-MoO$_3$/TiO$_2$ nanocomposite appears to have a uniform distribution of semi-spherical

particles with crystal as the structure, these semi-spheres had relatively smooth surfaces. The partial sizes of α-MoO$_3$ and its nanocomposite are not in nano-size that refers to the poly-crystal. TiO$_2$ is a commercial material with a micro-size.
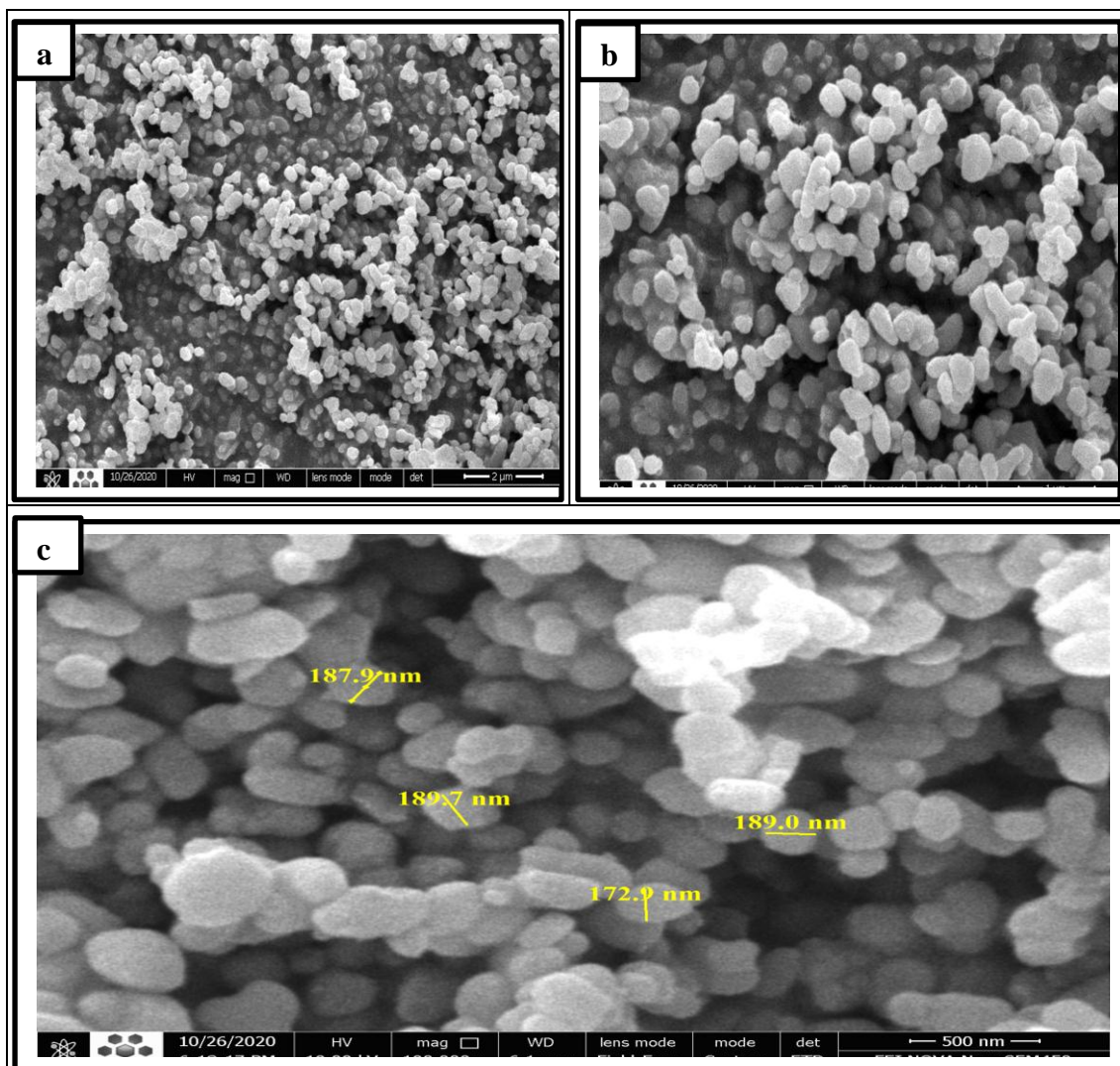
Figure (3-4). SEM images of synthesis α-MoO$_3$/TiO$_2$ nanocomposite, a) the overall product, b) a magnified region of the surface structure, c) more magnified to appear spherical shape.

3.1.3 Fourier-transform Infrared Spectroscopy (FTIR)

The FTIR technique was used to investigate the characterization of samples that using as photocatalysts (prepared α-MoO$_3$, α-MoO$_3$/TiO$_2$ nanocomposite, and commercial TiO$_2$) in this work.

Figure (3-5) shows the synthesized α-MoO$_3$ displays many distinct peaks at certain frequencies, as the three strong peaks appear: at a frequency of 995 cm^{-1} sharp associated with Mo=O stretching vibration an indicator of the layered orthorhombic α-MoO$_3$ phase, the sharp peak also occurs at 866 cm^{-1} that beyond to the stretching mode of oxygen in Mo-O-Mo bonds, and the last appears as broadband at 557 cm^{-1}, which due to the bending vibration of oxygen atom linked to three metal atoms. Moreover, at 588 cm^{-1} the band is the result of the α-MoO$_3$ single bond. The bands at 1626 cm^{-1} and 3356 cm^{-1} were attributed to the stretching and bending of O-H groups of adsorbed water on the surface synthesized α-MoO$_3$ due to the adsorption of H$_2$O from the environment [142, 146].
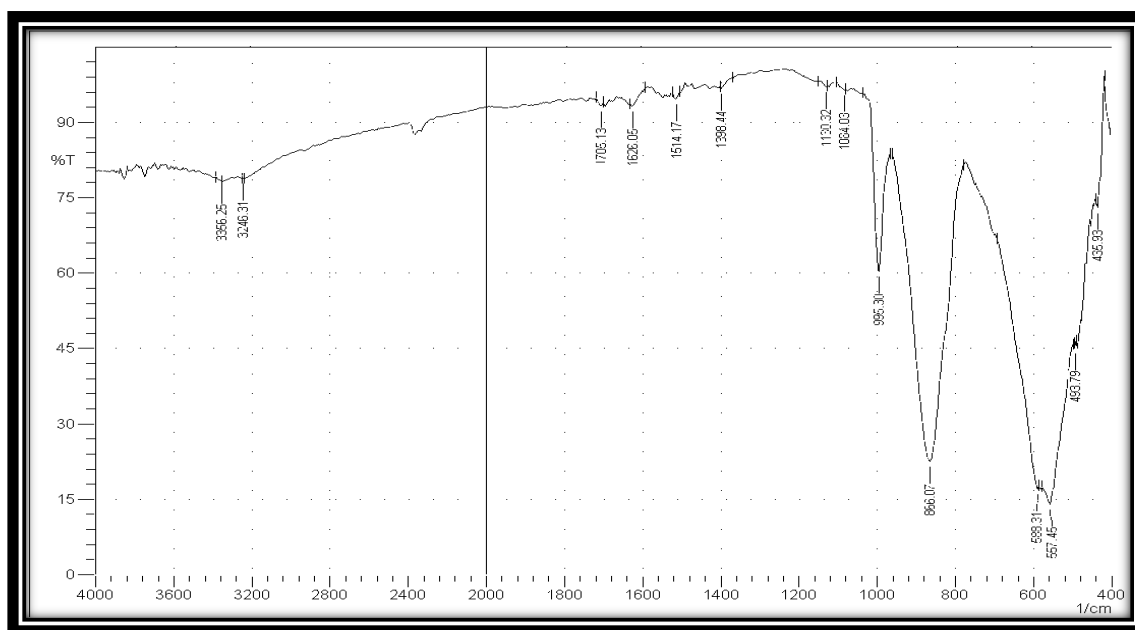
Figure (3-5). Spectrum (FTIR) of synthesis α-MoO$_3$.

Figure (3-6) explains the spectrum of the commercial rutile-TiO$_2$ that appears in the bands at 3429 cm^{-1} and 1653 cm^{-1}, which are attitudes to the stretching and bending modes of the O-H bond of absorption water molecular as moisture. The peak at 675 cm^{-1} beyond the Ti-O stretching, this band is regarded TiO$_2$ characteristic peak. Besides, the band at 597 cm^{-1} related to the Ti-O-Ti stretching vibration [147].
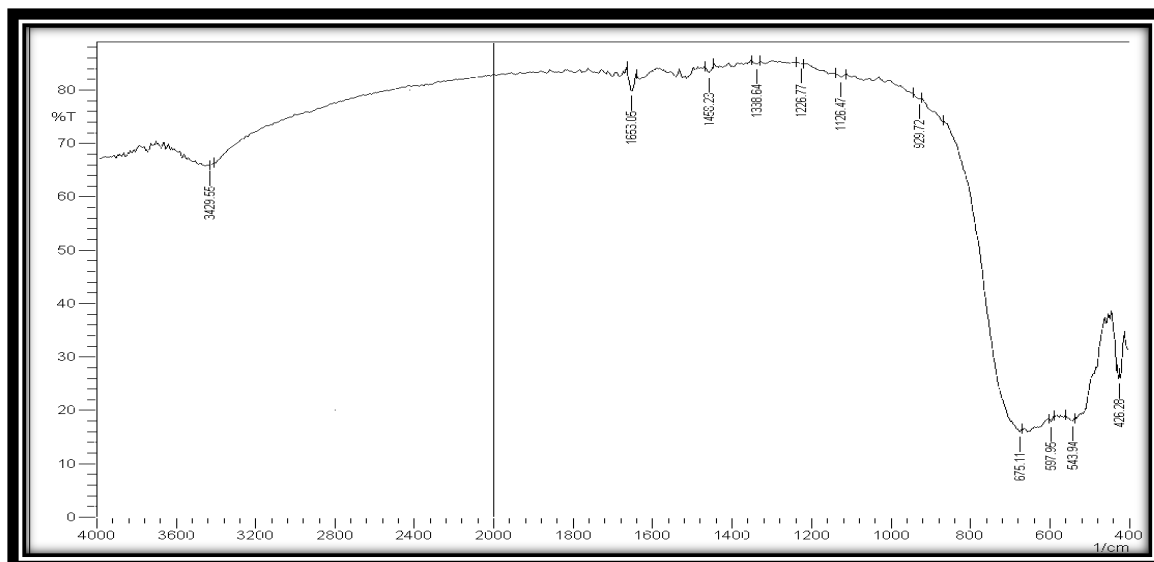
Figure (3-6). Spectrum (FTIR) of commercial TiO$_2$.

Based on Figure (3-7), the spectrum of synthesized α-MoO$_3$/TiO$_2$ nanocomposite appears the peaks at 1653 cm^{-1} and 3464 cm^{-1} related with OH group bending and stretching absorbed of water, respectively. Also, appearance the peak at 675 cm^{-1} associated with Ti-O stretching which is a characteristic peak for TiO$_2$. Besides, the peak at 559 cm^{-1} attitudes to the Mo-O single bond for α-MoO$_3$ [80].
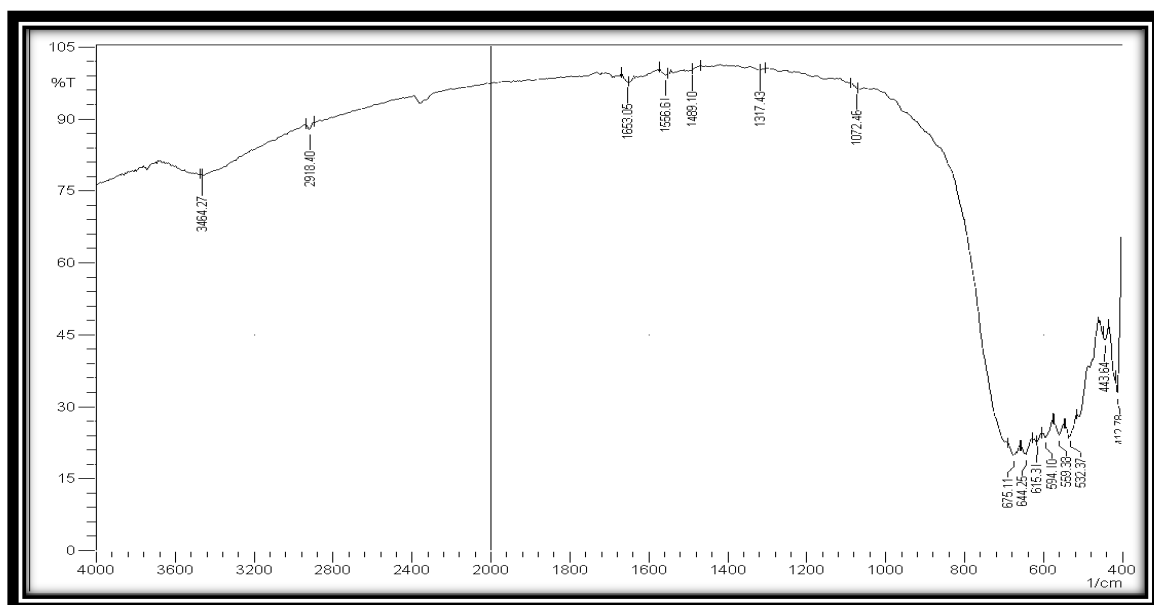
Figure (3-7). Spectrum (FTIR) of synthesis α-MoO$_3$/TiO$_2$ nanocomposite.

3.1.4 Band Gap Energy Measurements

The Tauc equation (2-3) was useful to calculate the band gap energies in eV unite that are plotted in Figures (3-8) and measured for all

samples in a table (3-2). The results of band gap energies were found that the band gap for α-MoO$_3$ is direct, while for TiO$_2$ and α-MoO$_3$/TiO$_2$ nanocomposite it is indirect.
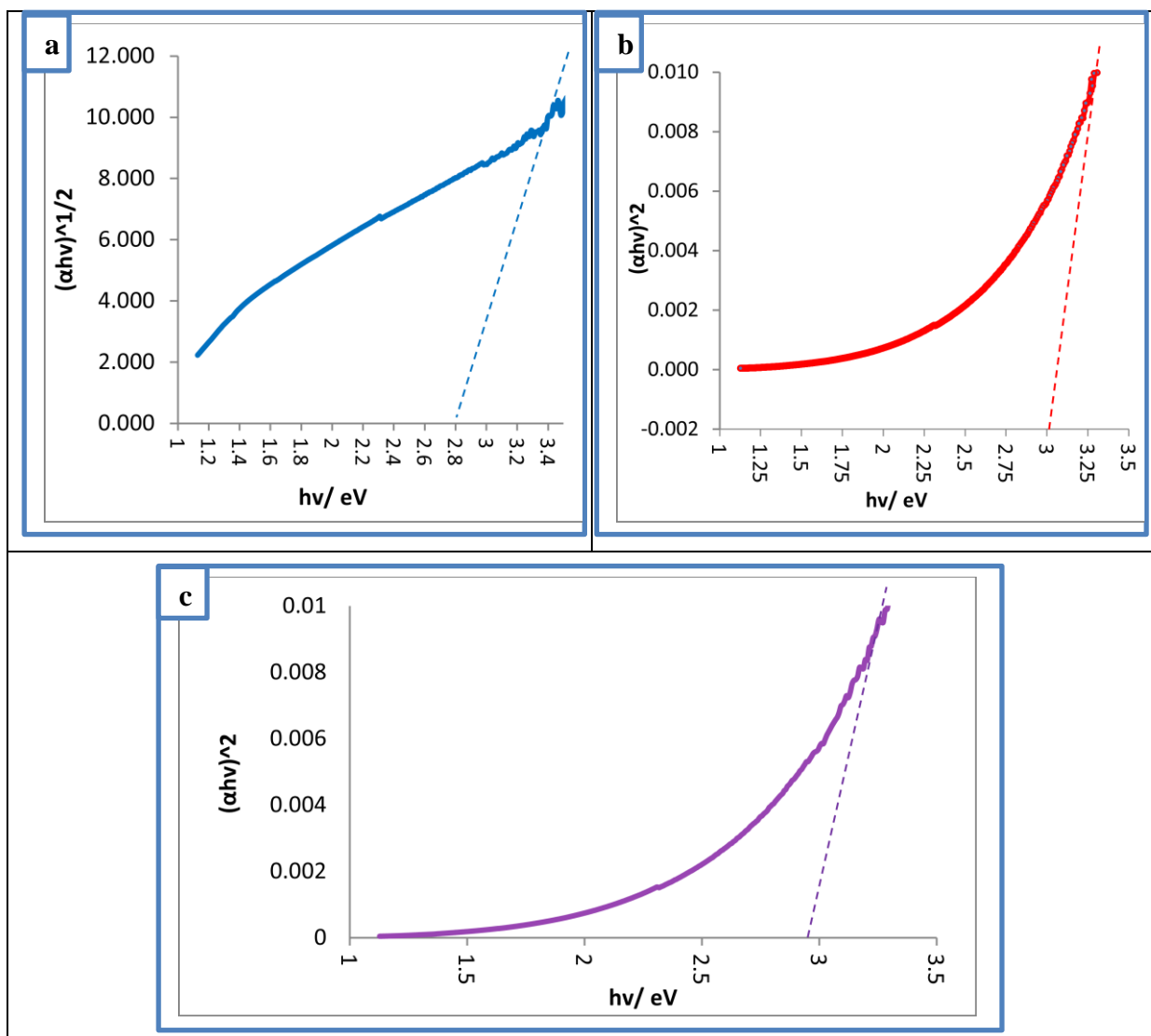
Figure (3-8). Tauc plot for a) α-MoO$_3$ as direct band gap, b) TiO$_2$ as indirect band gap, c) α-MoO$_3$/TiO$_2$ nanocomposite as indirect band gap.

Table (3-2). The band gap energies measured using UV-Visible Scan for all samples.

Sample	*α-MoO$_3$*	*TiO$_2$*	*α-MoO$_3$/TiO$_2$*
B$_g$ (eV)	**2.8**	**3.0**	**2.95**

3.2 Photocatalytic Reaction of Chlorazol Black BH Dye Decolorization

3.2.1 Primary experiments for photocatalyst samples

Initially, to determine the best photocatalyst among the prepared and commercial photocatalysts, using 50 ppm of chlorazol black BH dye, 0.1 g from all photocatalysts (TiO$_2$ commercial, prepared α-MoO$_3$, and prepared α-MoO$_3$/TiO$_2$ nanocomposite), initial pH of dye solution 7.6 at 18 ºC, and with the adsorption time at 15 min and 30 min was used, and adsorbtion time of 30 min was the best to reach the equilibrium time. And found in tables (3-3),(3-4) and figure(3-9), the fast reaction(high rate constant) and best photodecolorization efficiency for chlorazol black BH are with using prepared α-MoO$_3$/TiO$_2$ nanocomposite at 100 min equal to 0.0098 min-^{1} 56.54008 %, respectively. That attitude increases the lightness of α-MoO$_3$, and elevated the acidity of their surface after incorporated with TiO$_2$ which leads to an increase in the hydroxyl ions adsorption [134, 137], that generated under exposure to the suspension solution of photocatalysts to UV light and produce hydroxyl radicals [148, 149]. From the other side, this modification of the surface will increase the separation of charges on photocatalyst surface (electron-hole) and inhibited the recombination process [150].

Table (3-3). The Ln (C$_o$/C$_t$) of initial experiments (0.1 g) dose with (50 ppm in 100 mL D.W) solution of chlorazol black BH dye.

Time (min) \ Sample	ln(C$_o$/C$_t$)		
	TiO$_2$	α-MoO$_3$	α-MoO$_3$/TiO$_2$
0	0	0	0
10	0.050431	0.160343	0.29191
20	0.067823	0.223144	0.362115
30	0.085522	0.310155	0.457425
40	0.092691	0.351398	0.505216
50	0.129325	0.394415	0.562785
60	0.151967	0.439367	0.655876
70	0.182978	0.474458	0.705886
80	0.239673	0.554997	0.76758
90	0.260726	0.594476	0.804621
100	0.326684	0.621688	0.833331
k $_{app}$/min^{-1}	**0.0029**	**0.007**	**0.0098**

Table (3-4). The PDE % of initial experiments (0.1 g) dose with (50 ppm in 100 mL D.W) solution of chlorazol black BH dye.

Time (min) \ Sample	PDE%		
	TiO_2	α-MoO_3	α-MoO3/TiO_2
0	0	0	0
10	4.918033	14.81481	25.31646
20	6.557377	20	30.37975
30	8.196721	26.66667	36.70886
40	8.852459	29.62963	39.66245
50	12.13115	32.59259	43.03797
60	14.09836	35.55556	48.10127
70	16.72131	37.77778	50.63291
80	21.31148	42.59259	53.5865
90	22.95082	44.81481	55.27426
100	**27.86885**	**46.2963**	**56.54008**

In this work, only commercial rutile-TiO_2 and α-MoO_3/TiO_2 nanocomposite were used, with α-MoO_3 being left out, via application experiments for decolorizing of chlorazol black BH dye from aqueous solution in presence of various parameters such as (photocatalyst dose, initial pH, and temperature). Because the amount of α-MoO_3 generated by the hydrothermal method is very limited, and the time is lost due to corona (Covide 19).
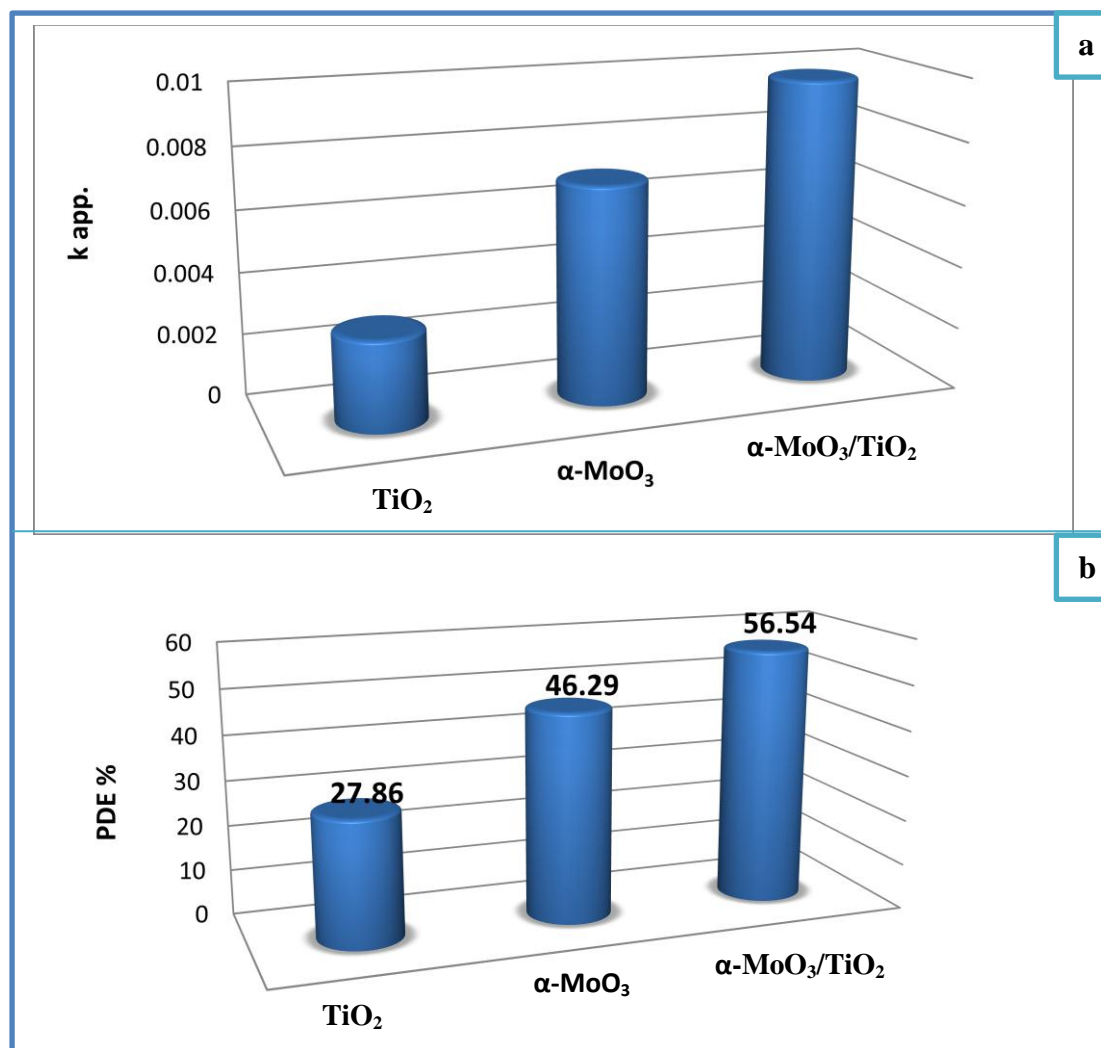
Figure (3-9). (a) The change of the k $_{app}$ with photocatalyst samples (b) Effect of samples on photodecolorization efficiency.

3.2.2 Effect of Parameters on Photocatalytic Reaction of Decolorization of Chlorazol Black BH Dye.

The effect of parameters on decolorization was done using photocatalysts TiO_2 and $\alpha\text{-}MoO_3/TiO_2$ nanocomposite.

3.2.2.1 Effect of Dose Catalyst on Dye Solution

The effect of the dose has been studied for commercial TiO_2 and the synthesized $\alpha\text{-}MoO_3/TiO_2$ nanocomposite on the photocatalytic decolorization of chlorazol black BH dye solution was performed at temperature 291.15 K and pH = 7.6 with a light intensity equal to $2.95 x 10^{-7}$ Enstine s^{-1}.

A. Effect of Dose for Commercial TiO_2 Photocatalyst on Dye solution:

This effect is necessary to determine the cost-benefit amount before and after the modification of the photocatalyst surface.

Table (3-5): The change of the Ln (C_o/C_t) with irradiation time at the different dose of commercial TiO_2 via photocatalytic decolorization of chlorazol black BH dye.

Doses (g) / Time (min)	Ln (C_o/C_t)					
	0.100	**0.200**	**0.300**	**0.400**	**0.500**	**0.600**
0	0.000	0.000	0.000	0.000	0.000	0.000
10	0.050	0.070	0.210	0.150	0.124	
20	0.067	0.176	0.451	0.239	0.315	0.133
30	0.085	0.240	0.540	0.293	-	0.470
40	0.092	0.294	0.568	-	-	-
50	0.129	0.389	-	-	1.243	-
60	0.151	0.413	1.145	-	1.618	0.693
70	0.182	0.445	1.212	0.852	1.713	0.693
80	0.239	0.453	1.597	0.997	2.001	-
90	0.260	0.478	1.682	1.220	2.224	-
100	0.326	0.495	1.851	1.508	2.512	0.980
k_{app}/ min^{-1}	0.0029	0.0059	0.0186	0.0199	**0.025**	0.0104

Table (3-6). The change of the (PDE %) with irradiation time at a different dose of commercial TiO_2 via photocatalytic decolorization of chlorazol black BH dye.

Doses (g) / Time (min)	PDE %					
	0.100	**0.200**	**0.300**	**0.400**	**0.500**	**0.600**
0	0.000	0.000	0.000	0.000	0.000	0.000
10	4.918	8.854	19.008	13.934	11.711	12.499
20	6.557	18.750	36.363	21.311	27.027	12.499
30	8.196	23.958	41.735	25.409	30.630	37.499
40	8.852	25.520	43.388	27.868	41.441	56.249
50	12.131	32.291	46.280	32.786	71.171	62.499
60	14.098	33.854	68.181	40.163	80.180	49.999
70	16.721	35.937	70.247	57.377	81.981	49.999
80	21.311	36.458	79.752	63.114	86.486	43.749
90	22.950	38.020	81.404	70.491	89.189	62.499
100	**27.868**	**39.062**	**84.297**	**77.868**	**91.891**	**62.499**
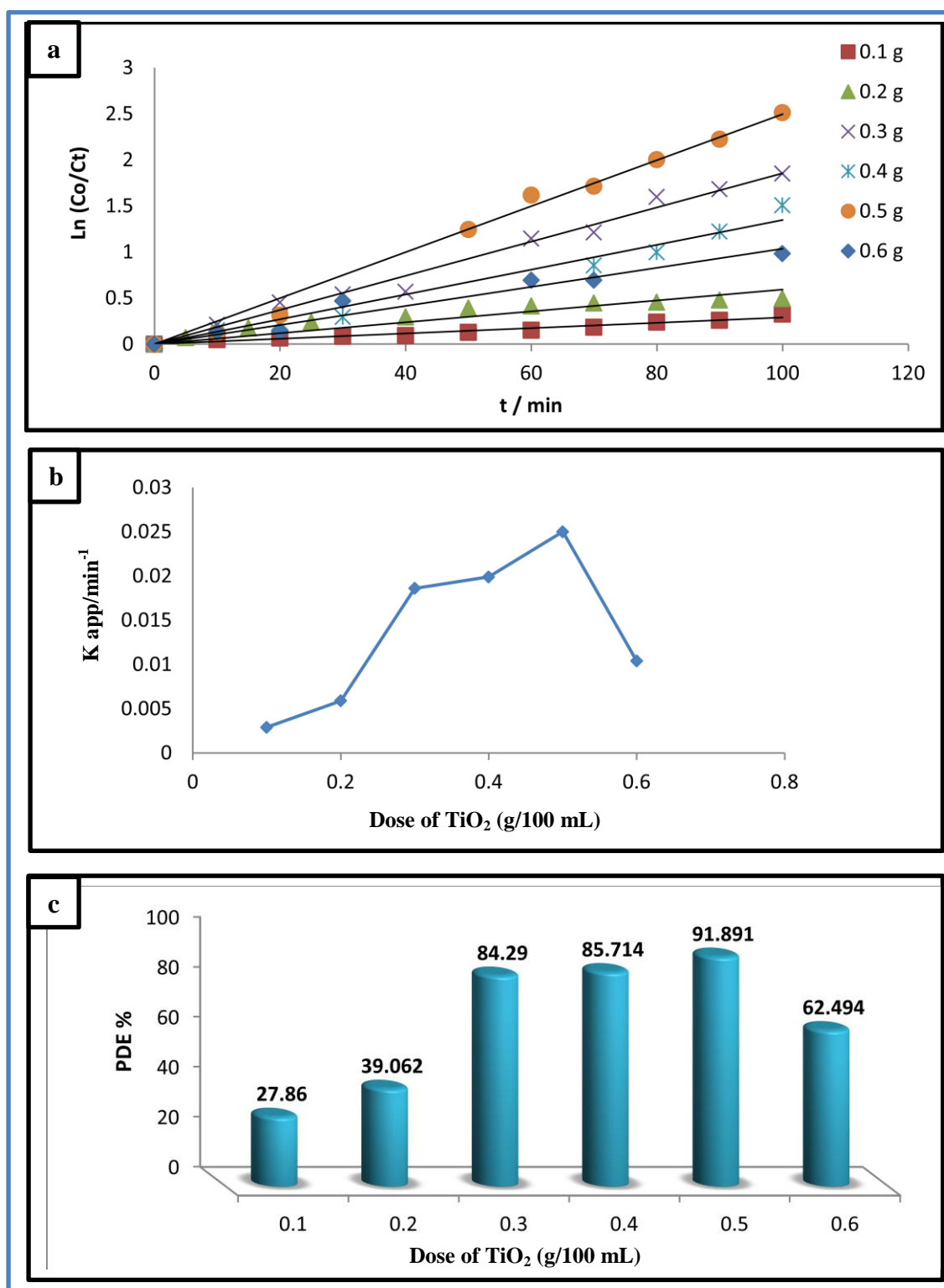
Figure (3-10). (a) The change of the Ln (C_o/C_t) with Irradiation time at a different dose of commercial TiO_2, (b) Relationship between (k app) apparent rate constant and a different dose commercial TiO_2, (c) Effect of a different dose of commercial TiO_2 on (PDE%) photodecolorization efficiency.

B. Effect of Dose for (α-MoO$_3$ /TiO$_2$) Nanocomposite Photocatalyst on Dye Solution:

Table (3-7). The change of the Ln (C$_o$/C$_t$) with irradiation time at a different dose of prepared (α-MoO$_3$/TiO$_2$) nanocomposite via photocatalytic decolorization of chlorazol black BH dye.

Doses (g) / Time (min)	Ln (C$_o$/C$_t$)					
	0.100	**0.200**	**0.300**	**0.400**	**0.500**	**0.600**
0	0.000	0.000	0.000	0.000	0.000	0.000
10	0.291	0.126	0.240	0.618	0.305	0.693
20	0.362	0.156	0.357	0.711	0.487	0.860
30	0.457	0.193	0.425	1.023	0.784	1.060
40	0.505	0.219	0.480	1.507	0.974	1.312
50	0.562	0.321	0.578	2.122	-	1.312
60	0.655	-	0.687	2.720	1.645	1.871
70	0.705	-	0.835	3.508	2.251	2.564
80	0.767	0.517	0.933	4.019	2.944	2.564
90	0.804	0.608	1.058	4.424	4.043	3.258
100	0.833	0.657	1.241	5.117	4.736	3.258
k$_{app}$/ min^{-1}	0.0098	0.0066	0.0121	**0.0483**	0.039	0.0335

Table (3-8). The change of the (PDE %) with irradiation time at a different dose of prepared (α-MoO$_3$/TiO$_2$) nanocomposite via photocatalytic decolorization of chlorazol black BH dye.

Doses (g) / Time (min)	PDE %					
	0.100	**0.200**	**0.300**	**0.400**	**0.500**	**0.600**
0	0.000	0.000	0.000	0.000	0.000	0.000
10	25.316	11.917	21.387	46.107	26.315	49.999
20	30.379	14.507	30.057	50.898	38.596	57.692
30	36.708	17.616	34.682	64.071	54.385	65.384
40	39.662	19.689	38.150	77.844	62.280	73.076
50	43.037	27.461	43.930	88.023	73.684	73.076
60	48.101	28.497	49.710	93.413	80.701	84.615
70	50.632	30.051	56.647	97.005	89.473	92.307
80	53.586	40.414	60.693	98.203	94.736	92.307
90	55.274	45.595	65.317	98.802	98.245	96.153
100	**56.540**	**48.186**	**71.098**	**99.401**	**99.122**	**96.15384**
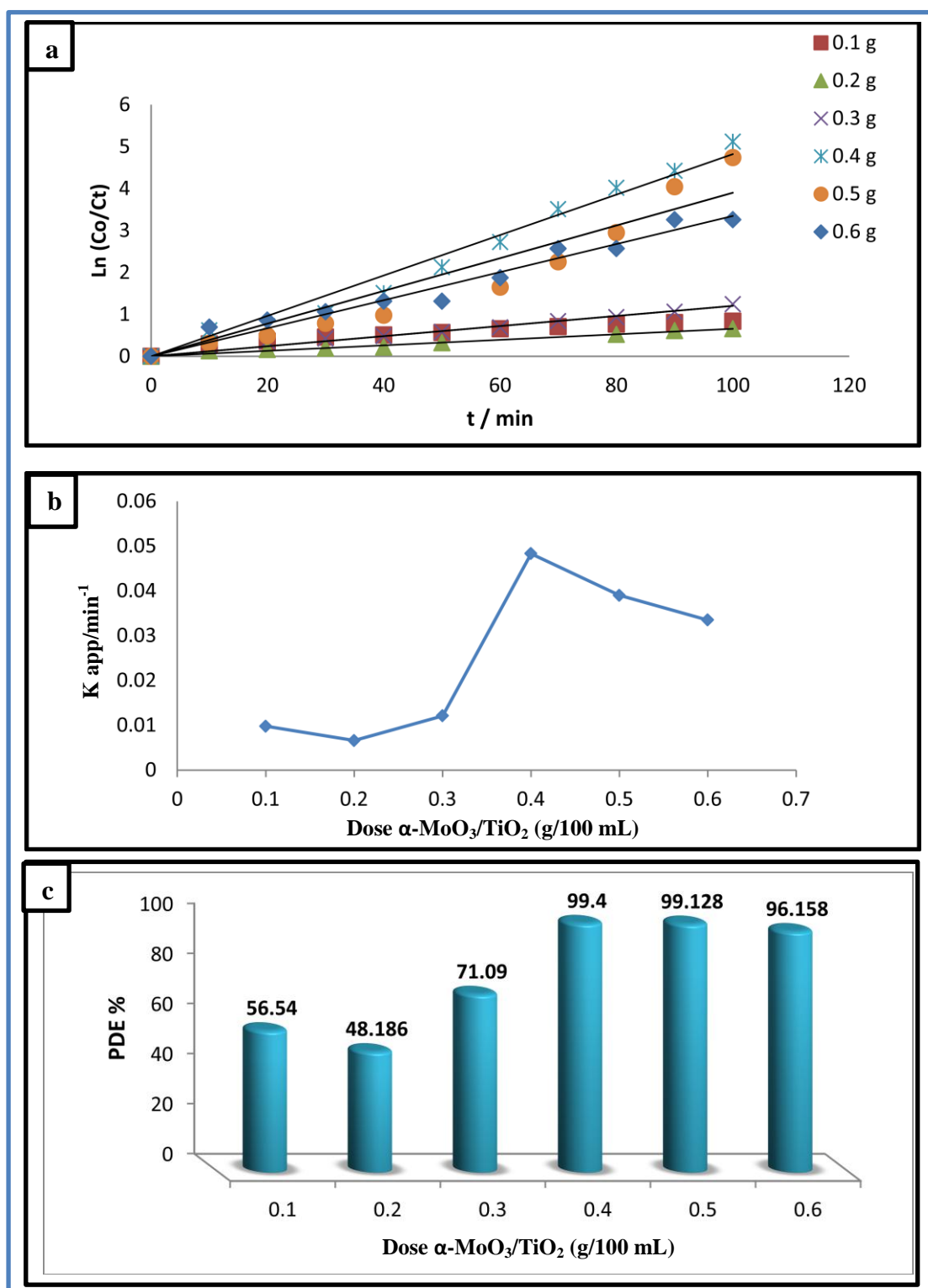
Figure (3-11). (a) The change of the Ln (C_0/C_t) with Irradiation time at a different dose of prepared α-MoO₃ /TiO₂ nanocomposite, (b) Relationship between the (k app) apparent rate constant and a different dose prepared α-MoO₃ /TiO₂, (c) Effect of a different dose of prepared α-MoO₃/TiO₂ on (PDE%) photodecolorization efficiency.

Based on the results from tables (3-5) to (3-8) and figures (3-10) and (3-11) obtained, that the apparent rate constant (k_{app}) and photodecolorization efficiency (PDE %) increases with increasing the dose of the photocatalyst from 0.1 g to 0.5 g and 0.4 g for using the commercial TiO_2 and prepared α-MoO_3/TiO_2 nanocomposite and the PDE % equal 91.891 and 99.401 respectively. Following these results, the rate constant and efficiency of the photoreaction reduces after these values that due to the screening effect, which results in high turbidity of the photocatalyst solution and will decrease the light passing through the solution [151].

3.2.2.2 Effect of Temperature

The effect of temperature has been performed in various ranges (283.15 - 298.15) K for the photocatalytic decolorization of chlorazol black BH dye. To maintain temperatures within the specified range, a water bath containing ice was used.

A. Effect of Temperature on Dye Solution by Commercial TiO_2:

The experimental condition includes a 50 ppm initial dye concentration, a dose of commercial TiO_2 (0.5 g /100mL), a pH = 7.6, and a light intensity equal to $2.95x10^{-7}$ Enstine s^{-1}.

Table (3-9). The change of the Ln (C_o/C_t) with irradiation time at different temperatures of commercial TiO$_2$ via photocatalytic decolorization of chlorazol black BH dye.

Time (min) \ t / K	Ln (C_o/C_t)			
	283.15	**288.15**	**291.15**	**298.15**
0	0.000	0.000	0.000	0.000
10	0.253	0.270	0.124	0.562
20	0.410	0.487	0.315	0.729
30	0.545	0.625	-	0.881
40	0.888	0.747	-	0.961
50	1.238	1.125	1.243	1.094
60	1.581	1.740	1.618	1.156
70	2.033	1.902	1.713	1.351
80	2.726	2.538	2.001	1.593
90	3.063	2.790	2.224	1.654
100	3.574	3.349	2.512	1.811
k$_{app}$/min^{-1}	**0.0315**	0.0279	0.0201	0.0198

Table (3-10). The change of the (PDE %) with irradiation time at different temperatures of commercial TiO$_2$ via photocatalytic decolorization of chlorazol black BH dye.

Time (min) \ t / K	PDE %			
	283.15	**288.15**	**291.15**	**298.15**
0	0.000	0.000	0.000	0.000
10	22.429	23.684	11.711	43.027
20	33.644	38.596	27.027	51.792
30	42.056	46.491	30.630	58.565
40	58.878	52.631	41.441	61.752
50	71.028	67.543	71.171	66.533
60	79.439	82.456	80.180	68.525
70	86.915	85.087	81.981	74.103
80	93.457	92.105	86.486	79.681
90	95.327	93.859	89.189	80.876
100	**97.196**	**96.491**	**91.891**	**83.665**
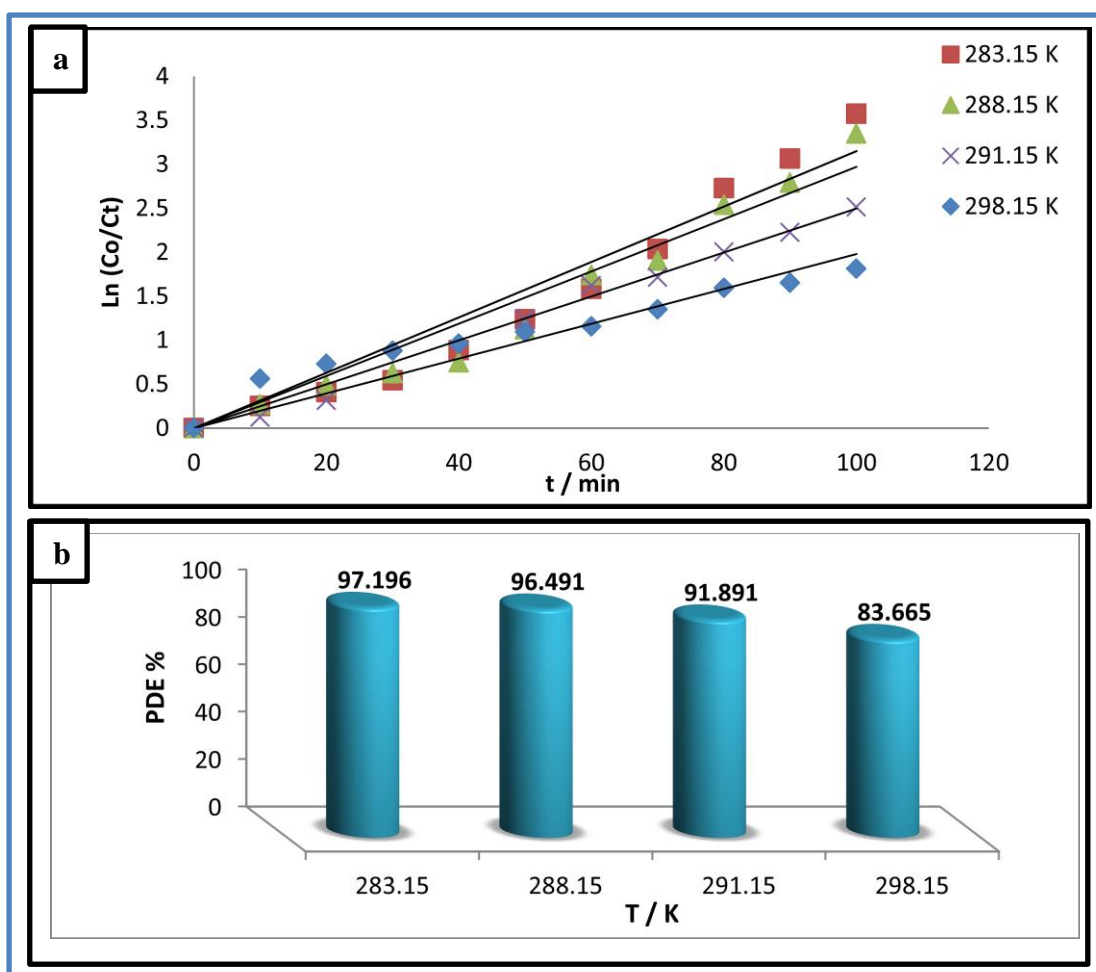
Figure (3-12). (a) The change of the Ln (C_o/C_t) with Irradiation time at different temperatures of commercial TiO$_2$, (b) Effect of the different temperature of commercial TiO$_2$ on (PDE%) photodecolorization efficiency.

Table (3-11). Relationship between (1/T) with ln k_{app} and ln (kapp/T) of commercial TiO$_2$ via photocatalytic decolorization of chlorazol black BH dye

t (ºC)	T(K)	1/T	k_{app}/ min^{-1}	ln k_{app}	ln($k_{app.}$/T)
10	283.15	3.5316	0.0315	-3.4577	-9.1037
15	288.15	3.4704	0.0279	-3.5791	-9.2426
18	291.15	3.4112	0.0201	-3.9070	-9.5808
25	298.15	3.3540	0.0198	-3.9220	-9.6196

a

$y = 3.1895x - 20.365$
$R^2 = 0.9255$

ln(k app/T)

(1000/T)

b

$y = 2.911x - 13.736$
$R^2 = 0.9043$

ln k app
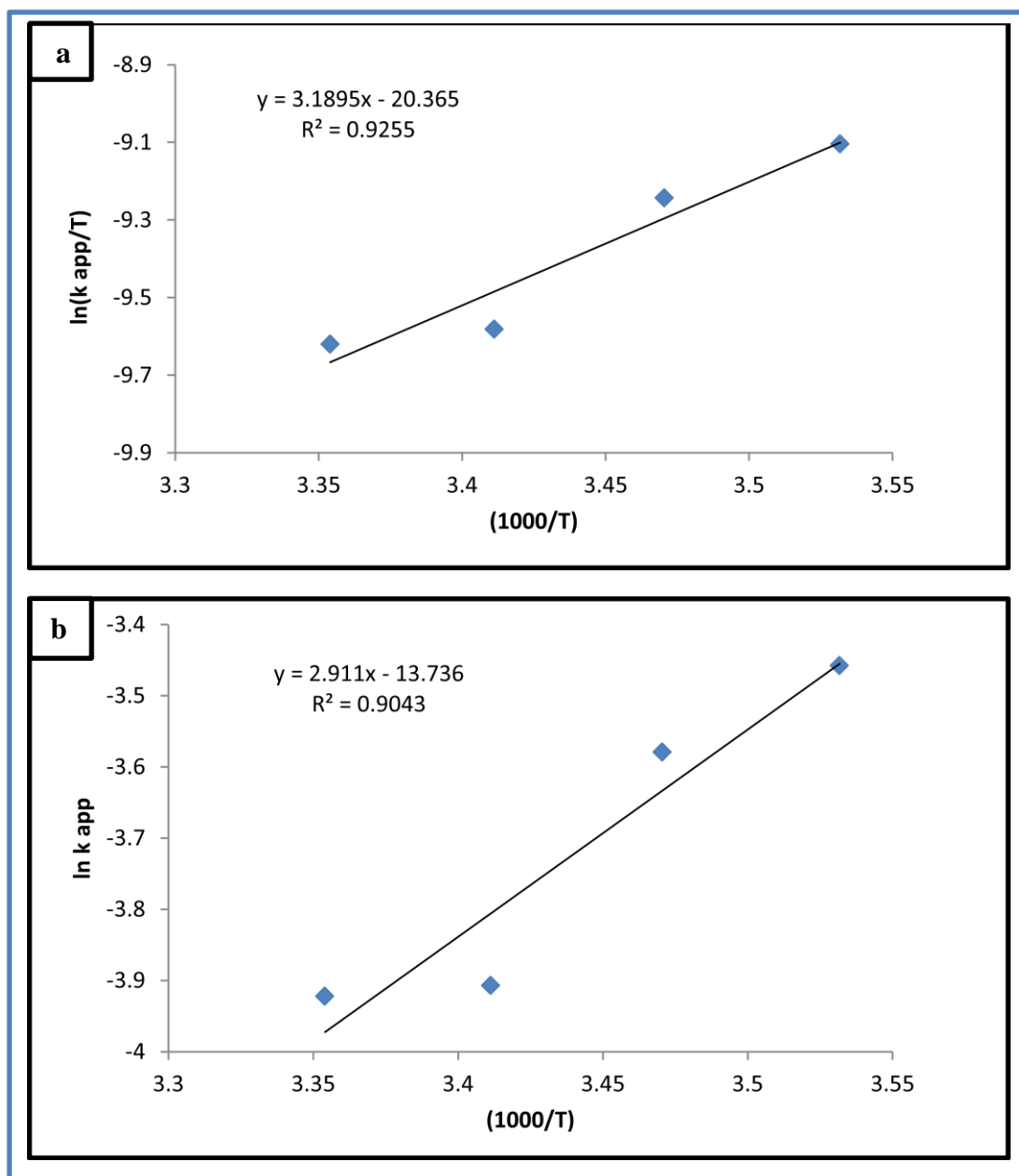
(1000/T)

Figure (3-13). (a) Eyring–Polanyi equation plot ln (k $_{app}$/T) VS. 1000/T (b) Arrhenius equation plot by commercial TiO$_2$ via photocatalytic decolorization of chlorazol black BH dye.

B. Effect of Temperature on Dye Solution by α-MoO$_3$/TiO$_2$ Nanocomposite:

The experimental condition includes a 50 ppm initial dye concentration, a dose of prepared α-MoO$_3$/TiO$_2$ (0.4 g /100mL), a pH = 7.6, and a light intensity equal to $2.95 x 10^{-7}$ Enstine s^{-1}.

Table (3-12). The change of the Ln (C_o/C_t) with irradiation time at different temperatures of prepared α-MoO₃/TiO₂ nanocomposite via photocatalytic decolorization of chlorazol black BH dye.

t / K Time (min)	Ln (C_o/C_t)			
	283.15	288.15	291.15	298.15
0	0.000	0.000	0.000	0.000
10	0.238	0.316	0.618	0.770
20	0.420	0.453	0.711	0.956
30	0.484	0.716	1.023	1.160
40	0.624	0.816	1.507	1.273
50	-	1.122	2.122	1.496
60	-	1.768	2.720	1.565
70	1.417	2.220	3.508	1.877
80	-	2.461	4.019	2.094
90	2.397	2.780	4.424	2.372
100	3.208	3.761	5.117	4.897
k_{app}/min⁻¹	0.0264	0.0314	**0.0483**	0.0333

Table (3-13). The change of the (PDE %) with irradiation time at different temperatures of prepared α-MoO₃/TiO₂ nanocomposite via photocatalytic decolorization of chlorazol black BH dye.

| t / K Time (min)	PDE %			
	283.15	288.15	291.15	298.15
0	0.000	0.000	0.000	0.000
10	21.212	27.131	46.107	53.731
20	34.343	36.434	50.898	61.567
30	38.383	51.162	64.071	68.656
40	46.464	55.813	77.844	72.014
50	54.545	67.441	88.023	77.611
60	65.656	82.945	93.413	79.104
70	75.757	89.147	97.005	84.701
80	83.838	91.472	98.203	87.686
90	90.909	93.798	98.802	90.671
100	**95.959**	**97.674**	**99.401**	**99.253**
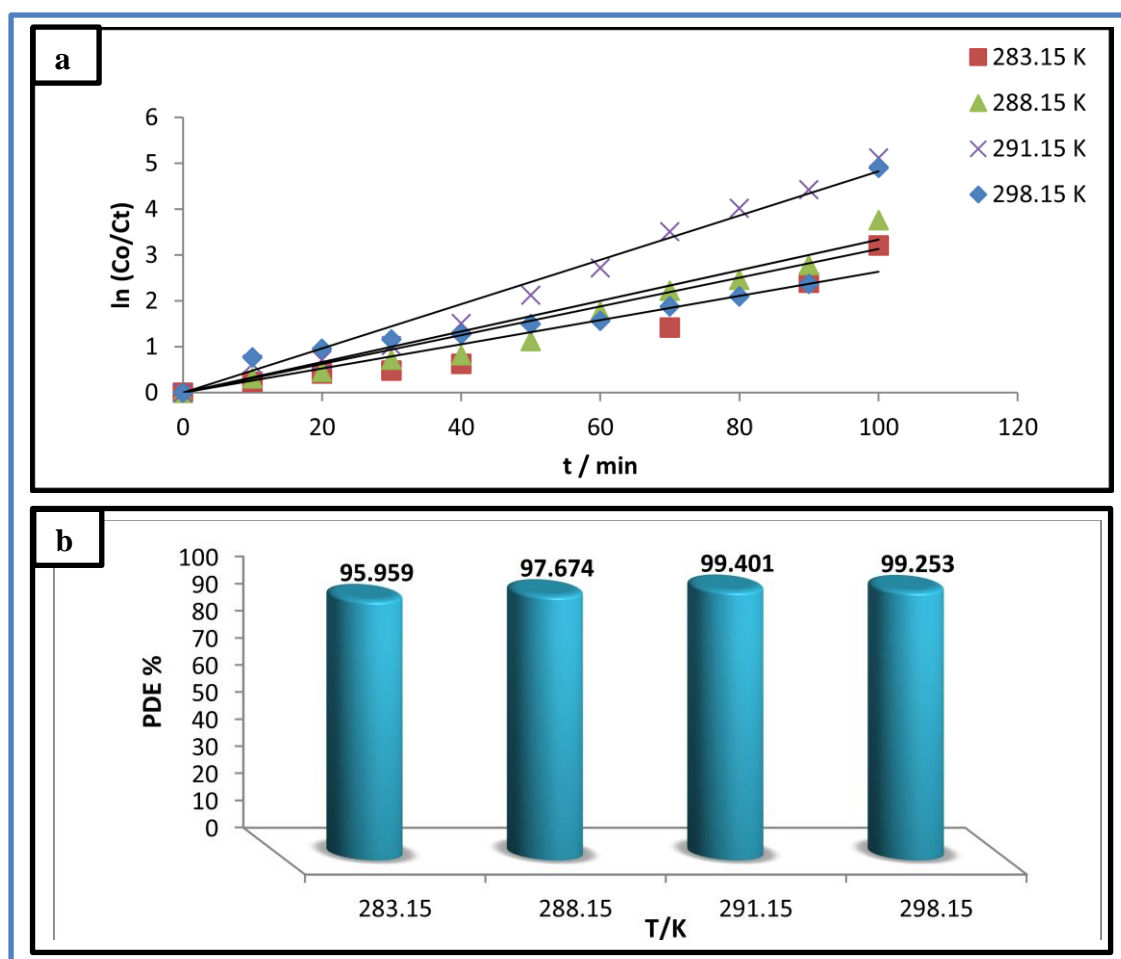
Figure (3-14). (a) The change of the Ln (C_0/C_t) with Irradiation time at a different temperatures of prepared α-MoO₃/TiO₂ nanocomposite, (b) Effect of the different temperatures of prepared α-MoO₃/TiO₂ nanocomposite on (PDE%) photodecolorization efficiency.

Table (3-14). Relationship between (1/T) with ln kapp and ln (k_{app}/T) of prepared (α-MoO₃/TiO₂) nanocomposite via photocatalytic decolorization of chlorazol black BH dye.

t (ºC)	T(K)	1/T	k_{app}/ min^{-1}	ln k_{app}	ln($k_{app.}$/T)
10	283.15	3.5316	0.0264	-3.6343	-9.2803
15	288.15	3.4704	0.0314	-3.4609	-9.1244
18	291.15	3.4346	0.0483	-3.0303	-8.7041
25	298.15	3.3540	0.0333	-3.4021	-9.0997

a $y = -1.2645x - 4.6926$
$R^2 = 0.1462$

ln(kapp./T) vs (1000/T)

b $y = -1.5552x + 1.9798$
$R^2 = 0.2059$

ln k app. vs (1000/T)
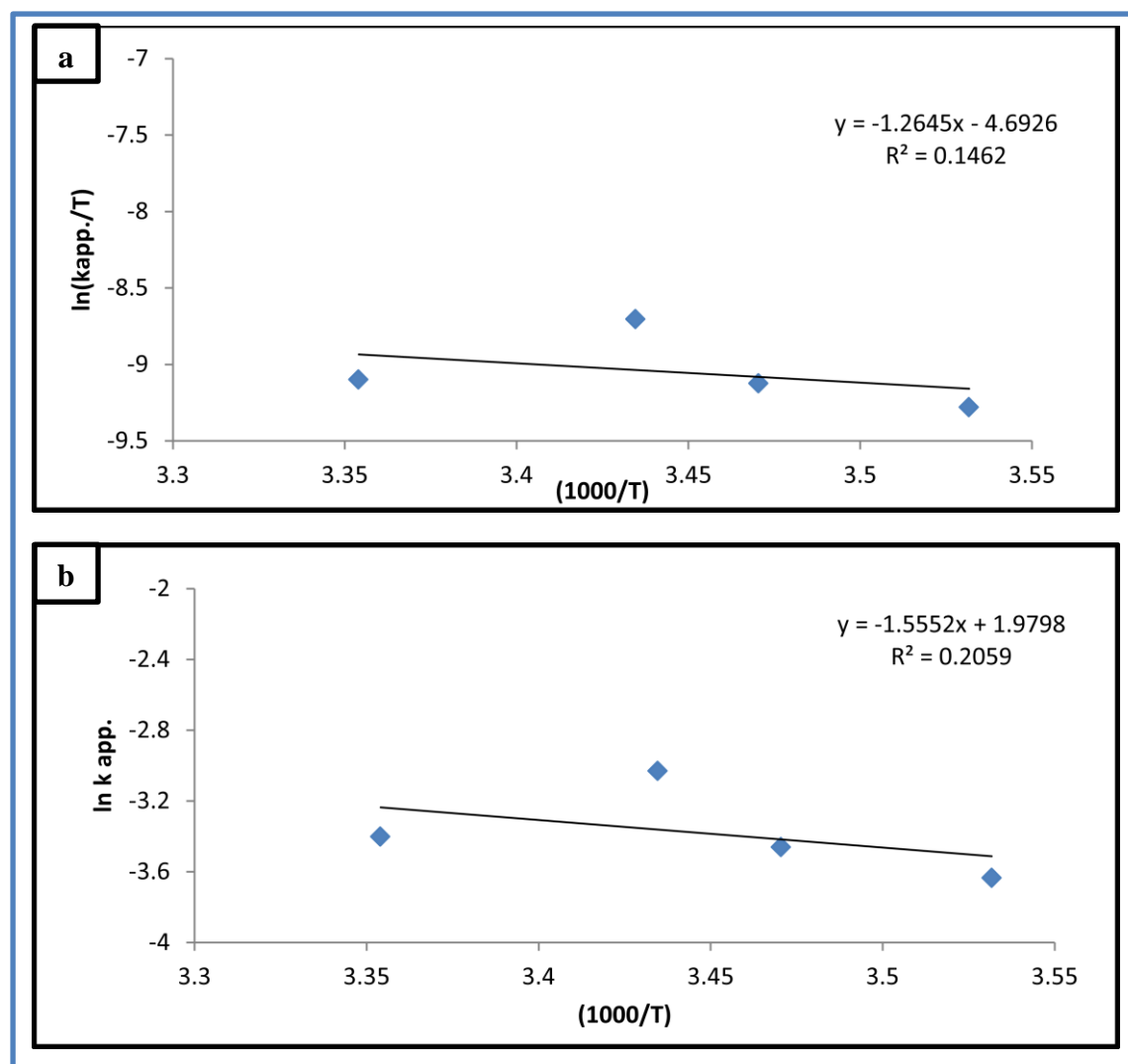
Figure (3-15). (a) Eyring–Polanyi equation plot ln (k $_{app}$/T) VS. 1000/T (b) Arrhenius equation plot by prepared (α-MoO₃/TiO₂) nanocomposite via photocatalytic decolorization of chlorazol black BH dye.

Table (3-15). The calculated activation kinetic and thermodynamic functions for decolorization of chlorazol black BH dye using commercial TiO₂ and prepared (α-MoO₃/ TiO₂) nanocomposite.

Samples	E_a /kJ mol^{-1}	$\Delta H^{\#}$/kJ mol^{-1}	$\Delta S^{\#}$/ J mol^{-1} K^{-1}	$\Delta G^{\#}$/kJ mol^{-1}
TiO₂	-24.202	-26.510	-366.821	80.290
(α-MoO₃/TiO₂)	12.929	10.513	-236.554	79.385

58

Depending on the results shown in the tables from (3-9) to (3-15) and figures from (3-11) to (3-14), the photocatalyst reaction was accelerated to the decolorization of the chlorazol black BH dye when the temperature was increased with the α-MoO$_3$/TiO$_2$ nanocomposite, but with the using TiO$_2$, it is found the opposite.

The activation energy after incorporation of TiO$_2$ with α- MoO$_3$ surface increased from (-24.202 kJ mol^{-1}) to (12.929 kJ mol^{-1}) for TiO$_2$ and α-MoO$_3$/TiO$_2$ nanocomposite respectively, the negative value of (E$_a$) may indicate that the studied photoreaction has multi-steps binding, one of which may be exothermic then conversion at a very low positive activation energy value via a series of chain reactions. This case leads to dye decolorize at temperatures ranging from 283.15 to 298.15 K, and as the temperature rises, the catalyst may become deactivated. The change in enthalpies (ΔH$^{\#}$) was positive for α-MoO$_3$/TiO$_2$ nanocomposite which indicated the reaction endothermic, this case is a favor in photoreaction, while, the change in enthalpies (ΔH$^{\#}$) was negative for using TiO$_2$ that referred to be as an exothermic reaction [116]. The change in Gibbs free energy (ΔG$^{\#}$) is positive for both reactions using TiO$_2$ and nanocomposite, which indicated to non-spontenous reaction. The change in entropy (ΔS$^{\#}$) for both reactions is negative that due to reduce the random dye solution after the decolorization reaction. From the other side, the positive values of (ΔH$^{\#}$) and (ΔG$^{\#}$)   using nanocomposite attitude to increase in the solvated intermediate between dye and hydroxide radical ˙OH [152].

3.2.2.3 Effect of Initial pH of the Solution on Dye Decolorization.

The effect of initial pH has been performed using a range of pH from 4 to 9 and at conditions: the concentration of dye 50 ppm in 100 mL, at 291.15 K, doses of photocatalysts commercial TiO$_2$, α-MoO$_3$/TiO$_2$ nanocomposite at 0.5 g, and 0.4 g respectively, and same the light intensity.

A. Effect of Initial pH of Chlorazol Black BH Dye Solution by Commercial TiO₂:

Table (3-16). The change of the Ln (C₀/Cₜ) and irradiation time at a different initial pH of chlorazol black BH dye by commercial TiO₂.

Time (min) / pH	Ln (C_o/C_t)				
	4.31	**5.04**	**6.02**	**7.6**	**9**
0	0.000	0.000	0.000	0.000	0.000
10	0.516	0.095	-	0.124	0.332
20	0.725	-	-	0.315	0.650
30	1.131	0.788	1.945	0.365	0.707
40	1.419	1.011	2.100	-	0.832
50	1.642	-	2.282	1.243	0.866
60	2.181	1.704	2.793	1.618	0.995
70	2.517	2.397	3.198	1.713	1.056
80	2.740	2.397	3.198	2.001	1.120
90	3.433	7.495	3.891	2.224	1.238
100	4.820	8.628	3.891	2.512	1.316
k_{app}/min^{-1}	0.0392	**0.058**	0.0432	0.0246	0.0151

Table (3-17). The change of the (PDE %) and irradiation time at a different initial pH of chlorazol black BH dye by commercial TiO₂.

Time (min) / pH	PDE %				
	4.31	**5.04**	**6.02**	**7.6**	**9**
0	0.000	0.000	0.000	0.000	0.000
10	40.322	9.090	10.204	11.711	28.260
20	51.612	27.272	83.673	27.027	47.826
30	67.741	54.545	85.714	30.630	50.724
40	75.806	63.636	87.755	41.441	56.521
50	80.645	63.636	89.795	71.171	57.971
60	88.709	81.818	93.877	80.180	63.043
70	91.935	90.909	95.918	81.981	65.217
80	93.548	90.909	95.918	86.486	67.391
90	96.774	99.944	97.959	89.189	71.014
100	**99.193**	**99.982**	**97.959**	**91.891**	**73.188**
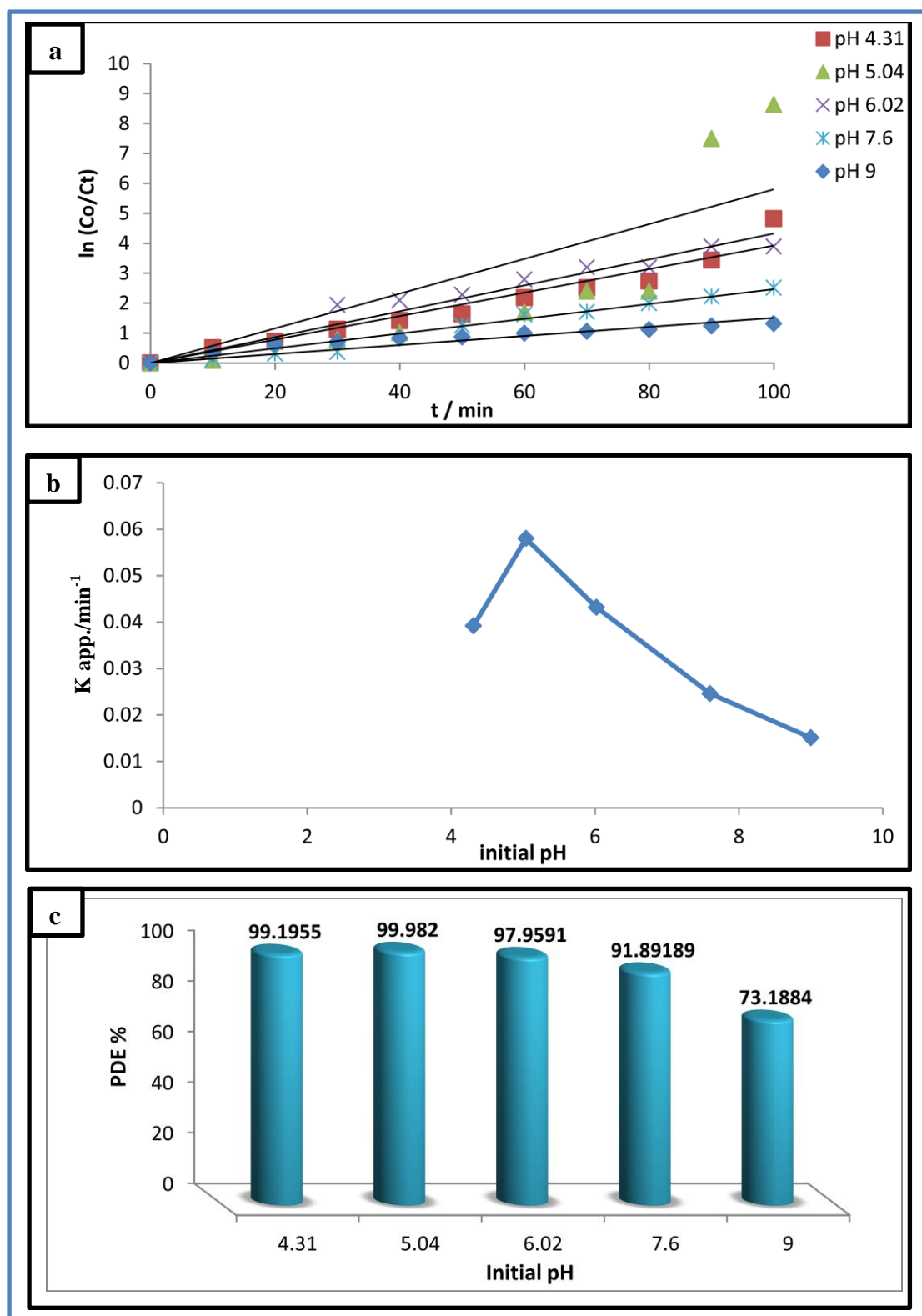
Figure (3-16). (a) The change of the Ln (C_o/C_t) with Irradiation time at a different pH solution of commercial TiO₂, (b) Relationship between the (k app) apparent rate constant and the different pH solution of commercial TiO₂, (c) Effect the different pH solution of commercial TiO₂ on (PDE%) photodecolorization efficiency.

B. Effect of Initial pH of Chlorazol Black BH dye Solution by α-MoO₃/TiO₂ Nanocomposite.

Table (3-18). The change of the Ln (C_o/C_t) and irradiation time at a different initial pH of chlorazol black BH dye by (α-MoO₃/TiO₂) nanocomposite.

Time pH (min)	Ln (C_o/C_t)				
	4.01	**5.15**	**6.02**	**7.6**	**9**
0	0.000	0.000	0.000	0.000	0.000
10	0.169	0.167	0.563	0.618	0.067
20	0.510	0.262	0.955	0.711	0.119
30	0.810	0.667	1.341	1.023	0.153
40	0.916	0.801	1.466	1.507	0.181
50	1.504	1.312	1.871	2.122	0.209
60	1.609	1.584	2.228	2.720	0.239
70	1.860	2.159	2.788	3.508	0.277
80	2.420	2.747	3.481	4.019	0.317
90	3.806	3.258	4.174	4.424	0.350
100	3.806	4.356	4.174	5.117	0.367
k_{app}/min^{-1}	0.0336	0.0343	0.042	**0.0483**	0.004

Table (3-19). The change of the (PDE %) and irradiation time at a different initial pH of chlorazol black BH dye by (α-MoO₃/TiO₂) nanocomposite.

Time pH (min)	PDE %				
	4.01	**5.15**	**6.02**	**7.6**	**9**
0	0.000	0.000	0.000	0.000	0.000
10	15.555	15.384	43.076	46.107	6.508
20	40	23.076	61.538	50.898	11.242
30	55.555	48.717	73.846	64.071	14.201
40	60	55.128	76.923	77.844	16.568
50	77.777	73.076	84.615	88.023	18.934
60	80	79.487	89.230	93.413	21.301
70	84.444	88.461	93.846	97.005	24.260
80	91.111	93.589	96.923	98.203	27.219
90	97.777	96.153	98.461	98.802	29.585
100	**97.777**	**98.717**	**98.461**	**99.401**	**30.769**
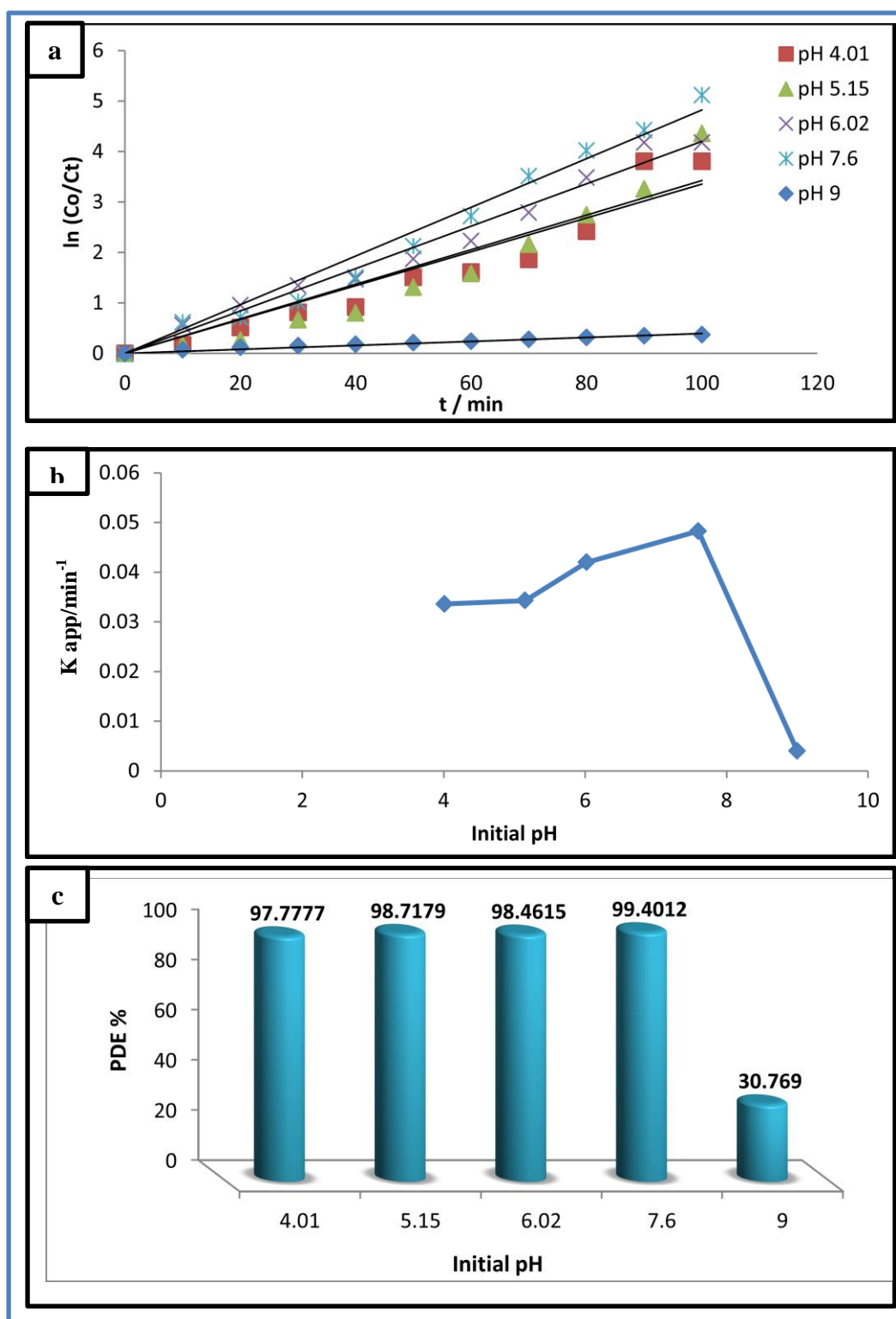
Figure (3-17). (a) The change of the Ln (C_o/C_t) with Irradiation time at the different pH solution of (α-MoO₃ /TiO₂) nanocomposite, (b) Relationship between the (k app) apparent rate constant and the different pH solution of (α-MoO₃/TiO₂) nanocomposite, (c)Effect of the different pH solution of (α-MoO₃/TiO₂) nanocomposite on (PDE%) photodecolorization efficiency.

The results above mentioned from tables (3-16) to (3-19) and figures (3-15) and (3-16) explained that the rate constant and efficiency of these photoreactions to the nanocomposite increases with the increase of the initial pH of the chlorazol black BH dye solution but decreased with using the commercial TiO_2. The optimum initial pH values for using commercial TiO_2, and (α-MoO_3/ TiO_2) nanocomposite are 5.04 and 7.6 with efficiency PDE% are 99.982 and 99.401 respectively. That attitude to be positively charged with TiO_2 and nanocomposite before mention pH. In contrast, after more value of this pH, the efficiency and rate constant of this photoreaction reduced, which indicates to negatively charge have occurred on TiO_2 and nanocomposite surfaces with increasing the hydroxyl ion adsorption. This case will cause coulombic repulsion between the negatively charged surface of the photocatalyst and the electronic density of lone pair electron on dye structure in the basic medium [153].

3.3 Suggested Mechanism for Dye Decolorization

The decolorization of the chlorazol black BH dye under UV-A light and photocatalysts produces a hydroxyl radical ($^{\bullet}OH$), which degrades the chromophores groups on dye and produces CO_2 and H_2O, as well as inorganic products as final products. Figure (3-17) displays the suggested decolorization mechanism for chlorazol black BH dye [116] under photocatalytic and light.
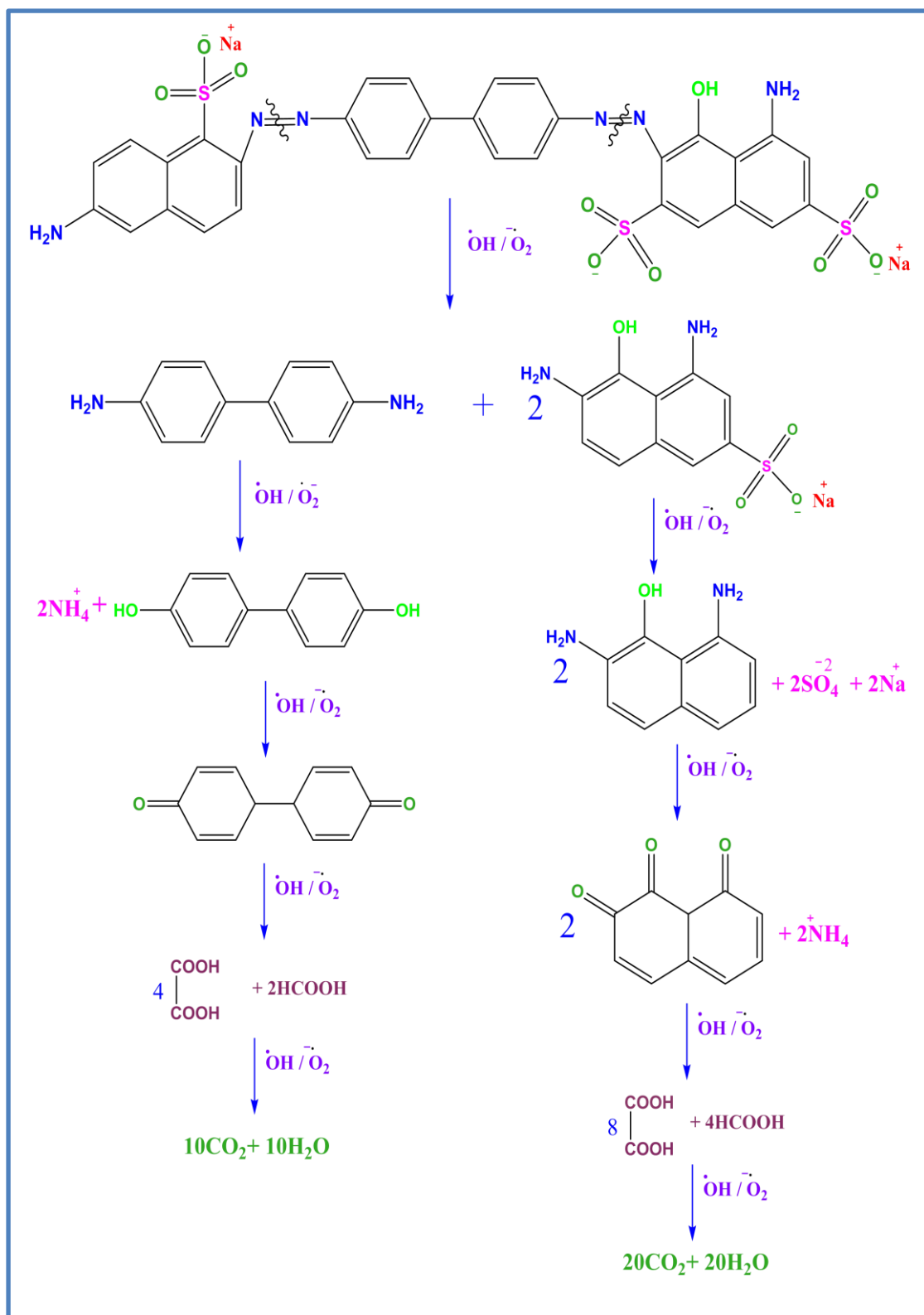
Figure (3-18). The schematic diagram mechanism for photodecolorization of chlorazol black BH dye [116].

3.4 Conclusions

This study focused on preparing the α-MoO$_3$ and then combining it with TiO$_2$ to produce α-MoO$_3$/TiO$_2$ nanocomposite, and then they were applied with chlorazol black BH dye solution to test their efficiency for dye decolorization as a photocatalysts. The main conclusions can be summarized as follows:

1) The preparation of α-MoO$_3$ nanobelts, were successfully prepared by hydrothermal method, when confirmed by XRD, SEM, FTIR, technique, and Bg measurements.

2) The preparation of α-MoO$_3$/TiO$_2$ nanocomposite, were successfully prepared by ultrasonic technique in aqueous solutions, where the surface of rutile-TiO$_2$ was modified by incorporating it with α-MoO$_3$.

3) XRD data results indicated the synthesis of α-MoO$_3$ is orthorhombic, and it's incorporated with rutile-TiO$_2$ as α-MoO$_3$/TiO$_2$ nanocomposite, depending on Scherer equation the mean crystallite sizes were calculated for commercial TiO$_2$, prepared α-MoO$_3$ nanobelts, and α-MoO$_3$/TiO$_2$ nanocomposite, and found to be in nano-sizes.

4) SEM images showed that the shapes of TiO$_2$ with its nanocomposite are semi-spherical and semi-spherical agglomerate respectively because of the large amount of TiO$_2$ dispersive and binding with α-MoO$_3$, while the α-MoO$_3$ is having nanobelts shape.

5) It can be concluded that the prepared α-MoO$_3$, commercial TiO$_2$, and α-MoO$_3$/TiO$_2$ are photocatalysts by plotting the Tauc equation, the band gaps of α-MoO$_3$ nanobelts, TiO$_2$, and its nanocomposite are direct band gap, indirect band gap, and indirect band gap, respectively.

6) The photodecolorization reactions of chlorazol black BH dye using the α-MoO$_3$ nanobelts, TiO$_2$, and α-MoO$_3$/TiO$_2$ nancomposite for 100 min are pseudo-first-order kinetic. The efficiency of this photoreaction using the α-MoO$_3$/ TiO$_2$ nanocomposite is higher than the use of both α-MoO$_3$ and TiO$_2$ at 18 ^{o}C and 400 mg/100 mL.

7) The activation energy of the photoreaction of Chlorazol black BH dye decolorization using prepared α-MoO$_3$/TiO$_2$ nanocomposite decreases compared with using α-MoO$_3$ and TiO$_2$ alone.

8) The optimum conditions for the photodecolorization reactions with TiO$_2$ where the dose was 0.5 g, temperature 283.15 K, and pH value was 5.04, while with α-MoO$_3$/TiO$_2$ nanocomposite the dose was 0.4 g, temperature 291.15 K, and pH value was 7.6.

3.5 Recommendations

In the future, the following recommendations should be used:

1) Calcination process for prepared α-MoO$_3$ and α-MoO$_3$/TiO$_2$ nanocomposite to obtain a new crystal size.

2) Preparation of α-MoO$_3$ using alcohol instead of D.W as solvent of precursor materials (Na$_2$MoO$_4$. 2H$_2$O) as solvothermal method, to change the morphology and optical properties of prepared α-MoO$_3$ and α-MoO$_3$/TiO$_2$ nanocomposite.

3) Doped certain transition metals on α-MoO$_3$ and α-MoO$_3$/TiO$_2$ nanocomposite to reduce the recombination process.

4) Studying the other characterization of the prepared α-MoO$_3$ and α-MoO$_3$/TiO$_2$ nanocomposite such as XPS, SEM-EDX, and surface area by BET.

5) Studying the zero point charge of the prepared α-MoO$_3$ and α-MoO$_3$/TiO$_2$ nanocomposite.

6) Application of the various conditions such as different doses, at different temperatures, various initial pH values of solution, and Fenton reaction to determine the optimum conditions using the α-MoO$_3$.

7) Incorporated α-MoO$_3$ with Al$_2$O$_3$ as a nanocomposite to use it as a petroleum catalyst to treat certain problems.

8) Study the properties of produced water after AOPs of dye solution such as pH, type and amounts of cationic and anionic…etc.

References

References

1. E. Guerra, M. Llompart, and C. Garcia-Jares, "Analysis of Dyes in Cosmetics: Challenges and Recent Developments", *Academic Open Access Publishing, (Cosmetics)*, Vol.5, no.3, pp.1-15, (2018).

2. F. F. Karam, N. H. Saeed, A. H. Al-Yasari, L.M. Ahmed and H. Saleh, "Kinetic Study for Reduced the Toxicity of Textile Dyes (Reactive yellow 14 dye and Reactive green dye) Using UV-A light/ZnO System", *Egypt. J. Chem.,* Vol. 63, no. 8. pp. 2987-2998 (2020).

3. L. M. Ahmed, M. A. Jassim, M. Q. Mohammed, and D.T. Hamza, "Advanced oxidation processes for carmoisine (E122) dye in UV-A/ZnO system: Influencing pH, temperature and oxidant agents on dye solution", *Journal of Global Pharma Technology*, vol. 10, no. 7, pp. 248-254,(2018).

4. N. Khalfaoui, H. Boutoumi, H. Khalaf, N. Oturan, and M. A. Oturan, "Electrochemical oxidation of the xanthene dye Rhodamine 6G by electrochemical advanced oxidation using Pt and BDD anodes",*Current Organic Chemistry*, Vol.16, no.18, pp. 2083-2090, (2012).

5. Z. S. Seddigi, "Removal of alizarin yellow dye from water using zinc doped WO_3 catalyst", *Bulletin of environmental contamination and toxicology*, Vol. 84, pp. 564-567, (2010).

6. M. A. Gondal, M. N. Sayeed, and Z. Seddigi, "Laser enhanced photo-catalytic removal of phenol from water using p-type NiO semiconductor catalyst", *Journal of Hazardous Materials*, Vol. 155, pp. 83-89, (2008).

7. L. M. Ahmed, "Bulk and Nanocatalysts Applications in Advanced Oxidation Processes", Oxidoreductase*,* M. A. Mansour ed., Licensee IntechOpen, , UK, DOI: 10.5772/intechopen.94234, ISBN: 978-1-83880-901-0, pp.1-15, (2020).

8. M. A. Rauf, and S.S. Ashraf, "Radiation induced degradation of dyes- an overview", *Journal of hazardous materials*, Vol.166, no.1, pp. 6-16, (2009).

References

9. S. G. Schrank, J. N. R. dos Santos, D. S. Souza, and E. E. S. Souza, "Decolourisation effects of Vat Green 01 textile dye and textile wastewater using H_2O_2/UV process", *Journal of Photochemistry and Photobiology A: Chemistry*, Vol.186, pp. 125-129, (2007).

10. A. L. N. Mota, L. F. Albuquerque, L. C Beltrame, O. Chiavone-Filho, A. Machulek Jr., and C. A. O. Nascimento, "Advanced oxidation processes and their application in the petroleum industry: a review", *Brazilian Journal of Petroleum and Gas*, Vol. 2, no. 3, pp. 122-142, (2009).

11. M. Pera-Titus, V. García-Molina, M. A. Baños, J. Giménez, and S. Esplugas," Degradation of chlorophenols by means of advanced oxidation processes: a general review", *Applied Catalysis B: Environmental*, Vol.47, no. 4, pp. 219-256, (2004).

12. F. Han, V. S. R. Kambala, M. Srinivasan, D. Rajarathnam, and R. Naidu, "Tailored titanium dioxide photocatalysts for the degradation of organic dyes in wastewater treatment: a review", *Applied Catalysis A: General*, Vol. 359, no. (1-2), pp. 25-40, (2009).

13. C. Hachem, F. Bocquillon, O. Zahraa, and M. Bouchy, "Decolourization of textile industry wastewater by the photocatalytic degradation process", *Dyes and pigments*, Vol. 49, no.2, pp.117-125, (2001).

14. M. Cheng, G. Zeng, D. Huang, C. Lai, P. Xu, C. Zhang, and Y. Liu, "Hydroxyl radicals based advanced oxidation processes (AOPs) for remediation of soils contaminated with organic compounds: a review", *Chemical Engineering Journal*, Vol.284, pp. 582-598, (2016).

15. K. Ayoub, E. D. van Hullebusch, M. Cassir, and A. Bermond, "Application of advanced oxidation processes for TNT removal: a review", *Journal of hazardous materials*, Vol.178, no. (1-3), pp.10-28, (2010).

References

16. L. Ahmed, and F. Hussein, "Roles of Photocatalytic Reactions of Platinized TiO$_2$ Nanoparticales", 1st ed. LAP Lambert Academia Published; ISBN-10: 3659538817, pp.108, (2014).

17. F. Hai, K. Yamamoto, K. Fukushi, "Hybrid Treatment Systems for Dye Wastewater", *Critical Reviews in Environmental Science and Technology,* Vol.37, no. 4, pp. 315-377, (2007).

18. T. Robinson, G. McMullan, R. Marchant, and P. Nigam, "Remediation of dyes in textile effluent: a critical review on current treatment technologies with a proposed alternative", *Bioresource Technology*, Vol.77, no.3, pp. 247-255, (2001).

19. B. E. A. Saleh, and M. C. Teich, "Fundamentals of photonics (Wiley series in pure and applied optics)", 1st ed., John Wiley, New York, ISBN-10 : 9780471839651, pp.992, (1991).

20. H. T. Grahn, "Introduction to Semiconductor Physics", world scientific, Pub Co., Singapore, pp.196, (1999).

21. A. Sobczyński, and A. Dobosz, "Water purification by photocatalysis on semiconductors", *Polish journal of environmental studies*, Vol.10, no.4, pp. 195-205, (2001).

22. A. J. Bard, "Semiconductor particles and arrays for the photoelectrochemical utilization of solar energy", *Berichte der Bunsengesellschaft für physikalische Chemie*, Vol. 92, no. 11, pp.1187-1194, (1988).

23. M. A. Fox, and M. T. Dulay, "Heterogeneous photocatalysis", *Chemical reviews*, Vol.93, no. 1, pp.341-357, (1993).

24. R. Vinu, and G. Madras, "Environmental remediation by photocatalysis", *Journal of the Indian Institute of Science*, Vol. 90, no. 2, pp.189-230, (2012).

References

25. A. Mills, and S. Le Hunte, "An overview of semiconductor photocatalysis", *Journal of photochemistry and photobiology A: Chemistry*, Vol. 108, no. 1, pp. 1-35, (1997).

26. O. Carp, C. L. Huisman, and A. Reller, "Photoinduced reactivity of titanium dioxide", *Progress in solid state chemistry*, Vol. 32, no.(1-2), pp. 33-177, (2004).

27. D. S. Bhatkhande, V. G. Pangarkar, and A. A. C. M. Beenackers, "Photocatalytic degradation for environmental applications–a review", *Journal of Chemical Technology & Biotechnology: International Research in Process, Environmental & Clean Technology*, Vol. 77, no. 1, pp.102-11, (2002).

28. K. Kabra, R. Chaudhary, and R. L. Sawhney, "Treatment of hazardous organic and inorganic compounds through aqueous-phase photocatalysis: a review", *Industrial & engineering chemistry research*, Vol. 43, no. 24, pp. 7683-7696, (2004).

29. M. M Khan, S. F. Adil, and A. Al-Mayouf, "Metal oxides as photocatalysts", *Journal of Saudi Chemical Society*, Vol. 19, no. 5, pp. 462-464, (2015).

30. A. J. Bard, "Photoelectrochemistry and heterogeneous photo-catalysis at semiconductors", *Journal of Photochemistry*, Vol. 10, no. 1, pp. 59-75, (1979).

31. A. Kudo, and Y. Miseki, "Heterogeneous photocatalyst materials for water splitting", *Chemical Society Reviews*, Vol.38, no. 1, pp. 253-278, (2009).

32. L. E. Smart, and E. A. Moore, "Solid state chemistry: an introduction", 4th ed. *CRC press*, pp. 494, Boca Raton, (2012).

33. C. Karthikeyan, P. Arunachalam, K. Ramachandran, A. M. Al-Mayouf, and S. Karuppuchamy, "Recent advances in semiconductor metal oxides with enhanced methods for solar photocatalytic applications", *Journal of Alloys and Compounds*, Vol. 828, pp.154281, (2020).

References

34. V. Singh, "Band Gap and Resistivity Measurements of Semiconductor Materials For Thin Films", *Journal of Emerging Technologies and Innovative Research (JETIR),* Vol. 4, no. 12, pp. 1200-1210, (2017).

35. M. N. Chong, B. Jin, C. W. Chow, and C. Saint, "Recent developments in photocatalytic water treatment technology: a review". *Water research*, Vol. 44, no. 10, pp. 2997-3027, (2010).

36. A. Fujishima, X. Zhang, and D. A. Tryk, "TiO$_2$ photocatalysis and related surface phenomena", *Surface science reports*, Vol. 63, no. 12, pp. 515-582, (2008).

37. D, Chatterjee, and S. Dasgupta, "Visible light induced photocatalytic degradation of organic pollutants", J*ournal of Photochemistry and Photobiology C: Photochemistry Reviews,* Vol. 6, no. (2-3), pp.186-205, (2005).

38. Y. Guo, X.Yang, F. Ma, K. Li, L. Xu, X. Yuan, and Y. Guo, "Additive-free controllable fabrication of bismuth vanadates and their photocatalytic activity toward dye degradation", *Applied Surface Science,* Vol. 256, no. 7, pp.2215-2222, (2010).

39. N. Serpone, "Relative photonic efficiencies and quantum yields in heterogeneous photocatalysis" *Journal of Photochemistry and Photobiology A: Chemistry*, Vol. 104, no. (1-3), pp. 1-12, (1997).

40. M. R. Hoffmann, S. T. Martin, W. Choi, and D. W. Bahnemann, "Environmental applications of semiconductor photocatalysis", *Chemical reviews*, Vol.95, no.1, pp.69-96, (1995).

41. M. Hayawi, M. Kareem, and L. Ahmed, "Synthesis of Spinel Mn$_3$O$_4$ and Spinel Mn$_3$O$_4$/ZrO$_2$ Nanocomposites and Using Them in Photo-Catalytic Decolorization of Fe (II)-(4, 5-Diazafluoren-9-One 11) Complex ", Periódico *Tchê Química*, Vol.17, no. 34, pp. 689-699, (2020).

References

42. S. Anandan, Y. Ikuma, and K. Niwa, "An overview of semi-conductor photocatalysis: modification of TiO_2 nanomaterials", *In Solid State Phenomena*, Vol. 162, pp. 239-260, (2010).

43. W. J. Kuang, H. Tolner, and Q. Li, "Cathode-luminescence diagnostics of MgO, MgO:Si, MgO:Sc, and MgCaO ", *Journal of the SID,* Vol.20, no.1, pp. 63- 69, (2012).

44. R.F. Pierret "Advanced semiconductor Fundemantals", 2nd ed, Modular series on solid state devices, Pearson Education, Inc. UpperSaddleRiver, NewJersey,07458, CH5, vol. VI, pp. 1-221, (2002).

45. A. L. Linsebigler, G. Lu, and J. T. Yates Jr, "Photocatalysis on TiO_2 surfaces: principles, mechanisms, and selected results", *Chemical reviews*, Vol.95, no. 3, pp.735-758, (1995).

46. M. Horie, and K. Fujita, "Toxicity of metal oxides nanoparticles". *In Advances in molecular toxicology*, Elsevier, Vol. 5, pp. 145-178, (2011).

47. N. A. Monteiro-Riviere, A. O. Inman, and L. W. Zhang, "Limitations and relative utility of screening assays to assess engineered nanoparticle toxicity in a human cell line", *Toxicology and applied pharmacology*, Vol. 234, no. 2, pp. 222-235, (2009).

48. S. Zhang, and L. Song, "Preparation of visible-light-active carbon and nitrogen codoped titanium dioxide photocatalysts with the assistance of aniline", *Catalysis Communications*, Vol.10, no.13, pp.1725-1729. (2009).

49. T. Theivasanthi, and M. Alagar, "Titanium dioxide (TiO_2) nanoparticles XRD analyses: an insight", *arXiv preprint arXiv*: *1307.1091*. pp.10, (2013).

50. H. Einaga, K. Mochiduki, and Y. Teraoka, "Photocatalytic oxidation processes for toluene oxidation over TiO_2 catalysts", *Catalysts*, Vol. 3, no. 1, pp. 219-231, (2013).

References

51. T. Alammar, A. Birkner, O. Shekhah, and A. V Mudring, "Sonochemical preparation of TiO_2 nanoparticles in the ionic liquid 1-(3-hydroxypropyl)-3-methylimidazolium-bis (trifluoromethylsulfonyl) amide", *Materials Chemistry and Physics*, Vol. 120, no. 1, pp. 109-113, (2010).

52. M. Pelaez, N. T. Nolan, S. C. Pillai, M. K. Seery, P. Falaras, A. G. Kontos, and M. H. Entezari, "A review on the visible light active titanium dioxide photocatalysts for environmental applications", *Applied Catalysis B: Environmental*, Vol. 125, pp. 331-349, (2012).

53. R. Liang, H. Cao, and D. Qian, "MoO_3 nanowires as electrochemical pseudocapacitor materials", *Chemical Communications*, Vol. 47, no. 37, pp.10305-10307, (2011).

54. Y. Wang, Y. Zhu, Z. Xing, and Y. Qian, "Hydrothermal synthesis of α-MoO_3 and the influence of later heat treatment on its electrochemical properties", *Int. J. Electrochem. Sci*, Vol. 8, no. 7, pp.9851-9857, (2013).

55. I. A. de Castro, R. S. Datta, J. Z. Ou, A. Castellanos-Gomez, S. Sriram, T. Daeneke, and K. Kalantar-zadeh," Molybdenum oxides–from fundamentals to functionality", *Advanced Materials*,Vol. 29, no. 40, pp.1-31, (2017).

56. A. Khitab, S. Ahmad, M. J. Munir, S. M. S. Kazmi, T. Arshad, and R. A. Khushnood, "Synthesis and applications of nano titania particles: A review", *Reviews on Advanced Materials Science*, Vol. 53, no. 1, pp. 90-105, (2018).

57. V. Jadkar, A. Pawbake, R. Waykar, A. Jadhavar, A. Mayabadi, A. Date, and S. Jadkar, "Synthesis of orthorhombic-molybdenum trioxide (α-MoO_3) thin films by hot wire-CVD and investigations of its humidity sensing properties", *Journal of Materials Science: Materials in Electronics,* Vol. 28, no. 21, pp.15790-15796, (2017).

58. Y. Zhu, Y. Yao, Z. Luo, C. Pan, J. Yang, Y. Fang, and Y. Guo, "Nanostructured MoO_3 for Efficient Energy and Environmental Catalysis", *Molecules*, Vol. 25, no. 1, pp.18, (2020).

References

59. X. Liu, Y. Wu, H. Wang, Y. Wang, C. Huang, L. Liu, and Z. Wang, "Two-dimensional β-MoO$_3$@ C nanosheets as high-performance negative materials for supercapacitors with excellent cycling stability". *RSC Advances*, Vol. 10, no. 30, pp.17497-17505, (2020).

60. S. Gulati, M. Sachdeva, and K. K. Bhasin, "Various synthetic routes for the preparation of nanoparticles", *In AIP Conference Proceedings*, Vol. 1953, no. 1, pp.1-4, (2018).

61. P. G. Jamkhande, N. W. Ghule, A. H. Bamer, and M. G. Kalaskar, "Metal nanoparticles synthesis: An overview on methods of preparation, advantages and disadvantages, and applications", *Journal of Drug Delivery Science and Technology*, Vol. 53, pp.1-11, (2019).

62. W. H. Abdelraheem, M. K. Patil, M. N. Nadagouda, and D. D. Dionysiou, "Hydrothermal synthesis of photoactive nitrogen-and boron-codoped TiO$_2$ nanoparticles for the treatment of bisphenol A in wastewater: Synthesis, photocatalytic activity, degradation byproducts and reaction pathways", *Applied Catalysis B: Environmental*, Vol. 241, pp. 598-611, (2019).

63. G. Yang, and S. J. Park, "Conventional and microwave hydrothermal synthesis and application of functional materials: A review", *Materials*, Vol. *12*, no. 7, pp.1177, (2019).

64. M. Rajamathi, and R. Seshadri, "Oxide and chalcogenide nanoparticles from hydrothermal/solvothermal reactions",*Current Opinion in Solid State and Materials Science*, Vol. 6, no. 4, pp.337-345, (2002).

65. W. T. Yao, and S. H. Yu, "Recent advances in hydrothermal syntheses of low dimensional nanoarchitectures", *International journal of nanotechnology*, Vol. 4, no. (1-2), pp.129-162, (2007).

66. S. Sōmiya, and R. Roy, "Hydrothermal synthesis of fine oxide powders", *Bulletin of Materials Science*, Vol. 23, no. 6, pp.453-460, (2000).

References

67. A. Chithambararaj, and A. C. Bose, "Hydrothermal synthesis of hexagonal and orthorhombic MoO_3 nanoparticles", *Journal of Alloys and Compounds*, Vol.509, no. 31, pp.8105-8110, (2011).

68. M. Safaei, R. Sarraf-Mamoory, M. Rashidzadeh, and M. Manteghian, "A Plackett–Burman design in hydrothermal synthesis of TiO_2-derived nanotubes ", *Journal of Porous Materials*, Vol. 17, no. 6, pp.719-726, (2010).

69. J. Li, Q. Wu, and J. Wu, "Synthesis of nanoparticles via solvothermal and hydrothermal methods", Handbook of Nanoparticles, M. Aliofkhazraei ed., Springer International Publishing, Switzerland, pp.296-323, (2016).

70. N. Asim, S. Ahmadi, M. A. Alghoul, F. Y Hammadi, K. Saeedfar, and K. Sopian, "Research and development aspects on chemical preparation techniques of photoanodes for dye sensitized solar cells", *International Journal of Photoenergy*, Vol. 2014, pp. 21, (2014).

71. J. Qian, M. Zhou, Y. Cao, X. Ai, and H. Yang, "Template-free hydrothermal synthesis of nanoembossed mesoporous $LiFePO_4$ microspheres for high-performance lithium-ion batteries", *The Journal of Physical Chemistry C*, Vol.114, no. 8, pp. 3477-3482, (2010).

72. D. F. Rivas, M. Ashokkumar, T. Leong, K. Yasui, T. Tuziuti, S. Kentish, and H. J. Gardeniers, "Sonoluminescence and sonochemiluminescence from a microreactor", *Ultrasonics sonochemistry*, Vol.19, no. 6, pp.1252-1259, (2012).

73. S. Gulati, M. Sachdeva, and K. K. Bhasin, "Various synthetic routes for the preparation of nanoparticles", *In AIP Conference Proceedings,* Vol. 1953, no. 1, pp. 1-5, (2018).

74. R. G. Compton, J. C. Eklund, and F. Marken, "Sonoelectrochemical processes: a review", *Electroanalysis*, Vol. 9, no. 7, pp. 509-522, (1997).

75. X. Wang, Y. Liu, Z. Hu, Y. Chen, W. Liu, and G. Zhao, "Degradation of methyl orange by composite photocatalysts nano-TiO_2 immobilized on activated carbons

of different porosities", *Journal of Hazardous Materials*, Vol. 169, no.(1-3), pp.1061-1067, (2009).

76. S. Bai, H. Liu, J. Sun, Y. Tian, S. Chen, J. Song, R. Luo and C. C. Liu, "Improvement of TiO_2 photocatalytic properties under visible light by WO_3/TiO_2 and MoO_3/TiO_2 composites", *Applied Surface Science*, Vol. 338, pp. 61-68, (2015).

77. M. E. Navgire, M. K. Lande, A. B. Gambhire, S. B. Rathod, D. V Aware, and S. R Bhitre, "Effect of poly (ethylene glycol) surfactant on carbon-doped MoO_3 nanocomposite materials and its photocatalytic activity", *Bulletin of Materials Science*, Vol. 34, no. 3, pp. 535-541, (2011).

78. M. Navgire, A. Yelwande, D. Tayde, B. Arbad, and M. Lande, "Photodegradation of molasses by a MoO_3-TiO_2 nanocrystalline composite material", *Chinese Journal of Catalysis*, Vol. 33, no. (2-3), pp. 261-266, (2012).

79. H. Yu, Y. Li, L. Zhao, G. Li, J. Li, H. Rong, and Z. Liu, "Novel MoO_3-TiO_2 composite nanorods films with improved electrochromic performance", *Materials Letters*, Vol. 169, pp. 65-68, (2016).

80. T. V. Kumar, K. V. Ramana, and R. B. Choudary, "Spectroscopic characterization of mechanically synthesized MoO_3-TiO_2 Composite Nano powders", *International Journal of Mechanical Engineering and Technology*, Vol. 8, no. 5, pp. 1051-1063, (2017).

81. Y. Zhao, Q. Sun, J. Luo, H. Chen, W. Cai, and X. Su, "Hydrothermal fabrication of TiO_2-MoO_3 nanocomposites with superior performance for water treatment", *Nano-Structures & Nano-Objects*, Vol. 13, pp. 93-99, (2018).

82. A Kubiak, W. Wojciechowska, B. Kurc, M. Pigłowska, K. Synoradzki, E. Gabała, and T. Jesionowski, "Highly Crystalline TiO_2-MoO_3 Composite Materials Synthesized via a Template-Assisted Microwave Method for Electrochemical Application", *Crystals*, Vol.10, no. 6, pp. 493, (2020).

References

83. V. K. Gupta, "Application of low-cost adsorbents for dye removal–a review", *Journal of environmental management*, Vol. 90, no. 8, pp. 2313-2342, (2009).

84. A. Ahmad, S. H. Mohd-Setapar, C. S. Chuong, A Khatoon, W. A. Wani, R. Kumar, and M. Rafatullah, "Recent advances in new generation dye removal technologies: novel search for approaches to reprocess wastewater", *RSC advances*, Vol. 5, no. 39, pp. 30801-30818, (2015).

85. W. J. Thomas, and B. Crittenden, "Adsorption technology and design", Butterworth-Heinemann, Melbourne, pp.271, (1998).

86. L. Tian, Z. Shi, Y. Lu, A. C. Dohnalkova, Z. Lin, and Z. Dang, "Kinetics of cation and oxyanion adsorption and desorption on ferrihydrite: roles of ferrihydrite binding sites and a unified model", *Environmental Science & Technology*, Vol. 51, no. 18, pp.10605-10614, (2017).

87. H. Zhao, X. Liu, Z. Cao, Y. Zhan, X. Shi, Y. Yang, and J. Xu, "Adsorption behavior and mechanism of chloramphenicols, sulfonamides, and non-antibiotic pharmaceuticals on multi-walled carbon nanotubes" *Journal of hazardous materials*, Vol. 310, pp. 235-245, (2016).

88. S. Horikoshi, and N. Serpone, "Can the photocatalyst TiO_2 be incorporated into a wastewater treatment method? Background and prospects", *Catalysis Today*, Vol. 340, pp.334-346, (2020).

89. N. Serpone, and A. V. Emeline, "Suggested terms and definitions in photocatalysis and radiocatalysis" *International journal of photoenergy*, Vol. 4, no.3, pp. 91-131, (2002).

90. D. C. Hurum, A. G. Agrios, K. A. Gray, T. Rajh, and M. C. Thurnauer, "Explaining the enhanced photocatalytic activity of Degussa P25 mixed-phase TiO_2 using EPR", *The Journal of Physical Chemistry B*, Vol. 107, no. 19, pp. 4545-4549, (2003).

References

91. J. M Herrmann, "Heterogeneous photocatalysis: fundamentals and applications to the removal of various types of aqueous pollutants", *Catalysis today*, Vol. 53, no. 1, pp. 115-129, (1999).

92. U. I. Gaya, "Heterogeneous photocatalysis using Inorganic Semiconductor Solids", 1st ed., *Springer Science*, Business Media Dordrecht, London, CH3, pp. 73-89, (2014).

93. B. Wu, J. Lee, S. Mubeen, Y. S. Jun, G. D. Stucky, and M. Moskovits, "Plasmon-Mediated Photocatalytic Decomposition of Formic Acid on Palladium Nanostructures", *Advanced Optical Materials*, Vol.4, no. 7, pp. 1041-1046, (2016).

94. H. Gerischer, and A. Heller, "The role of oxygen in photooxidation of organic molecules on semiconductor particles", *The Journal of physical chemistry*, Vol. 95, no. 13, pp.5261-5267, (1991).

95. F. Petronella, A. Truppi, C. Ingrosso, T. Placido, M. Striccoli, M. L. Curri, and R. Comparelli, "Nanocomposite materials for photocatalytic degradation of pollutants". *Catalysis Today*, Vol. 281, pp. 85-100, (2017).

96. I. Ali, "New generation adsorbents for water treatment" *Chemical reviews*, Vol.112, no. 10, pp. 5073-5091, (2012).

97. Z. Q. Guo, N. X. Miao, J. P. Zhou, Y. X. Lei, Q. U. Hassan, and M. M. Zhou, "Novel magnetic semiconductor $Na_2Fe_2Ti_6O_{16}$: synthesis, double absorption and strong adsorptive ability", *Journal of Materials Chemistry A*, Vol. 5, no. 33, pp. 17589-17600, (2017).

98. M. N. Akieh, M. Lahtinen, A. Väisänen, and M. Sillanpää, "Preparation and characterization of sodium iron titanate ion exchanger and its application in heavy metal removal from waste waters", *Journal of hazardous materials,* Vol. 152, no. 2, pp. 640-647, (2008).

References

99. M. Kaykhaii, M. Sasani, and S. Marghzari, "Removal of dyes from the environment by adsorption process", *Chem. Mater Eng.*, Vol. 6, no. 2, pp. 31-35, (2018).

100. N. Mohammadi, H. Khani, V. K. Gupta, E. Amereh, and S. Agarwal, "Adsorption process of methyl orange dye onto mesoporous carbon material–kinetic and thermodynamic studies", *Journal of colloid and interface science,* Vol. 362, no. 2, pp. 457-462, (2011).

101. J. Yang, D. Chen, Y. Zhu, Y. Zhang, and Y. Zhu, "3D-3D porous Bi_2WO_6/graphene hydrogel composite with excellent synergistic effect of adsorption-enrichment and photocatalytic degradation", *Applied Catalysis B: Environmental*, Vol.205, pp. 228-237, (2017).

102. A. Macías-García, M. G. Corzo, M. A. Domínguez, M. A. Franco, and J. M. Naharro, "Study of the adsorption and electroadsorption process of Cu (II) ions within thermally and chemically modified activated carbon", *Journal of hazardous materials*, Vol. 328, pp.46-55, (2017).

103. X. Luo, Y. Zhan, Y. Huang, L. Yang, X. Tu, and S. Luo, "Removal of water-soluble acid dyes from water environment using a novel magnetic molecularly imprinted polymer", *Journal of hazardous materials*, Vol. 187, no.(1-3), pp. 274-282, (2011).

104. S. Natarajan, H. C. Bajaj, and R. J. Tayade, "Recent advances based on the synergetic effect of adsorption for removal of dyes from waste water using photocatalytic process", *Journal of Environmental Sciences*, Vol. 65, pp. 201-222, (2018).

105. V. K. Gupta, "Application of low-cost adsorbents for dye removal–a review", *Journal of environmental management*, Vol. 90, no. 8, pp. 2313-2342, (2009).

References

106. A. Kausar, M. Iqbal, A. Javed, K. Aftab, H. N. Bhatti, and S. Nouren, "Dyes adsorption using clay and modified clay: A review", *Journal of Molecular Liquids*, Vol. 256, pp. 395-407, (2018).

107. Z. Carmen, and S. Daniela, "Textile organic dyes–characteristics, polluting effects and separation/elimination procedures from industrial effluents–a critical overview", In Organic pollutants ten years after the Stockholm convention-environmental and analytical update. T. Puzyn ed., Intech Open, ISBN 978-953-307-917-2, Vol. 10, ,London, UK, pp. 55-86, (2012).

108. E. Forgacs, T. Cserhati, and G. Oros, "Removal of synthetic dyes from wastewaters: a review", *Environment international*, Vol. 30, no. 7, pp. 953-971, (2004).

109. M. T. Yagub, T. K. Sen, S. Afroze, and H. M. Ang, "Dye and its removal from aqueous solution by adsorption: a review", *Advances in colloid and interface science*, Vol. 209, pp.172-184, (2014).

110. E. A. Clarke, and R. Anliker, "Organic dyes and pigments", In Anthropogenic compounds, The Handbook of Environmental Chemistry, 1st , O.Hutzinger ed., Springer, Berlin, Heidelberg, Vol. 3 / 3A., ISBN 978-3-662-15998-9, pp. 181-215, (1980).

111. V. K. Gupta, "Application of low-cost adsorbents for dye removal–a review", *Journal of environmental management,* Vol. 90, no. 8, pp. 2313-2342, (2009).

112. W. Ruan, J. Hu, J. Qi, Y. Hou, C. Zhou, and X. Wei, "Removal of dyes from wastewater by nanomaterials: a review", *Adv Mater Lett*, Vol. 10, no. 1, pp.09-20, (2019).

113. R. G. Saratale, G. D. Saratale, J. S. Chang, and S. P. Govindwar, "Bacterial decolorization and degradation of azo dyes: a review", *J Taiwan Inst Chem Eng,*Vol. 42, no.1, pp. 138–157, (2011).

References

114. M. Solís, A. Solís, H. I. Pérez, N. Manjarrez, and M. Flores, "Microbial decolouration of azo dyes: a review", *Process Biochemistry*, Vol.47, no.12, pp. 1723-1748, (2012).

115. N. SEKAR, "Direct dyes", " Handbook of textile and industrial dyeing", 1st ed., M. Clark ed. , Woodhead Publishing Limited, India, CH 12 , Vol. 1, no.116, pp. 425-443, (2011).

116. S. K. Abbas, Z. M. Hassan, and L. M. Ahmed, "Influencing the Artificial UV-A light on decolorization of Chlorazol black BH Dye via using bulk ZnO Suspensions", *In Journal of Physics: Conference Series* Vol. 1294, no. 5, pp.1-8, (2019).

117. G. Vijayaraghavan, and S. Shanthakumar, "Efficacy of alginate extracted from marine brown algae (Sargassum sp.) as a coagulant for removal of direct blue2 dye from aqueous solution", *Global Nest Journal*, Vol. 17, no. 4, pp.716-726, (2015).

118. Q. Duan, J. Lee, Y. Liu, and H. Qi, "Preparation and photocatalytic performance of MWCNTs/TiO$_2$ nanocomposites for degradation of aqueous substrate", *Journal of Chemistry*, Vol. 2016, pp. 8, (2016).

119. K. J. Samdani, D. W. Joh, M. K. Rath, and K. T. Lee, "Electrochemical mediatorless detection of norepinephrine based on MoO3 nanowires", *Electrochimica Acta*, Vol. 252, pp. 268-274, (2017).

120. B. Ohtani, "Photocatalysis A to Z—what we know and what we do not know in a scientific sense", *Journal of Photochemistry and Photobiology C: Photochemistry Reviews*, Vol. 11, no. 4, pp.157-178, (2010).

121. A. L. Patterson, "The Scherrer formula for X-ray particle size determination", *Physical review*, Vol. 56, no. 10, pp. 978, (1939).

122. I. P. Bincy, T. Srinivasan, S. N. Jaisankar, and V. Ramkumar, "Structure, growth and characterization of a new naphthalene family crystal for fluorescence and

third order nonlinear optical applications", *Solid State Sciences*, Vol. 89, pp. 85-92, (2019).

123. R. Saravanan, J. Aviles, F. Gracia E. Mosquera, and V. K. Gupta, "Crystallinity and lowering band gap induced visible light photocatalytic activity of TiO_2/CS (Chitosan) nanocomposites", *International journal of biological macromolecules*, Vol. 109, pp. 1239-1245, (2018).

124. S. Ahmed, "Photo Electrochemical Study of Ferrioxalate Actinometry at A Glassy Carbon Electrode", *Journal of Photochemistry and Photobiology A: Chemistry*, vol. 161, pp. 151-154, (2004).

125. M. Montalti, A. Credi, L. Prodi, and M. T. Gandolfi, "Handbook of photochemistry", 3rd ed., CRC press, pp.664, (2006).

126. A. W. Adamson, A. Vogler, H. Kunkely, and R. Wachter, "Photocalorimetry. Enthalpies of photolysis of trans-azobenzene, ferrioxalate and cobaltioxalate ions, chromium hexacarbonyl, and dirhenium decarbonyl", *Journal of the American Chemical Society*, Vol. 100, no. 4, pp.1298-1300, (1978).

127. B. Barrocas, O. C. Monteiro, M. M. Jorge, and S. Sério, "Photocatalytic activity and reusability study of nanocrystalline TiO_2 films prepared by sputtering technique", *Applied surface science*, Vol. 264, pp.111-116, (2013).

128. P. Intaphong, A. Phuruangrat, K. Karthik, T. Thongtem, and S. Thongtem, "Sonochemical synthesis and characterization of BiOCl nanoplates and their photodegradation of Rhodamine B", *Digest Journal of Nanomaterials & Biostructures (DJNB)*, Vol. 14, no. 3, pp. 593 - 599 , (2019).

129. S. I. Zuafuani, and L. M. Ahmed, "Photocatalytic decolourization of direct orange Dye by zinc oxide under UV irradiation", *International Journal of Chemical Sciences*, Vol. 13, no. 1, pp.187-196, (2015).

130. M. A. Tabbara, and M. M. El Jamal, "A KINETIC STUDY OF THE DISCLOLORATION OF METHYLENE BLUE BY Na_2SO_3, COMPARISON

References

WITH NaOH", *Journal of the University of Chemical Technology & Metallurgy*, Vol. 47, no. 3, pp. 275-282, (2012).

131. P. Atkins, and J. De Paula, "Physical chemistry for the life sciences", 2nd ed., Oxford University Press, USA, pp.590, (2011).

132. M.B. Rahmani, S.H. Keshmiri, J. Yua, A.Z. Sadek, L. Al-Mashat, A. Moafic, K. Latham, Y.X. Li, W. Wlodarski, and K. Kalantar-zadeh, "Gas sensing properties of thermally evaporated lamellar MoO_3", *Sensors and Actuators B: Chemical*, Vol.145, no.1, pp.13–19, (2010).

133. Q.P. Ding, H.B. Huang, J.H. Duan, J.F. Gong, S.G. Yang, X.N. Zhao, and Y.W. Du, "Molybdenum trioxide nanostructures prepared by thermal oxidization of molybdenum", *J. Cryst. Growth*, Vol. 294, no. 2, pp. 304–308, (2006).

134. T. M. Jawad, and L. M. Ahmed, "Direct Ultrasonic Synthesis of WO3/TiO2 Nanocomposites and Applying them in the Photodecolorization of Eosin Yellow Dye", *Periódico Tchê Química*, Vol. 17, no. 34, pp. 621-633, (2020).

135. E. Filippo, C. Carlucci, A. L. Capodilupo , P. Perulli , F. Conciauro , G. A. Corrente, G.Gigli and G. Ciccarell, "Enhanced Photocatalytic Activity of Pure Anatase TiO_2 and Pt-TiO_2 Nanoparticles Synthesized by Green Microwave Assisted Route", *Materials Research*, Vol. 18, no. 3, pp.473-481, (2015).

136. B. A. Mohammed, and L. M. Ahmed, "Improvement the photo-catalytic properties of ZnS nanoparticle with loaded manganese and chromium by co-precipitation method", *JGPT*, Vol. 10, no. 7, pp.129-138. (2018).

137. M. K. Hayawi, M. M. Kareem, and L. M., Ahmed "Synthesis of Spinel Mn_3O_4 and Spinel Mn_3O_4/ZrO_2 Nanocomposites and Using Them in Photo-Catalytic Decolorization of Fe (II)-(4, 5- Diazafluoren-9-One 11) Complex", *Periódico Tchê Química*, Vol. 17, no. 34, pp. 689- 699, (2020).

References

138. B. A. Mahammed, and L. M. Ahmed, "Enhanced Photocatalytic Properties of Pure and Cr-Modified ZnS Powders Synthesized by Precipitation Method", *Journal of Geoscience and Environment Protection*, Vol. 5, pp.101-111, (2017).

139. S. Silvestri, E. T. Kubaski, T. Sequinel, S. A. Pianaro, J. A. Varela, and S. M. Tebcherani, "Optical Properties of the MoO_3-TiO_2 Particulate System and Its Use as a Ceramic Pigment", *Particulate Science and Technology, An International Journal*, Vol. 31, no. 5, pp. 466-473, (2013).

140. R. Shannon, "Revised effective ionic radii and systematic studies of interatomic distances in halides and chalcogenides", *Acta Crystallographica A*, Vol. 32, no. 5, pp.751–767, (1976).

141. L.M. Ahmed, I. Ivanova, F.H. Hussein, and D.W. Bahnemann, "Role of platinum deposited on TiO_2 in photocatalytic methanol oxidation and dehydrogenation reactions", *International Journal of Photoenergy*, Vol.2014, pp. 1-10, (2014).

142. T. H. Chiang, and H. C. Yeh, "A novel synthesis of α-MoO_3 nanobelts and the characterization", *Journal of alloys and compounds*, Vol.585, pp. 535-541, (2014).

143. C. V. S. Reddy, E. H. Walker, C. Wen, and S. I. Mho, "Hydrothermal synthesis of MoO_3 nanobelts utilizing poly (ethylene glycol)", *Journal of Power Sources*, Vol.183, no.1, pp.330-333, (2008).

144. Y. Mo, Z. Tan, L. Sun, Y. Lu, and X. Liu, "Ethanol-sensing properties of α-MoO_3 nanobelts synthesized by hydrothermal method", *Journal of Alloys and Compounds*, Vol. 812, pp.5, (2020).

145. M. Pal, J. G Serrano, P. Santiago, and U. Pal, "Size-controlled synthesis of spherical TiO_2 nanoparticles: morphology, crystallization, and phase transition", *The Journal of Physical Chemistry C*, Vol. 111, no. 1, pp. 96-102, (2007).

References

146. P. Wongkrua, T. Thongtem, and S. Thongtem, "Synthesis of h-and α-MoO$_3$ by refluxing and calcination combination: Phase and morphology transformation, photocatalysis, and photosensitization", *Journal of Nanomaterials*, Vol. 2013, pp. 8, (2013).

147. M. Rashidzadeh, "Synthesis of high-thermal stable titanium dioxide nanoparticles", *International Journal of Photoenergy*, Vol. 2008, pp. 4, (2008).

148. Z. A.Hussain, F. H. Fakhri, H. F. Alesary and L. M. Ahmed, ZnO "Based Material as Photocatalyst for Treating the Textile Anthraquinone Derivative Dye (Dispersive Blue 26 Dye): Removal and Photocatalytic Treatment", *Journal of Physics: Conference Series*, Vol. 1664, no. 1, pp.1-15, (2020).

149. K. M. Jasim, and L. M. Ahmed, "TiO$_2$ nanoparticles sensitized by safranine O dye using UV-A light system", *In IOP Conference Series: Materials Science and Engineering*, Vol. 571, no. 1, pp. 1-9, (2019).

150. F. H. Fakhri, and L. M. Ahmed, "Incorporation CdS with ZnS as nanocomposite and Using in Photo-Decolorization of Congo Red Dye", *Indones. J. Chem.*, Vol. 19, no. 4, pp.936–943, (2019).

151. H. Chun, W. Yizhong, and T. Hongxiao, "Destruction of phenol aqueous solution by photocatalysis or direct photolysis", *Journal of Chemosphere*, Vol. 41, pp. 1205–1209, (2000).

152. L. M. Ahmed, "Photo-decolourization kinetics of acid red 87 dye in ZnO suspension under different types of UV-A light", *Asian Journal of Chemistry.*, Vol. 30, no. 9, pp.2134-2140, (2018).

153. C. Galindo, P. Jacques, and A. Kalt, " Photodegradation of the aminoazobenzene acid orange 52 by three advanced oxidation processes: UV/H$_2$O$_2$, UV/TiO$_2$ and VIS/TiO$_2$: comparative mechanistic and kinetic investigations", *Journal of Photochemistry and Photobiology A: Chemistry*, Vol. 130, no.1, pp.35-47, (2000).

الخلاصة

يتكون هذا المشروع من ثلاثة اجزاء رئيسية:

يتضمن الجزء الاول تحضير ثالث اوكسيد الموليبدينوم α-MoO$_3$ كاحزمة نانوية باستعمال طريقة الهيدروثيرمل. اذ تم بهذه الطريقة التحكم بابعاد المادة المحضرة بوساطة التفاعل بين(Na$_2$MoO$_4$.2H$_2$O) كمادة بادئة وحامض الهدروكلوريك المخفف (HCl). تم تحضير المتراكب النانوي بنسبة وزنية (MoO$_3$) 0.25 :(TiO$_2$) 9.75 باستخدام تقنية الموجات فوق الصوتية ، والتي تعتبر طريقة سريعة ، وبسيطة، و صديقة للبيئة.

الجزء الثاني يتعامل مع توصيف المحفزات المحضرة α-MoO$_3$ ، والمتراكب النانوي α-MoO$_3$/TiO$_2$ والتجاري TiO$_2$.حيث تم مطابقة نتائج تحليل حيود الاشعة السينية للمحضر α-MoO$_3$ومتراكبه مع TiO$_2$ وتأكيد تحضيرها بنجاح بناءا على ظهور قمم شديدة القوة عند مؤشرات ميلر (020)، (040)، و(060). وأشار تحليل المجهر الالكتروني الماسح الى شكل α-MoO$_3$ ووجد انه بهياة أحزمة نانوية، بينما كانت أشكال TiO$_2$ والمتراكب النانوي شبه- كروية وتجمعات شبه-كروية على التوالي. ومن خلال اطياف الاشعة تحت الحمراء تم تأكيد تحضيرα-MoO ومتراكبه النانوي α-MoO$_3$/TiO$_2$ نتيجة ظهور قمم من روابط الاوكسجين- فلزعند 675 cm^{-1} تعود الى Ti-O وعند 559 cm^{-1} تعود الى Mo-O. وتم حساب فجوة الحزمة (Bg) بواسطة معادلة Tauc ووجد انه جميع المحفزات المستخدمة هي محفزات ضوئية، واتضح انه TiO$_2$ التجاري ومتراكبه النانوي لهما حزمة فجوة غير مباشرة، بينما α-MoO$_3$ المحضر لديه حزمة فجوة مباشرة، اذ كانت قيم حزمة الفجوة للمحفزات الضوئية تساوي 2.8 eV, 2.95 eV, 3 eV على التوالي.

الجزء الثالث ركز على قدرة وأختبار كفاءة المحفزات الضوئية α-MoO$_3$، TiO$_2$، و متراكبه النانوي α-MoO$_3$/TiO$_2$ على أزالة لون صبغة الكلورازول السوداء BH كنموذج للدراسة. تم دراسة تأثير العوامل المختلفة على الأزالة اللونية للصبغة بأستخدام المحفزات الضوئية TiO$_2$ ومتراكبه النانوي α-MoO$_3$/TiO$_2$. حيث تتضمن العوامل المستخدمة كمية المحفز الضوئي، ودرجة الحرارة، والدالة الحامضية الابتدائية للمحلول. كما تم احتساب العوامل الثرموديناميكية بأستخدام معادلة Arrhenius ومعادلة Eyring-Polanyi ومعادلة Gibbs حيث تم اثبات بأن هذا التفاعل الضوئي هو باعث للحرارة، و أقل عشوائية ، وغير تلقائي مع استخدام TiO$_2$ ، بينما

مع أستخدام المتراكب النانوي α-MoO_3/TiO_2 يكون التفاعل ماص للحرارة، و أقل عشوائية، وغير تلقائي.

اذ تم الحصول على اقصى فعالية لأزالة اللون ضوئيا بأستخدام المتراكب النانوي α-MoO_3/TiO_2 ويعزا سبب ذلك الى زيادة حموضة α-MoO_3 بعد دمجه في الشبكة البلورية من TiO_2. حركيا يعد هذا التفاعل الضوئي تفاعل درجة اولى كاذبه بالاعتماد على صبغة كلورازول السوداء BH.

تحضير ودراسة المتراكب النانوي (MoO$_3$/TiO$_2$) وتطبيقه في الازالة اللونية

رسالة مقدمة الى

مجلس كلية العلومـ جامعة كربلاء وهي جزء من متطلبات نيل شهادة الماجستير في الكيمياء

تقدمت بها

اماني جبار عبيد

بكلوريوس علوم كيمياء (2016) / جامعة كربلاء

بأشراف

أ .د . لمى مجيد احمد